NCHRP 17-22 FINAL REPORT VOLUME II

DEVELOPMENT OF CRASH RECONSTRUCTION PROCEDURES FOR ROADSIDE SAFETY APPURTENANCES

by

Brian A. Coon

TABLE OF CONTENTS

1 INTRODUCTION 0
1.1 Purpose of Research 0
1.2 Crash Reconstruction 1
1.3 Absent Reconstruction Procedures 2
1.4 Research Approach 3
2 Prior Work 5
2.1 Hutchinson and Kennedy Study 5
2.2 Cooper Study 6
2.3 Probability Models 6
2.4 Crash Reconstruction 7
2.4.1 Rigid Barrier Impact Reconstruction Procedure 7
2.4.2 Longitudinal Barrier Special Studies 9
2.4.3 NCHRP Project 17-11 10
2.4.4 Reconstruction Procedure for Pole Accidents - Labra and Mak 11
2.4.5 Reconstruction Procedure for Pole Accidents - Kent and Strother 13
3 Reconstruction Procedure 16
3.1 Literature Review 16
3.2 Crash Test Results 17
4 Available Information 18
4.1 Crash Site Information 18
4.1.1 Scale Diagrams 19
4.1.2 Photographic Evidence 21
4.1.3 Post-Impact Trajectory 21
4.1.4 Object Interaction 22
4.1.5 Vehicle Data Sources 22
4.2 Roadside Characteristics 23
4.3 Environmental Conditions 23
5 Device Identification 24
5.1 Longitudinal Barriers 24
5.2 Guardrail End Terminals 25
5.3 Crash Cushions 26
5.4 Concrete Barriers 26
5.5 Poles and Luminaries 27
5.6 Others 27
6 Development of Reconstruction Procedures 29
6.1 General Engineering Principles 29
6.2 Full-Scale Crash Testing 30
6.3 Component Testing 30
6.4 Software 31
6.4.1 LS-DYNA 31
6.4.2 CRASH3 31
6.4.3 BARRIER VII 32
6.4.4 Other Software Codes 33

7 EXAMPLE OF PROCEDURES 34
7.1 Longitudinal Barriers 34
7.2 Guardrail End Terminals 36
7.3 Crash Cushions 39
8 CONCLUSIONS 41
9 FUTURE WORK 42
10 REFERENCES ..... **Error! Bookmark not defined.**
11 APPENDICES 48

Crash Reconstruction Technique for Longitudinal Barriers Appendix A

Reconstruction Techniques for Guardrail End Terminals Appendix B

Crash Cushion Identification and Reconstruction Techniques Appendix C

1 INTRODUCTION

When a vehicle exits the traveled way and encroaches on the roadside, the best chance for reducing crash severity is to offer roadsides free of fixed objects and other hazards [1]. However, logistics and economy frequently prohibit the removal of all roadside hazards. Design alternatives, in order of preference, include:

Remove the obstacle.

Relocate the obstacle.

Make the object breakaway or safely traversable.

Shield the object with a longitudinal barrier or crash cushion.

As a last alternative, delineate the obstacle.

The determination of the benefit-to-cost ratio for each alternative requires an accurate understanding of the real-world conditions where ran-off-road crashes occur. Most importantly, this includes the distribution of the angles and speeds at which vehicles exit the roadway. This information can then be used for refining the guidelines for roadside safety countermeasures and for calibrating roadside safety simulation models, such as the Roadside Safety Analysis Program (RSAP), as well as identifying the roadside features involved in the greatest number of serious crashes.

1.1 Purpose of Research

This research was developed for National Cooperative Highway Research Program (NCHRP) Project 17-22, entitled “Identification of Vehicular Impact Conditions Associated with Serious Ran-Off-Road Crashes.” The primary goal of NCHRP Project 17-22 is to identify the vehicle types, impact conditions, and site characteristics associated with serious injury and fatal crashes involving roadside features and safety devices.

NCHRP Project 17-22 is a retrospective examination of ran-off-road crashes by performing crash reconstruction of such crashes from the National Automotive Sampling System (NASS) Crashworthiness Data System (CDS) by the National Highway Traffic Safety Administration (NHTSA). The distribution of the impact speeds, angles, and orientations will be used to create a database that can then be used to identify a practical worst-case testing regimen.

Real-world data on ran-off-road crashes will help designers spend safety dollars on improvements that will have the greatest likelihood of reducing serious injuries and fatalities. These improvements will also serve to foster the spectrum of commonly available roadside design alternatives for appropriate field conditions.

1.2 Crash Reconstruction

Analysis of ran-off-road crashes requires the application of accurate crash reconstruction methodologies. Crash reconstruction involves using engineering principles, such as conservation of energy and conservation of momentum, to determine how a crash occurred and to estimate the initial speed and position of the vehicle.

Crash reconstruction primarily entails calculating energy losses and gains after the vehicle leaves the roadway. This requires qualitative and quantitative information about the crash; while the logistical specifics of a particular crash may be unique, ran-off-road crashes generally involve specific groups of objects, such as trees, embankments, or guardrails. The fixed-object impact frequency for fatal crashes by object struck from the Fatality Analysis Reporting System (FARS) data for 2000 is shown in Table 1 [2].

Table 1. Object Struck as First Harmful Event From 1999 FARS Data.

Object	Frequency
Tree	2,997
Embankment	1,213
Guardrail	1,078
Utility Pole	1,018
Ditch	887
Curb	681
Culvert	592
Fence	490
Sign Support	368
Other Post/Support	308
Concrete Barrier	275
Bridge Rail	158
Bridge Pier/Abutment	155
Wall	119
Luminaire Support	103
Boulder	79
Building	79
Shrubbery	56
Bridge Parapet	36
Equipment	26
Fire Hydrant	25
Other Longitudinal Barrier	23
Snow Bank	23
Traffic Signal Support	22
Unknown	22
Impact Attenuator	11
Other Fixed Object	506
Other Object (not fixed)	135
Total	11,485

1.3 Absent Reconstruction Procedures

Many ran-off-road crashes, such as those with rigid walls or poles, can be reconstructed using well-established reconstruction procedures [3]. However, impacts with longitudinal barriers, crash cushions, and many other roadside hazards do not have reconstruction procedures available

in literature. Because of the prevalence of crashes involving roadside hazards lacking available reconstruction procedures, the development of appropriate reconstruction procedures for these devices is required.

1.4 Research Approach

The development of new reconstruction procedures involves a comprehensive examination of the existing procedures, an examination of full-scale and component testing performed, and the availability and applicability of computer simulation software. This generalized approach will allow for new procedures to be developed and for future additions to the database with vehicle fleet changes, future speed limits changes, and other changes that may affect the nature of ran-off-road crashes.

This dissertation is divided into ten chapters. This first chapter serves as an introduction and overview of the work. Chapter 2 examines the prior work in the field of crash reconstruction. Both a perspective of ran-off-road crashes and crash reconstruction are discussed.

Chapter 3 discusses the nature of reconstruction procedures and a general methodology for developing reconstruction procedures. This includes examining reconstruction procedures in literature and the availability and analysis of crash test results.

The information available to reconstruct a crash is delineated in Chapter 4. Sources of data include scale diagrams, photographic evidence, and police reports. Chapter 4 also suggests other resources for obtaining data, such as the National Automobile Dealer's Association (NADA) and the American Automobile Manufacturer's Association (AAMA).

Due to the hundreds of roadside devices and obstacles, with some designs of devices barely distinguishable from others, Chapter 5 examines device identification. Correct identification of a roadside device is critical to accurate reconstructions. This includes the identification of longitudinal barriers, guardrail end terminals, crash cushions, concrete barriers, *et cetera*.

Chapter 6 details procedures required to develop reconstruction procedures. The use of basic engineering principles, full-scale crash test data, component testing, as well as the use of computer software is discussed.

Examples of three reconstruction procedures are detailed in Chapter 7. These procedures, listed in detail in the Appendix, were developed for longitudinal barriers, energy-absorbing guardrail end terminals, and inertial barriers (sand barrels).

Chapter 8 lists the conclusions of the research effort of developing reconstruction procedures to aid in the identification of the real-world conditions where ran-off-road crashes occur. This information will allow better test procedures for determining the suitability of an appurtenance for use on the National Highway System (NHS). Ultimately, this will lead to a safer roadside environment, which will save lives and reduce injuries during ran-off-road crashes.

Opportunities for future work are discussed in Chapter 9. This includes the development of reconstruction procedures for additional roadside devices and the examination of the effects of impact orientation.

2 PRIOR WORK

Identification of the real-world conditions where ran-off-road crashes occur requires that the encroachment rates and conditions (impact angle, speed, and vehicle orientation) be identified. An examination of prior studies reconstructing significant numbers of ran-off-road accidents is helpful to identify procedures that have proved successful previously and to identify potential pitfalls to be avoided.

Research determining vehicle encroachment rates have focused on two areas: (1) the use of vehicle tracks along the roadside to estimate encroachment angles and lengths and (2) the use of accident records and crash reconstruction.

2.1 Hutchinson and Kennedy Study

Hutchinson and Kennedy (H&K) performed the landmark study of vehicle encroachments in medians through the examination of vehicle tracks in 1966 [4]. This consisted of planned, weekly coverage of entire lengths of selected highway segments to locate and evaluate evidence of vehicle encroachments. Much of the data from the H&K study was collected during winter months on snow-covered medians of rural divided highways with speed limits of 112.7 km/h (70 mph).

Surveillance was performed by two-man teams who patrolled the highway in specially marked, slow-moving vehicles. A visual record of each encroachment consisted of a sketch of the path of the vehicular movement with dimensions, highway cross-section dimensions, type of median

cover, approximate time of occurrence, and other pertinent data. A visual record of each encroachment was compiled with a series of colored and black and white pictures.

The encroachment data from the H&K study is the basis of the runout lengths in the Roadside Design Guide. Additionally, the data was also used for the development of the computer simulation program ROADSIDE.

2.2 Cooper Study

Cooper performed an extensive study in Canada through the use of vehicle tracks in 1978 [5]. Cooper collected encroachment data during the summer/autumn months of June through October along the roadsides of both divided and undivided highways. Most of the highways had 80.5 - 96.6 km/h (50 - 60 mph) speed limits.

Cooper found markedly lower encroachment lengths than H&K. Much debate has been given to whether the encroachment lengths from the H&K and Cooper studies are similar. It has been shown that once both studies are corrected to match encroachment angle distributions from real-world data, there appears to be good agreement between the two studies [6].

2.3 Probability Models

Mak developed an encroachment model under NCHRP Project 22-9, “Improved Procedures for Cost-Effectiveness Analysis of Roadside Features.” Project 22-9 was the basis for the Roadside Safety Analysis Program (RSAP) [7]. Mak determined a base or average encroachment frequency based on highway type and traffic volume and then modifying the base frequency to account for specific highway characteristics such as vertical and horizontal alignment, number of lanes, and annual traffic growth factor.

RSAP determines the probability of an accident given an encroachment using the Monte Carlo simulation technique where a large number of encroachments are simulated and those causing crashes are identified. Given information on the roadway design and the location of roadside obstacles, the encroachment models will use a series of conditional probabilities to estimate the ran-off-road crash costs associated with a given design. The designer can use this information to evaluate alternative designs.

2.4 Crash Reconstruction

The field of crash reconstruction is an extremely mature field [8]. Vehicle kinematics and kinetics, the reconstruction of rear-end collisions, and even the determination of whether or not brakes had been applied by the analysis of light bulb filaments are well-documented and mature areas of engineering [**Error! Bookmark not defined.**]. Research on the development of generalized reconstruction procedures for categories of roadside objects is of particular interest to this research.

2.4.1 Rigid Barrier Impact Reconstruction Procedure

Mak, Sicking and Lock developed procedures for reconstructing rigid barrier impacts [9]. The procedure is based on the principle of conservation of energy, utilizing empirical relationships derived from full-scale crash test results. Computer simulation of the impacts is performed using a new subroutine developed for the software package CRASH3 [10].

The new subroutine, CMB, implements an iterative scheme to produce an initial estimate of the energy lost during the rigid barrier impact. CMB uses vehicle crush energy and the length of barrier contact to produce an initial estimate of the energy lost during the rigid barrier impact.

This energy loss is then added to the CRASH3 trajectory analysis to produce an initial estimate of the original impact speed. If the vehicle crush energy then matches the energy associated with the lateral velocity of the impacting vehicle, the result is believed to be reasonably accurate. If not, the vehicle crush energy is adjusted appropriately and a new estimate of the impact speed is generated. This iterative procedure has been found to give reasonably good estimates of impact speed when compared with full-scale crash tests.

Also examined in this study were cases where vehicle rollover occurred. The computer software program HVOSM was used to determine energy losses from roll distances. These curves, known as Kildare Curves, are shown in Figure 1 [**Error! Bookmark not defined.**]. It was found that roll distance is relatively unrelated to the tripping mechanism. That is to say, roll distances are not greatly affected whether high tire side forces are applied instantaneously or whether they are applied slowly.

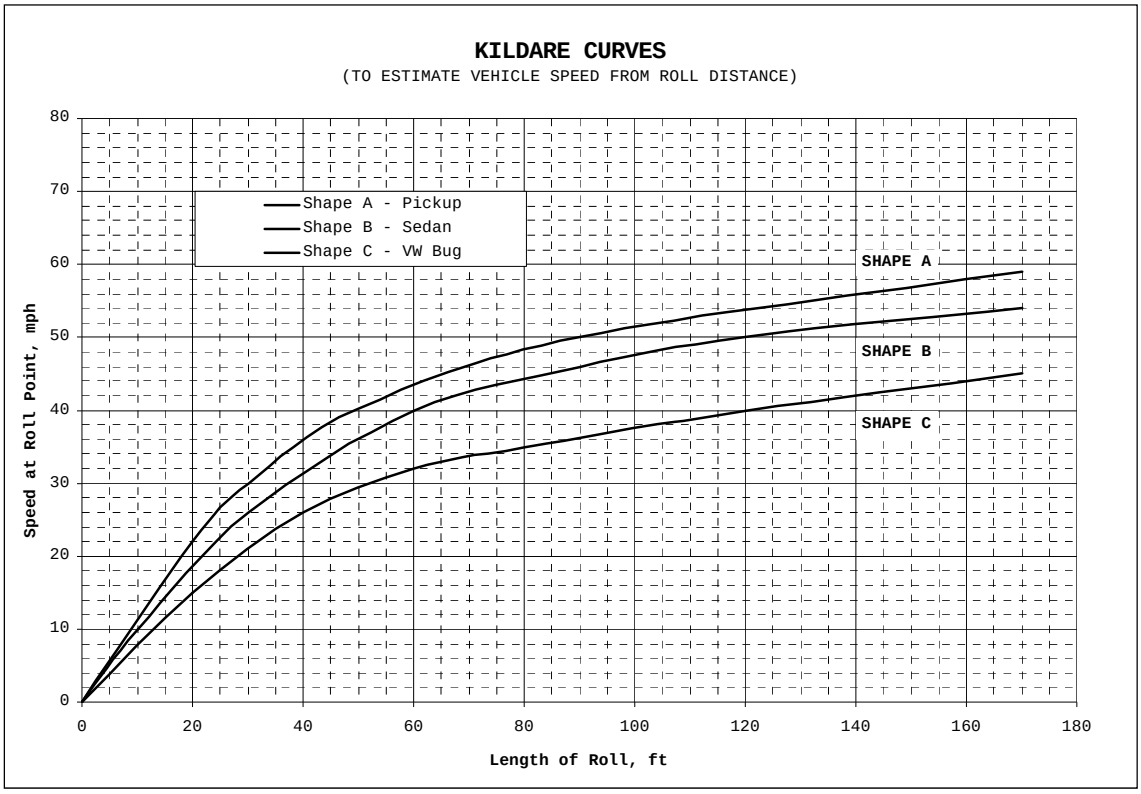

Figure 1. Curves developed using HVOSM to simulate vehicle rollover accidents [**Error! Bookmark not defined.**].

2.4.2 Longitudinal Barrier Special Studies

The Longitudinal Barrier Special Studies (LBSS) file was developed to augment the National Accident Sampling System (NASS), which is a probability sample of all police-reported crashes occurring in the U.S. from year to year [11]. The LBSS file, which was revised to meet changing analytical requirements, was cleaned and recoded to ensure consistent coding of data from year to year. This was found to be essential in developing a usable, clean database.

Scientex researchers examined several reconstruction procedures to determine the most appropriate method(s). Features of the procedures taken into consideration included the time and

effort required to develop or modify the procedure, any previous use of the procedure, and an evaluation of the previous efforts.

For barrier Length-Of-Need (LON) speed reconstructions, the basic principle of conservation of energy was used. The total energy absorbed in a crash comes from the following three components:

$$E_{total} = E_{vehicle\ crush} + E_{barrier\ deformation} + E_{vehicle\ trajectory} \quad [1]$$

The energy due to vehicle crush was found using the visual method and equations from Campbell [12]. The extent of the crush was determined visually by inspecting crash vehicles. Barrier deformation energy was obtained from curves of impact severity index versus maximum dynamic deflection (number of failed posts was used for cable systems) developed for flexible longitudinal barriers. This is the same impact severity index that was used in NCHRP Report 230 and is currently still implemented in NCHRP Report 350 and is equal to:

$$IS = \tfrac{1}{2} mV^2 \sin^2 \theta \quad [2]$$

Where:

IS = Impact Severity (Severity Index)
m = Mass of impacting vehicle
V = Velocity of impacting vehicle
θ = Impact Angle

These curves were based on a series of computer simulations performed using BARRIER VII as part of work performed by Calcote [13]. In order to adjust for differences between the permanent and dynamic deflections, a scaling factor was used. This scaling factor was created

by dividing the dynamic deflection by the permanent deflection of several full-scale crash tests on standard guardrails.

Vehicle trajectory was based on the energy absorbed using equations of motion. Adjustments were made for skidding and sliding. For rotating vehicles, the distance traveled was based on the angle of rotation and the radius. The energy absorbed by the rotation was also calculated.

2.4.3 NCHRP Project 17-11

Research to improve the trajectory data used in the encroachment model is included in NCHRP Project 17-11 "Recovery-Area Distance Relationships for Highway Roadsides" [14]. This effort developed relationships between recovery-area distance, sideslopes and other factors for various highway functional classes and design speeds. This project also involved the creation of a crash database.

2.4.4 Reconstruction Procedure for Pole Accidents - Labra and Mak

An examination of existing simulation and analytical models was performed for pole crashes by Labra and Mak [15]. Software programs designed for reconstructing pole accidents, including DASF, LUMINAIRE, MODASF, and UTILITY POLE were deemed unusable due to the significant amounts of information required to reconstruct the accident, including the structural properties of individual poles and the physical properties of a luminaire transformer base. Therefore, a procedure to create a new subroutine for the well-validated CRASH was developed. Examined analytical models made assumptions and simplifications in order to keep the mathematics and calculations at a manageable level. The key assumption was that the post failed in a shear mode and that shearing is instantaneous once the shear strength or base fracture energy

is reached. While this assumption is valid for metal bases, timber poles cannot adequately be modeled, since wooden posts fail mostly in a bending mode with fiber striping.

Pole impacts were divided into three categories: (1) no noticeable pole damage, (2) partial fracture of the pole, and (3) complete separation of the post. In cases where there was no noticeable pole damage, the pole was treated as a rigid object. It was assumed that the pole did not absorb energy and that all energy dissipation that occurred was due to vehicle crush. Equations for the fracture of wooden utility poles are shown in Table 1 and graphically represented in Figure 2.

Table 2. Equations Used to Derive Figure 2.

Pole Circumference (in.)	Extent of Fracture	Breakaway Fracture Energy (ft-lb)	Curve Segment
≤ 26	None	0	1
	Partial	½ (20,000 – (1.4 x 10^{-5}) $C^{4.38}$)	3
	Complete	20,000	4
>26	None	0	5
	Partial	½ ((1.4 x 10^{-5}) $C^{4.38}$ - 20,000)	3
	Complete	(1.4 x 10^{-5}) $C^{4.38}$	2

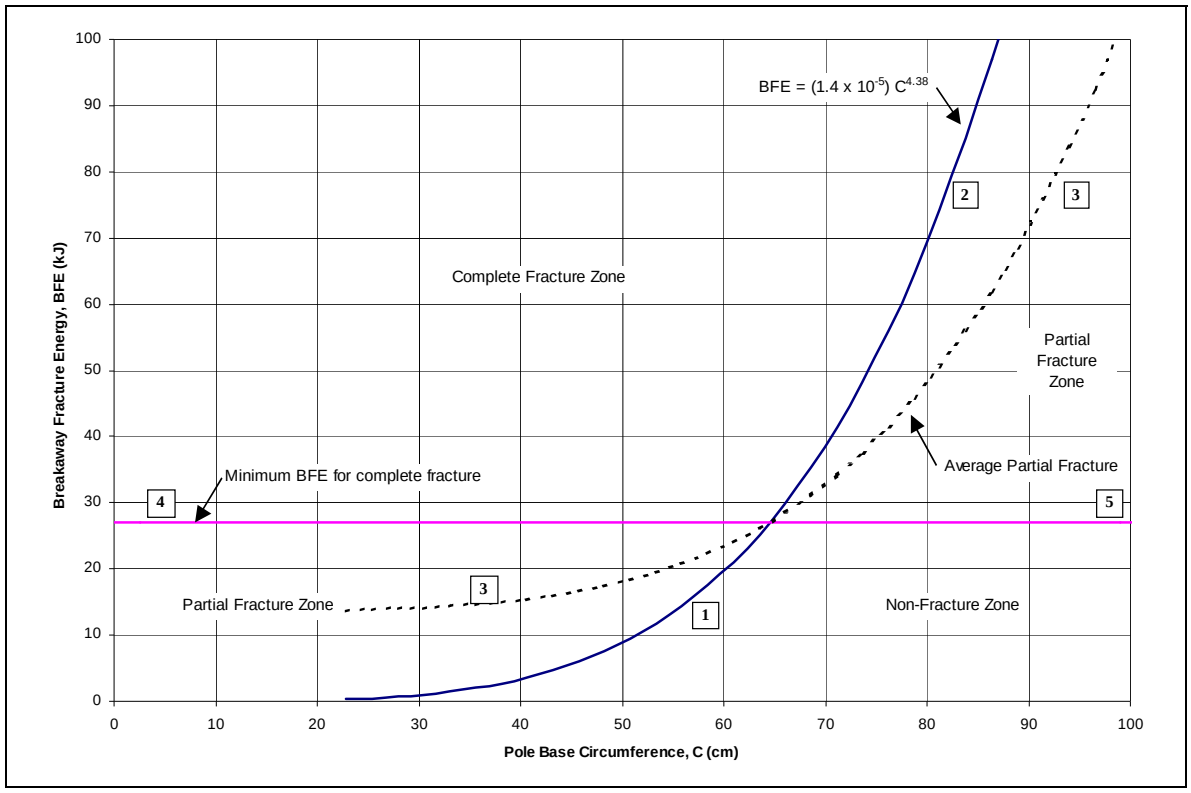

Figure 2. Relationship between Pole Diameter and Fracture Energy.

The study determined that the minimum elements required for a complete reconstruction of a pole impact are: (1) material and type of pole or base, (2) length of pole, (3) cross-sectional dimensions at base of pole, (4) type of base / anchoring mechanism, (5) type of breakaway

design, and (6) damage extent of the pole. It was found to be desirable to have the following information: (1) height of break / length of broken segment, (2) cross-sectional dimensions at the top and bottom of the broken segment, (3) final resting position of the pole, and (4) manufacturer of the breakaway device.

The analytical procedure for the five full-scale impacts varied between -5.5% and 45.9% of the actual energies. However, the procedure was never coded into subroutines for CRASH and its numerical intensity far exceeds its level of accuracy if performed manually. While the procedure was never coded into subroutines for CRASH, this methodology provides a usable way to reconstruct pole impacts.

2.4.5 Reconstruction Procedure for Pole Accidents - Kent and Strother

This study performed a literature review, a series of one-eighth scale-model pole/pendulum impacts, and an analytical study using static analysis and dynamic finite element modeling of vehicle/pole impacts [16]. A methodology was developed correlating the scale-model testing of several species of wood to full-scale impacts. It was assumed that the pole or tree in question acts as a cantilevered beam when impacted with no significant base translation and/or rotation in addition to a fracture.

The implementation of this methodology requires the following additional data be known during the reconstruction:

The geometry of the struck pole/tree (diameter and height).

Species of wood making up the pole or tree in question (however, the accident reconstructionist can assume the pole or tree was constructed of a material that will absorb a minimum amount of energy).

The moisture content of the pole or tree in question (poles can generally be assumed to be of low moisture content (i.e. less than six percent), trees generally have moisture contents greater than 20 percent).

The nature of damage to the pole or tree, including the completeness and height of the fracture.

A graphical summary of the methodology for reconstructing pole impacts is shown in Figure 3. Wood species and moisture content may be necessary to accurately reconstruct wood pole impacts. However, the acquisition of this data would require expertise generally beyond that of the average technician unless properly educated.

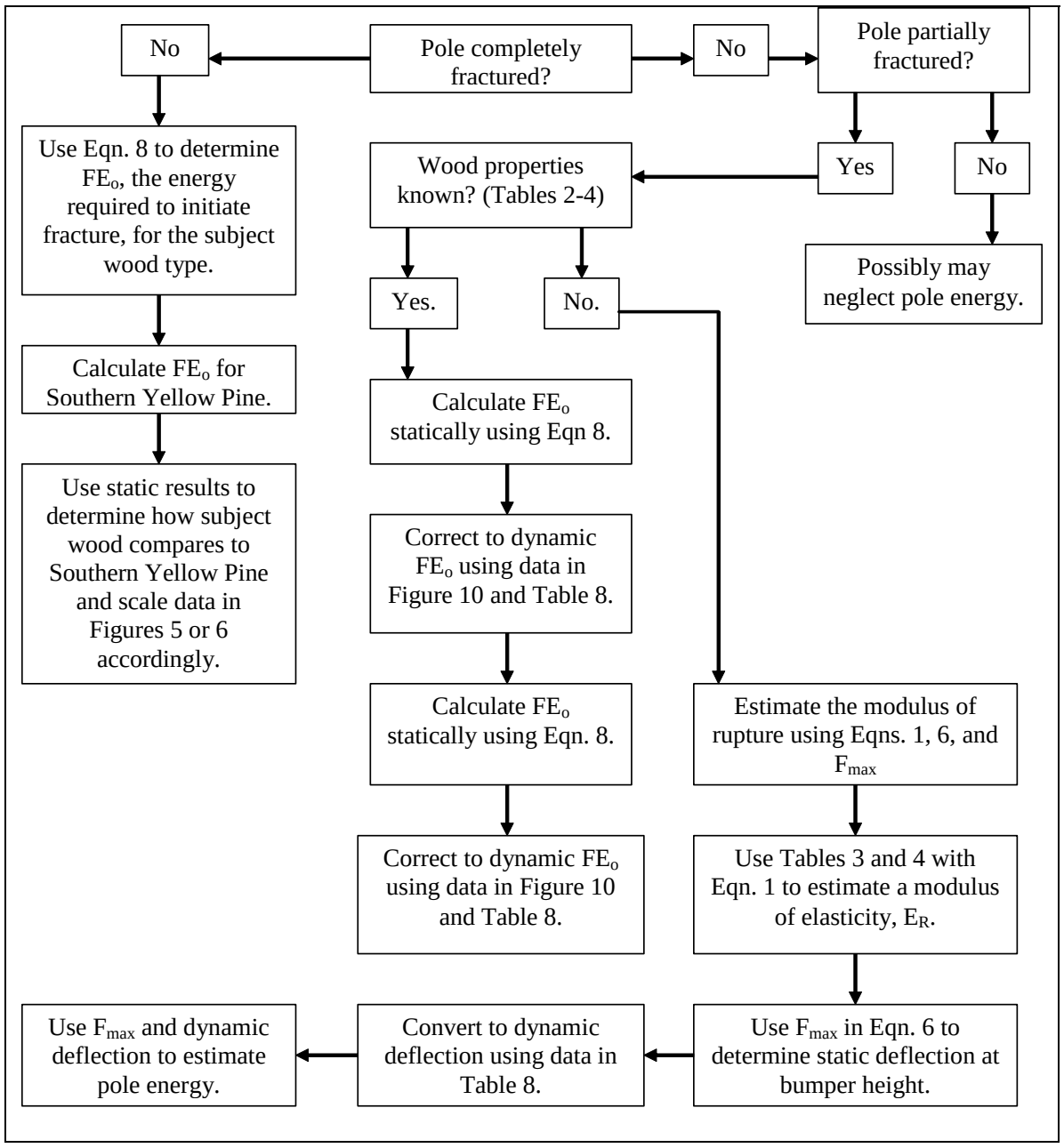

Figure 3. Kent and Strother Method of Reconstructing Pole Impacts.
(Equations listed are found in Reference **Error! Bookmark not defined.**)

3 RECONSTRUCTION PROCEDURE

Considerable numbers of crashes must be reconstructed in order to obtain a statistically significant sample for the prediction of impact angle and speed. Additionally, changes in the vehicle fleet, such as increases in the percentages of Sport Utility Vehicles (SUVs) or the introduction of significant numbers of light-weight hybrid vehicles, require that the vehicle types, impact conditions, and site characteristics involving roadside hazards be reviewed on a periodic basis. Therefore, it is anticipated that ongoing research will be needed in order to address future data needs.

Due to the inevitability of future additions to the database, reconstruction procedures must be developed on a categorical basis as much as possible. This allows for continuity and uniformity between reconstructions; a case-by-case reconstruction introduces undesirable variability in the reconstructed speeds and angles and should be avoided. Because of these concerns, a deliberative approach must be taken when developing new crash reconstruction procedures.

3.1 Literature Review

The development of new reconstruction procedures must first focus on a comprehensive literature review. Reconstruction procedures have been developed for many roadside objects, including trees, breakaway poles, luminaries, *et cetera*. Additionally, the Society of Automotive Engineers (SAE) publishes an annual database of articles on crash reconstruction [**Error! Bookmark not defined.**].

3.2 Crash Test Results

The availability of full-scale crash test results is invaluable in the development of reconstruction procedures. Several governmental agencies and private entities are involved in the testing of vehicles and objects that may be impacted by vehicles, including the Midwest Roadside Safety Facility, Texas Transportation Institute, and the Insurance Institute for Highway Safety.

In 1978, the New Car Assessment Program (NCAP) in the United States was initiated with the primary purpose of providing consumers with a measure of the relative safety potential of vehicles in frontal crashes [17]. NCAP now has comprehensive crash test information on many vehicles, including frontal- and side- crash test results. This data is available at the following web site:

http://www.nhtsa.dot.gov/NCAP/

Roadside appurtenances in the United States and Europe require crash testing under NCHRP Report 350 and its European counterpart, EN 1317. Roadside appurtenances include crash cushions, end terminals, and trailer-mounted attenuators. The Federal Highway Administration (FHWA) requires full-scale crash testing before devices are approved for use on the NHS. A comprehensive list of devices approved for use on the NHS, along with limited crash analysis, is available at the following web site:

http://www.fhwa.dot.gov/safety/fourthlevel/hardware/listing.cfm?code=cushions

Crash test results of simulated moose impacted by a vehicle have even been performed at the Swedish Road and Transport Research Institute [18]. Determination of what information is available should be performed before a reconstruction procedure is developed.

4 AVAILABLE INFORMATION

The primary limitation on the accuracy of a crash reconstruction is the availability of information; the development of a reconstruction procedure relies on the anticipated information available to reconstruct the crash. Due to the retrospective nature of NCHRP Project 17-22, available information is reliant upon the NASS CDS data developed within NHTSA. The NASS CDS program is a continuous data collection effort that collects in-depth data on an annual sample of approximately 5,000 crashes.

Due to privacy restrictions and NHTSA policy, crash site location information is not available to anyone outside of the NASS program; police accident reports, which do contain the location information, are only kept for one year beyond the data collection year. Therefore, the collection of additional information pertaining to the crash itself, the vehicle, the occupant(s), injury severity, *et cetera*, is limited to the information provided in the CDS cases. However, supplemental data collection can be performed through analysis of the information available through the CDS program.

4.1 Crash Site Information

Information available about the specific crash site is limited in the CDS system. General categories exist, such as “first object contacted” which may only be identified as a “fence / wall / building.” A manual review of available evidence, such as field forms, scale diagrams, and photographs, is required to determine the actual object impacted.

The critical information, including the roadside object struck and the corresponding damage information is critical to the reconstruction of a ran-off-road crash. This information is required

to determine the energy absorbed by the impacted object during the crash. It is anticipated that identification of these devices can be determined through photographic analysis of the scene.

4.1.1 Scale Diagrams

The scale diagram is the only source of information indicating vehicle dynamics and trajectory. Vehicle encroachment angle, orientation, traveled path, lateral extent of encroachment, and vehicle orientation must be determined from scale diagram information. Frequently, these diagrams are of a poor quality and are of an undeterminable scale due to computer imaging of the written documents. An example of a typical scale diagram is shown in Figure 4.

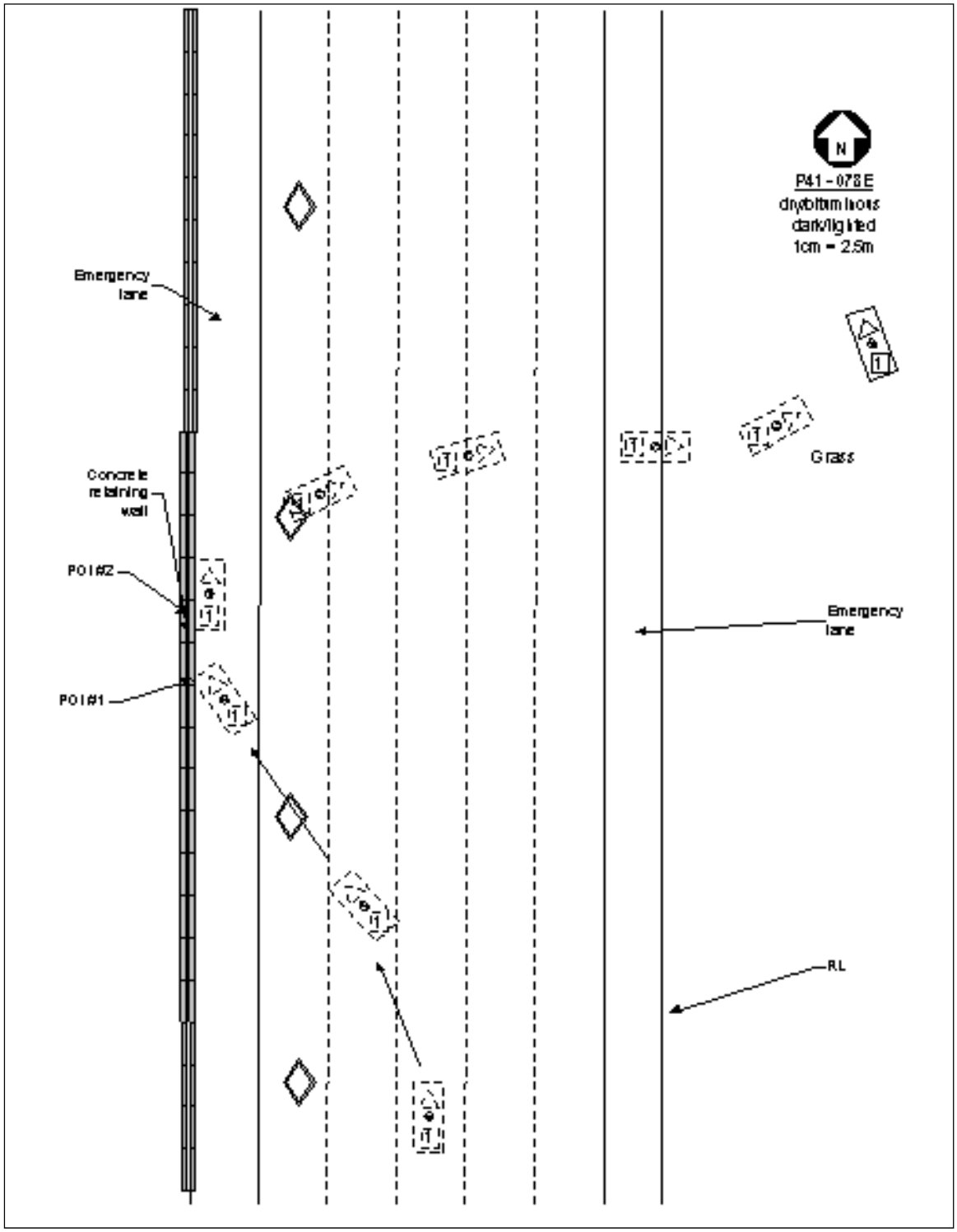

Figure 4. NASS Case 2000-041-078.

4.1.2 Photographic Evidence

Photographic evidence is extremely beneficial in the determination of unique factors affecting individual crashes. Special factors include the existence of snowdrifts along the side of the road, the visual condition of the roadside and shoulder, as well as other environmental and geometric considerations that may not be specifically available in the crash record itself.

The conditions of the roadside area where the vehicle ran off the road are not generally documented and must be gleaned from photographic data. These conditions, in addition to embankments or sideslopes, are difficult to determine through only photographic analysis and may require a modest amount of supplemental data collection.

Additionally, curbs, shoulder types, and other smaller roadway geometrics are not generally available from scale drawings. These must be observed through photographic evidence.

Finally, photographic evidence provides a valuable check of database integrity. Verification of vehicle crush profile, vehicle type, and other information explicitly listed in the CDS database should correspond to available photographic evidence. This provides additional assurance of the quality of the database.

4.1.3 Post-Impact Trajectory

Post-impact vehicle trajectory, which is frequently essential to the reconstruction of an impact with a roadside object, can be determined through rolling friction, damage caused by subsequent impacts, and other traditional methods. Post-impact trajectory is essential, since the kinetic

energy of the vehicle after an impact with a roadside obstacle must be quantified in the energy balance equations.

4.1.4 Object Interaction

Device interaction must be ascertained from scale diagrams and photographic evidence. While not critical for fixed-object impacts that do not yield, such as large trees or poles, objects that attenuate energy on impact, either by design or by intrinsic nature, are critical to a reconstruction. Device interaction and device identification are both of paramount importance and are discussed further in Section 5.

4.1.5 Vehicle Data Sources

Vehicle data is essential in the accurate reconstruction of an impact. At a minimum, the general vehicle category and mass must be identified. This allows for the rough reconstruction of a crash using categorical crush parameters. However, more accurate reconstruction results can be obtained through more accurate vehicle data. Examples of vehicle data include:

Widths & Lengths
Height & Ground Clearance
Curb Weight
Tire & Wheel Size
Optional Equipment Weights
Center of Gravity Calculations
Headlamp Data
Recall Information
Acceleration Speeds/Distance
Braking Distance
VIN Number Analysis
Interior Dimensions
Manufacturing Materials Used

One source for vehicle data is the NADA; a more comprehensive data source is available through the AAMA [19,20].

4.2 Roadside Characteristics

The determination of the condition of surfaces traversed by the vehicle during the excursion is critical in predicting frictional coefficients. Although lower coefficients of friction are typically associated with wet surfaces, one exception is gravel. It is not uncommon to have higher frictional coefficients with wet, loose gravel than with dry, hard-packed gravel.

The data available on roadside conditions varies from extremely precise to exceedingly vague. An example of this is found in NASS Case #1997-002-157. In this case, the displaced rock, small rock walls, and roadside data are clearly and painstakingly annotated.

However, many other cases do not have this level of detail. Without this data accurately recorded or able to be gleaned from photographic evidence, the difficulty of the reconstruction effort is greatly increased.

4.3 Environmental Conditions

Environmental conditions greatly affect the frictional coefficient between the tires and the roadway surface. The single most important factor affecting tire friction force in practice is the presence of water (in its various forms). Generally, lower coefficients of friction are associated with wet and/or icy surfaces. Accurate recording of the road condition is essential. An example where verification of the record was possible through photographic evidence is Case #2000-002-019. In this record, the roadway was listed as “level/dry/clear,” but police photography shows

significant amounts of snow next to the roadside and what appears to be a wet asphalt surface. NASS photography obviously was not taken at the stated environmental conditions.

Device Identification

With literally hundreds of roadside devices, with some designs of devices barely distinguishable from others, device identification is a difficult task for the reconstructionist. While two devices' appearance may be similar, the nature of their behavior during an impact can be markedly different. Correct identification of a roadside device is critical to accurate reconstructions.

The Roadside Design Guide describes roadside safety devices currently approved for use on the NHS. However, the depth required for exact identification generally exceeds the depth of the Guide. This requires additional research, including documentation from manufacturers and extensive literature reviews. General information about specific roadside safety appurtenances is useful in performing an initial investigation, with examples to follow.

4.4 Longitudinal Barriers

Flexible longitudinal barriers are a special type of safety fence designed to protect errant vehicles from roadside hazards. Longitudinal barriers are identified by several qualities dealing with the physical construction and components. Factors that must be examined include: post type, post embedment, post spacing, beam type, and soil conditions. Each of these factors can significantly affect the behavior of the system.

Other factors to consider when identifying longitudinal barriers include how the barrier is terminated, the number, position, and type of blockouts, and any other hardware used to fasten the rail to the posts. The detail to which a barrier needs to be identified is dependent upon the

required precision of the reconstruction; this precision may require verification of the original device specifications.

4.5 Guardrail End Terminals

While longitudinal barriers protect errant vehicles from roadside hazards, the introduction of these barriers onto the highway requires that the ends of the barriers be protected in an effective manner. This protection is achieved most commonly with guardrail end terminals. Approximately nineteen guardrail end terminals are currently approved under NCHRP Report 350 for usage on the NHS. The similarity in appearance among end treatments can cause confusion in determining the appropriate methods and values to be used to reconstruct a crash. Guardrail end terminals can generally be categorized by their energy-absorbing qualities. Energy-absorbing end terminals rely on an impact head to kink, cut, or extrude the guardrail; in the case of box-beam guardrail, the terminal either bursts the beam or crushes pultruded fiberglass/epoxy tubes within the beam. There are six unique designs of energy absorbing end terminals: the Box Beam Bursting Energy Absorbing Terminal (BEAT) family, the Beam Eating Steel Terminal (BEST), the ET-2000 family, the FLared End Terminal (FLEAT) family, the Sequential Kinking Terminal (SKT), and the Wyoming Box Beam End Terminal (WY-BET). These terminals have distinctly different force-deflection behaviors, as well as significantly different masses, which must be differentiated before performing a reconstruction. Each of the energy-absorbing terminals is identified by its distinguishing characteristics. The appearance of the deformed guardrail section, which is unique to each end terminal, is also examined.

Non-energy-absorbing terminals still attenuate some energy; these devices, particularly the Slotted Rail Terminal (SRT) are difficult to identify since the after-impact appearance, even to the trained investigator, of different versions of the SRT are almost identical.

4.6 Crash Cushions

Crash cushions, such as inertial barriers (sand barrels) are designed to protect an errant vehicle from impacting a fixed object by gradually decelerating the vehicle to a safe stop or by redirecting the vehicle way from the obstacle. There are over two-dozen general designs of crash cushions currently in use on the NHS. Of these designs, some families have over a dozen different approved configurations. In particular, designs such as the HiDro Sandwich and the HexFoam Sandwich, which share a common crash cushion design with completely different energy-absorbing cartridges, make identification of crash cushions exceedingly difficult. Crash cushion identification requires the identification of the design of the crash cushion and the verification of the energy-absorbing cartridge, if any.

4.7 Concrete Barriers

Concrete barriers, such as Portable Concrete Barriers (PCBs) and Rigid Concrete Barriers (RCBs), are concrete barriers designed to have several functions: (1) to protect traffic from entering work areas, such as excavations or material storage sites; (2) to provide positive protection for workers; (3) to separate two-way traffic; (4) to protect construction such as falsework for bridges and other exposed objects; and (5) to separate pedestrians from vehicular traffic [**Error! Bookmark not defined.**]. Concrete barriers have many different designs and sizes. These include F-Shape barriers, New Jersey safety shape barriers, GM-Shape barriers, and

single-slope barriers. The orientation of the slopes and the heights of these barriers vary greatly. These cannot be identified without visual identification.

An additional consideration with portable concrete barriers is the connection between barriers. There are several types of connections that must be identified due to their significant effect on barrier performance. An example of one connection is the pin and loop connection. This type of connection is very common because it accommodates changes in curvature and grade. However, pin and loop connections cannot generate a lateral resisting moment until the barriers have significantly contacted each other and undergone a significant amount of rotation.

4.8 Poles and Luminaries

Pole and luminaire reconstruction vary greatly from crash to crash on how much data is required to reconstruct the impact. As mentioned previously, the minimum elements required for a complete reconstruction of a pole or luminary impact are: (1) material and type of pole or base, (2) length of pole, (3) cross-sectional dimensions at base of pole, (4) type of base / anchoring mechanism, (5) type of breakaway design, and (6) damage extent of the pole. It is desirable to have the following information: (1) height of break / length of broken segment, (2) cross-sectional dimensions at the top and bottom of the broken segment, (3) final resting position of the pole, and (4) manufacturer of the breakaway device.

4.9 Others

Other devices, such as Trailer-Mounted Attenuators (TMAs), vehicle arresting systems, and other similar devices, are also commonly seen on the NHS. These devices can vary greatly and must be identified individually.

5 DEVELOPMENT OF RECONSTRUCTION PROCEDURES

The development of reconstruction procedures is a combination of the application of general engineering principles, physical testing, computer simulation, and common sense. Specific analytical procedures are not applicable to a generalized reconstruction procedure: however, the following topics are almost always involved in the development of a crash reconstruction procedure.

5.1 General Engineering Principles

Reconstruction procedures primarily involve calculating energy losses and gains after leaving the roadway. Energy changes during ran-off-road crashes can generally be divided into five categories:

Roadside hardware and terrain damage

Vehicle crush and fixed object damage

Vehicle-ground interaction, including braking and side-slip

Vehicle rollover

Vehicle elevation changes

Energy changes during a crash can be solved using either conservation of energy or conservation of momentum. While both energy and momentum are always conserved, kinetic energy is almost always not conserved in real-world impacts. If conservation of energy is applied, energy losses due to vehicle crush, friction, the generation of elastic waves, *et cetera*, must be determined. If the impact is considered perfectly plastic, conservation of momentum can be applied and energy losses do not need to be explicitly calculated.

However, dealing with momentum is more difficult than dealing with mass and energy because momentum is a vector quantity, having both a magnitude and a direction. Momentum is conserved in the principle directions while energy is conserved as a scalar value.

For the reconstruction of longitudinal barrier impacts, conservation of energy is used. For the reconstruction of inertial barriers (sand barrels), conservation of momentum is used. In the case of energy-absorbing end terminals, both conservation of energy and conservation of momentum are used. These procedures are provided in detail in Section 7.

5.2 Full-Scale Crash Testing

As discussed in Section 3.2, crash test information is an invaluable tool when developing a reconstruction procedure. Since full-scale crash testing is designed to mimic real-world crash conditions, full-scale crash testing should, in theory, be representative of the real-world impacts. Full-scale crash tests are generally fully instrumented events. This includes data such as accelerometer traces, high-speed video, rate gyros, and frequently instrumented hardware. Unfortunately, for various reasons, many manufacturers are unable to share specific crash test data or component test information. This limitation requires a significant increase in the amount of resources required to determine the physical behavior of a roadside safety device.

5.3 Component Testing

Component testing is frequently required to understand the effects of individual components on a system. An example of component testing is the dynamic evaluation of guardrail posts embedded in soil [21]. Changes in soil stiffness can drastically affect the overall performance of a system and require detailed analysis.

5.4 Software

Computer simulation software is frequently used in crash reconstruction. Literally hundreds of commercially available, public domain, and proprietary software codes have been developed since the advent of the computer. While a detailed discussion of the many programs is beyond the scope of this research, it is of paramount importance that software be chosen that matches the detail and purposes of the reconstruction and that the application of the software does not violate any restrictive assumptions upon which the software is based. Several software programs and brief descriptions are listed below. These software codes are not an exhaustive list but merely codes with which the author is familiar.

5.4.1 LS-DYNA

LS-DYNA, an explicit, nonlinear finite element program, developed by the Livermore Software Technology Corporation (LSTC), is the standard finite element software used for roadside safety simulation [22,23]. LS-DYNA is a general-purpose program used to analyze the nonlinear dynamic response of two- and three-dimensional inelastic structures.

LS-DYNA is capable of simulating complex real-world problems, and can economically test prototype response to real-world events. Simulation accuracy has been proven through experimental data correlation.

5.4.2 CRASH3

CRASH3 (Calspan Reconstruction of Accident Speeds on the Highway) is a simplified mathematical software analysis of automobile accident events [24]. CRASH3 is able to

determine the change in velocity, Delta-V, and the Equivalent Barrier Speed (EBS) by combining data on the damage crush profile with the Collision Deformation Classification (CDC) and the mass of the vehicle. Delta-V and EBS are then calculated by a direct application of the principles of linear momentum.

5.4.3 BARRIER VII

BARRIER VII, a computer simulation code used extensively in the roadside safety community to model longitudinal barriers, has been shown to be accurate in simulating longitudinal barrier impacts [25, 26, 27, 28, 29, 30]. BARRIER VII uses an idealized two-dimensional structural framework that allows the simulation of beams, cables, springs, columns, viscous damping links, friction damping links, and posts impacted by a vehicle idealized as a rigid body of arbitrary shape surrounded by a cushion of discrete inelastic springs.

BARRIER VII uses a highly sophisticated barrier model and a somewhat simplified vehicle model. BARRIER VII allows for the configuration of vehicle specifications, barrier design, and impact parameters.

BARRIER VII uses idealized vehicles of an arbitrary shape that interact with the barrier through defined points. The part of the vehicle boundary that may interact with the barrier is defined by specifying a number of points at which point contact with the barrier may be made. A discrete, nonlinear spring is then associated with each point.

BARRIER VII uses an idealized, two-dimensional structural framework of an arbitrary shape to represent the barrier. Discrete structural members possessing geometric and material

nonlinearities are used, including beams, cables, columns, springs, dampers, posts, and composite members.

5.4.4 Other Software Codes

Computer simulation programs, including GUARD, CRUNCH, and NARD, have been specifically designed for the simulation of roadside barrier accidents. However, many of these guardrail simulation programs have not gained the confidence of analysts due to a variety of problems including coding errors, poor analytical formulations, and restrictive assumptions [31]. The limitations and assumptions of any computer program must be understood prior to its implementation. The suitability of other codes to particular reconstruction applications may be valid as long as the assumptions upon which the software is based are not violated.

6 EXAMPLE OF PROCEDURES

For this research, three reconstruction procedures were developed. These procedures are designed to reconstruct general categories of crashes: impacts with the length of need of longitudinal barriers (Appendix A), impacts with energy-absorbing end terminals (Appendix B), and impacts with inertial barriers, also known as sand barrels (Appendix C). Summaries of the individual procedures are provided below.

6.1 Longitudinal Barriers

The first procedure, "Crash Reconstruction Technique for Longitudinal Barriers," details an iterative procedure for reconstructing crashes involving longitudinal barriers using the computer program BARRIER VII. Strong-post, W-beam guardrail is the most common system found along highways in the United States, with an installed base of over 250 million feet and accounting for 43% of the impacts with guardrail [**Error! Bookmark not defined.**, 32, 33]. In both the G4 (2W) and modified G4 (1S) strong-post guardrail systems, the W-beam rail is fastened to the post with a bolt that passes through a wood blockout and is fastened to the guardrail post with a hex nut [34]. These blockouts are used to position the rail away from the posts, thus reducing the probability of wheel snag. A typical installed G4(1S) system is shown in Figure 5.

Figure 5. G4(1S) Strong Post Guardrail System.

During a flexible barrier impact, initial vehicle kinetic energy is dissipated through several means: vehicle crush, barrier rail deformation (including axial, bending, and flattening deformations), rotation of the post in the soil, plastic deformation or fracture of the posts, rolling friction between the vehicle and the ground, and barrier-vehicle friction. Summing these energy losses and adding them to the vehicle kinetic energy at the point when it departed the guardrail provides a reasonable estimate of the initial kinetic energy (and therefore velocity) of the vehicle. The software package BARRIER VII was used to develop relationships between these energy losses and to design a simplified crash reconstruction technique [35, 36].

Correlations were found between a vehicle's departure angle, velocity, type of vehicle, and the energy dissipated by friction, vehicle crush, barrier deformation, post deformation, and rolling friction. Two significant observations were found in regards to the behavior of strong-post guardrail systems: (1) significant portions of the initial vehicle energy were found to be dissipated through friction, which is linearly related to the angle of impact and (2) the energy to

cause permanent post deflections was determined to be roughly equivalent to the amount of energy dissipated by the rail elements of that system.

Crash reconstructions were performed for the three strong-post guardrail system impacts available in literature. Comparisons of the BARRIER VII program output with full-scale crash results proved to be accurate within 3%.

6.2 Guardrail End Terminals

The second procedure, "Reconstruction Techniques for Guardrail End Terminals," provides a comprehensive literature review of guardrail end terminals and details procedures for reconstructing impacts with guardrail end terminals using the principles of conservation of momentum and conservation of energy. Guardrail end terminals protect the end of flexible longitudinal barriers, which are introduced onto the roadside to protect errant vehicles from roadside hazards. Left untreated, the ends of the barrier can penetrate into the occupant compartment. A typical guardrail end terminal is shown in Figure 6.

a) Installed SKT-350 System

b) After-Crash SKT-350 System

Figure 6. SKT-350, Sequential Kinking Terminal.

For energy-absorbing guardrail end terminals, reconstruction is performed using conservation of momentum during the initial portion of the impact where the guardrail end terminal is accelerated by the impacting vehicle. Soon after the impacting vehicle and end terminal have reached the same velocity, the end terminal begins attenuating energy through a kinking, bursting, crushing, or extruding process depending on the terminal type. The average force required to attenuate the energy was determined through literature, accelerometer traces, and traditional engineering dynamics equations. This average force can be used to determine estimated energy dissipations for any given deflection, since the attenuated energy is the area underneath the force-deflection curve.

For non-energy-absorbing terminals, conservation of momentum equations and the rotational and fracture energies of the posts are used to estimate impact velocity. These terminals do not absorb significant amounts of energy during impact and are designed to protect the passenger compartment from guardrail penetration and to eliminate extreme decelerations.

Accelerometer data, vehicle kinematics, and conservation of energy and momentum equations were used to estimate average force levels required by each guardrail end terminal type to attenuate energy. Weights, energy-absorbing mechanisms, and force-deflection characteristics of energy-absorbing end terminals were documented for use in reconstructing terminal crashes. These characteristics are shown in Table 3.

Table 3. Terminal Head Summary.

	Faceplate Size mm (in.)	Head Mass kg (lb)	Head Length m (in.)	Average Force kN (kips)
BEAT	508x508 (20x20)	59 (130)	1.21 (83.3)	87 (20) to 122.5 (32.1)
BEAT-MT				
BEAT-SSCC*				87 (20) to 122.5 (32.1) (Stage 1) 129 (29) (Stage 2)
BEST-350	502x610 (20x24)	125 (275)	1.63 (64.25)	83.4 (18.7) to 100 (22.5)
ET-2000	508x521 (20x20.5)	122 (268)	1.28 (50.25)	53.2 (12) to 94.7 (21.3)
ET-2000 PLUS	381x711 (15x28)	79 (175)	1.44 (56.75)	
FLEAT-350	357x497 (14x19.6)	54.5 (120)	1.56 (61.3)	60.2 (13.5) to 74.5 (16.7)
FLEAT-350 MT	357x497 (14x19.6)	54.5 (120)	1.56 (61.3)	First Head: Identical to FLEAT-350 Both Heads: 120.4 (17) to 149 (33.4)
REGENT	457x457 (18x18)	21 (46)	N/A	N/A
SKT-350	508x508 (20x20)	78 (172)	2.11 (83.3)	46.7 (10.5) to 67.6 (15.2)
WY-BET*	508x508 (20x20)	57 (125)	0.96 (37.875)	Stage 1: 80.1 (18) to 95.27 (21.4) Stage 2: 155 (35)
WY-BET (MB)*				

* The BEAT-SSCC and the WY-BET both have two stages

Comparisons of the program output with full-scale crash results of energy-attenuating terminals proved to be accurate within ±10 km/h (±6 mph) for most terminals. For the SRT, a reconstruction methodology using conservation of energy and correlation of the energy dissipated by the rail to the energy dissipated by the fracture of the BCT and CRT posts correlated well with recent versions of the SRT.

6.3 Crash Cushions

The third procedure, “Literature Review and Reconstruction Techniques for Crash Cushions,” assists the reconstructionist in the identification of the various types of crash cushions and details procedures for reconstructing crashes involving inertial barriers (sand-filled barrels). Crash cushions are protective devices that shield fixed objects from errant vehicle impacts by gradually decelerating a vehicle to a safe stop for head-on impacts or, in most instances, redirecting a vehicle away from the object for side impacts. A typical crash cushion is shown in Figure 7.

Figure 7. A TRACC Crash Cushion.

In order to reconstruct an impact with a crash cushion, the reconstructionist must first be able to identify the specific type of device impacted. The third procedure documents crash cushions

certified for use on the NHS under NCHRP Reports 230 and 350 by their distinguishing characteristics, including physical appearance, number of bays, method of energy dissipation, *et cetera*.

Initially, it was envisioned that techniques for reconstructing impacts for several crash cushions would be developed. Unfortunately, for various reasons, many manufacturers of crash cushions are unable to share specific crash test data or component test information. Therefore, reconstruction techniques were developed only for two common crash cushions, inertial barriers (sand barrels) and the Box-Beam-Bursting, Energy-Attenuating Terminal Single-Sided Crash Cushion (BEAT-SSCC). The BEAT-SSCC is detailed in the second procedure due to its shared impact head and relationship to the BEAT family of end terminals, median barriers, and bridge pier protection systems.

For inertial barriers (sand-filled barrels), a crash reconstruction procedure using the principles of conservation of momentum was derived. Methods for estimating impact velocity from post-impact damage and vehicle exit velocity produced velocities that correlated extremely well with full-scale crash data. This methodology was shown to be very precise, but accuracy was shown to be dependant on the velocity of a vehicle as it departs a sand barrel array.

7 CONCLUSIONS

Procedures for identifying and reconstructing impacts with several types of roadside devices are presented in this dissertation. These procedures rely on engineering principles such as conservation of energy and conservation of momentum to determine the impact speed and angle of an errant vehicle impacting a roadside safety feature.

These methodologies will be used in NCHRP Project 17-22, entitled “Identification of Vehicular Impact Conditions Associated with Serious Ran-Off-Road Crashes” in order to determine the angles and speeds during an off-road excursion. The identification of the real-world conditions where ran-off-road crashes occur will allow better test procedures for determining the suitability of an appurtenance for use on the NHS. This information can then be used to determine the benefit-to-cost ratio of installing a safety appurtenance to shield that hazard for a more efficient use of roadside safety funding. Ultimately, this will lead to a safer roadside environment, which will save lives and reduce injuries during ran-off-road crashes.

8 FUTURE WORK

An extensive examination of the REACT crash cushion was performed in order to determine a suitable reconstruction procedure. It was determined that, at a minimum, detailed finite element modeling would be required to analyze the system and create an acceptably accurate reconstruction procedure. Additionally, dynamic physical testing of the REACT system and its components would be required to determine strain rate and temperature dependent behavior. Because of these requirements, an acceptable reconstruction procedure for the REACT was not achieved during this research, and thus, not reported herein. Due to the commonality of self-restoring systems, this is considered essential future work.

Side impacts into end terminals, crash cushions, and poles need to be examined to determine the frequency of side-impact crashes and performance of the safety devices during these crashes. While head-on impacts are the only method currently used to certify roadside safety hardware, should significant instances of severe injuries or deaths be associated with side impacts of roadside hardware, these test procedures should be reevaluated.

Non-tracking impacts into longitudinal barriers and impacts where the vehicle penetrates the barrier are not sufficiently well examined. Future work should consider the reconstruction of impacts where significant yawing of the vehicle has occurred, as this has been seen in real-life crashes [37].

9 REFERENCES

AASHTO, “Roadside Design Guide 2002,” American Association of State Highway and Transportation Officials, Washington, DC, 2002.

National Highway Traffic Safety Administration (NHTSA), Fatality Analysis Reporting System (FARS), United States Department of Transportation, 1975 - Present.

Fricke, LB, “Traffic Accident Reconstruction, Volume 2 of the Traffic Accident Investigation Manual,” Northwestern University Traffic Institute, 1990.

Hutchinson, JW and TW Kennedy, “Medians of Divided Highways – Frequency and Nature of Vehicle Encroachments,” Engineering Experiment Station Bulletin 487, University of Illinois, 1966.

Cooper, PJ, “ Analysis of Roadside Encroachment Data Analysis from Five Provinces and its Application to an Off-Road Vehicle Trajectory Mode l,” British Columbia Research Council, Vancouver, Canada, 1981.

Sicking, DL, “Reexamination of the Roadside Encroachment Data,” Discussion, Transportation Research Record, Transportation Research Board, Paper No. 99-1138, 1999.

Mak, KK, “Roadside Safety Analysis Program – User’s Manual,” National Cooperative Highway Research Program, Transportation Research Board, National Research Council, Washington, DC, 1997.

Society of Automotive Engineers (SAE), “Accident Reconstruction Technology Collection,” Warrendale, PA, 2001.

Mak, KK, DL Sicking and JR Lock, “Rollover Caused by Concrete Safety Shaped Barriers,” Federal Highway Administration (FHWA), Report Number FHWA-RD-88-220, January 1989.

McHenry, RR and JP Lynch, "User’s Manual for the CRASH Computer Program," Calspan Report No. ZQ-5708-V-3, Contract No. DOT-HS-5-01124, January 1976.

Erinle, O., W Hunter, M Bronstad, F Council, R Stewart, and K Hancock, “Analysis of Guardrail and Median Barrier Accidents Using the Longitudinal Barrier Special Studies (LBSS) File,” Vols. 1 & 2, Federal Highway Administration, Report No, FHWA/RD-92/098, February 1994.

Campbell, KL, “Energy Basis for Collision Severity,” SAE Paper No. 740565, Proceedings of the 3rd International Conference on Occupant Protection, Troy, MI, July 1974.

Calcote, LR, “Development of a Cost-Effectiveness Model for Guardrail Selection,” Final Report, Federal Highway Administration, Report No. FHWA-RD-78-74, January 1980.

Mak, KK and RP Bligh, “Recovery-Area Distance Relationships for Highway Roadsides, Phase I Report,” NCHRP Project 17-11, January 1996.

Labra, JJ, and KK Mak, “Development of Reconstruction Procedure for Pole Accidents,” Final Report, Contract No. DTNH22-80-C-07014, National Highway Traffic Safety Administration, Washington, DC, November 1980.

Kent, RW, and CE Strother, “Wooden Pole Fracture Energy in Vehicle Impacts,” Advances in Safety

Technology, Society of Automotive Engineers, February 1998.

National Highway Transportation Safety Administration (NHTSA), Washington, DC.

Gens, M, "Konstruktion av älgattrapp avsedd för krockprovnings-ändamål," ("Construction of a Definitive Moose Model for Crash Test Purposes") In Swedish, Institutionen för fordonsteknik, Kungliga Tekniska Högskolan, Stockholm, Sweden, 2000.

National Automobile Dealer's Association (NADA), McLean, VA 22102.

American Automobile Manufacturer's Association (AAMA), Twinsburg, OH 44087.

Coon, BA, "Dynamic Testing and Simulation of Guardrail Posts Embedded in Soil," Master's Thesis, University Of Nebraska - Lincoln, December 1999.

Reid, JD, "Recent Progress in Roadside Safety Simulation," Fourth Annual LS-DYNA User's Conference, Minneapolis, MN, September 1996.

LSTC, "LS-DYNA User's Manual," Version 950, Livermore Software Technology Corporation, Livermore, CA, May 1999.

CRASH3 User's Guide and Technical Manual, NHTSA, US Dept of Transportation.

Post, ER, CY Tuan and SA Ataullah, "Comparative Study of Kansas and FHWA Guardrail Transition Designs Using BARRIER VII Computer Simulation Model," Transportation Research Report TRP-03-012-88, Midwest Roadside Safety Facility, University of Nebraska – Lincoln, December 1988.

Ataullah, S, "An Analytical Evaluation of Future Nebraska Bridgerail-Guardrail Transition Designs Using Computer Simulation Model BARRIER VII," M.S. Thesis, Civil Engineering Department, University of Nebraska – Lincoln, August 1988.

Tuan, CY, ER Post, S Ataullah, and JO Brewer, "Development of Kansas Guardrail to Bridgerail Transition Using BARRIER VII," Transportation Research Record No. 1233, Transportation Research Board, National Academy Press, Washington, DC, 1989.

Bligh, RP, and DL Sicking, "Applications of Barrier VII in the Design of Flexible Barriers," Transportation Research Record 1233, Transportation Research Board, National Research Council, Washington, DC 1989, pp. 117–123.

Mak, KK, RP Bligh, and DH Pope, "Wyoming Tube-Type Bridge Rail and Box-Beam Guardrail Transition," Transportation Research Record No. 1258, Transportation Research Board, National Academy Press, Washington, DC, 1990.

Wollyung, R, M Carpino, A Scanlon, and B Gilmore, "Performance of Timber Bridge Railings Under Vehicle Impact Using Barrier VII Simulation," Proceedings of 76th Annual Meeting of the Transportation Research Board, Paper No. 971384, January 1997.

Ray, MH, "The Use of Finite Element Analysis in Roadside Hardware Design," International Journal of Crashworthiness, Vol 2, No 4, Woodhead Publishing, London, UK, 1997.

Barth, KE, JF Davalos, RG McGinnis, and MH Ray, "Development of an Improved Roadside Barrier System," NCHRP Project 22-17, National Cooperative Highway Research Program, National

Academies of Science, Washington, DC, March 2001.

Reid, JD, “Steel Post Simulation for the Buffalo Guardrail System,” AMD Vol. 225, Crashworthiness, Occupant Protection and Biomechanics in Transportation Systems, American Society of Mechanical Engineers, 1997.

AASHTO-ARTBA-AGC, “A Guide to Standardized Highway Barrier Hardware,” American Association of State Highway and Transportation Officials, Washington, DC, 1995.

Powell, GH, “Computer Evaluation of Automobile Barrier Systems,” Federal Highway Administration No. FHWA-RD-73-73, August 1970.

Powell, GH, “BARRIER VII: A Computer Program for Evaluation of Automobile Barrier Systems,” Report No. FHWA-RD-73-51, Federal Highway Administration, Washington, DC, April 1973.

Rabanal, JD, CIDAUT, Center for Automobile Development, Spain, Personal Correspondence, 2003.

APPENDIX A.

Crash Reconstruction Technique for Longitudinal Barriers

I INTRODUCTION

Flexible longitudinal barriers are designed to protect errant vehicles from roadside hazards. However, since these barriers must be placed between the traveled roadway and the hazard, there is a greater risk of a crash with the guardrail than the initial hazard. Guardrail impacts are the third most common fixed-object impact, after only trees and embankments [1,2].

Since the placement of roadside safety appurtenances increases the risk of an impact at significant capital costs for installation and maintenance, the placement of these devices must be deliberative. Risk estimates must be performed to determine the probability, angle, and speed of a vehicle impacting any specific roadside hazard.

The validity of the risk estimates depends upon, among other factors, an accurate estimate of the impact conditions, including speed, angle, and vehicle orientation. This information can only be developed from the accurate reconstruction of real-world crashes. Crash reconstruction involves using engineering principles, such as conservation of energy and conservation of momentum, to determine how a crash occurred and to estimate the initial speed and position of the vehicle.

NCHRP (National Cooperative Highway Research Program) Project 17-22, entitled "Identification of Vehicular Impact Conditions Associated with Serious Ran-Off-Road Crashes," involves using crash reconstruction techniques to estimate vehicle speed and angle of run-off-road crashes. This procedure details the reconstruction technique used for longitudinal barrier crashes.

During a flexible barrier impact, initial vehicle kinetic energy is dissipated through several means: vehicle crush, barrier rail deformation (including axial, bending and flattening deformations), rotation of the post in the soil, plastic deformation or fracture of the posts, rolling friction between the vehicle and the ground, and barrier-vehicle friction. Summing these energy losses and adding them to the kinetic energy in the vehicle at the point when it departed the guardrail provides a reasonable estimate of the initial kinetic energy (and therefore velocity) of the vehicle. The usage of the software package BARRIER VII was used to develop relationships between these energy losses and to design a simplified crash reconstruction technique [3, 4].

10 2 DESCRIPTION OF STRONG-POST W-BEAM GUARDRAIL

It is well documented that the strong-post W-beam guardrail is the most common system found along highways in the United States, with an installed base of over 250 million feet [5, 6]. In both the G4 (2W) and modified G4 (1S) strong-post guardrail systems, the W-beam rail is fastened to the post with a bolt that passes through a wood blockout and is fastened to the guardrail post with a hex nut [7]. These blockouts are used to position the rail away from the posts, thus reducing the probability of wheel snag. A typical installed G4(1S) system is shown in Figure 1

Figure 8. G4(1S) Strong Post Guardrail System.

Extensive analyses have been performed on the National Highway Traffic Safety Administration's (NHTSA) National Accident Sampling System (NASS) database [8]. Part of the NASS database includes the Longitudinal Barrier Special Study file developed for the Federal Highway Administration (FHWA). It was found that 43% of impacts with guardrail

involved an impact with strong-post W-beam systems [9]. Because of its prevalence, it was chosen for the development of a reconstruction technique.

3 SELECTION OF SIMULATION SOFTWARE

The interaction of a vehicle with a roadside barrier is exceptionally difficult to simulate on a computer. BARRIER VII, a computer simulation code used extensively in the roadside safety community, has been calibrated to real-world full-scale crash tests of automobiles and has been shown to be accurate. BARRIER VII was developed to predict the behavior of a wide variety of roadside barrier systems [**Error! Bookmark not defined.**, **Error! Bookmark not defined.**]. BARRIER VII uses an idealized two-dimensional structural framework that allows the simulation of beams, cables, springs, ideal columns, viscous damping links, friction damping links, and posts impacted by a vehicle idealized as a rigid body of arbitrary shape surrounded by a cushion of discrete inelastic springs.

In 1980, Calcote examined the cost-effectiveness of guardrail using BARRIER VII [10]. In 1988 and 1989, Post *et al* examined guardrail transitions using BARRIER VII [11, 12, 13]. In 1989 and 1990, Bligh used BARRIER VII to evaluate flexible barriers and a box-beam to bridge rail transition [14,15].

In 1994, Ross used BARRIER VII to examine the deflections, accelerations, and other factors to evaluate the performance of roadside features on vans, minivans, pickup trucks, and four-wheel-drive vehicles [16]. In 1996, Reid *et al* developed a method for identifying the critical impact points for longitudinal barriers using BARRIER VII [17]. In 1996, Faller examined transitions to concrete barriers using BARRIER VII [18]. In 1996, Bierman *et al* performed an extensive

examination of BARRIER VII post parameters and comparisons with full-scale testing were performed [19]. In 1997, Wollyung examined timber bridge railings using BARRIER VII [20]. In 1998, Plaxico calibrated input data for guardrail posts using BARRIER VII using bogie impact data [21]. In 1999, Polivka *et al* used BARRIER VII to analyze and predict the dynamic performance of various long-span guardrail alternatives prior to full-scale vehicle crash testing [22].

In 2001, Faller used BARRIER VII to aid in the analysis and design of a bridge railing and approach guardrail system [23]. In 2002, Ross used BARRIER VII to provide vehicular accelerations, barrier deformation, and information from which the potential for wheel snagging on guardrail posts could be assessed [24].

Another factor in selecting BARRIER VII as the simulation software was that other guardrail simulation programs have never gained the confidence of analysts due to a variety of problems including coding errors, poor analytical formulations, and restrictive assumptions. Ray discussed these other computer simulation codes specifically designed for the simulation of roadside barrier accidents, including GUARD, CRUNCH, and NARD [25].

BARRIER VII has also been used and accepted by the Federal Highway Administration in lieu of full-scale testing and is suggested for use in NCHRP Report 350 [26,27]. Due to its prevalence and accepted accuracy when used within its theoretical limitations, a procedure to quantify energy losses during longitudinal barrier impacts was developed using BARRIER VII.

4 FLEXIBLE BARRIER KINETICS

Flexible barriers are designed to redirect an errant vehicle away from a roadside or median hazard. Resistive normal forces are developed laterally to redirect the vehicle during impact. However, these normal forces create frictional forces between the vehicle and the barrier, as well. These frictional forces act against redirection, creating a moment about the vehicle that tends to turn the vehicle towards the barrier.

The frictional force must equal the coefficient of friction multiplied by the normal force and must act in a direction determined by the angle of the barrier surface and the relative velocities of the automobile and barrier at the point of impact. This requires an iterative approach, since the barrier's deflection and reactive forces are dependant on the vehicle velocity and position, which are dependent on the barrier's deflection and reactive forces.

5 BARRIER VII SIMULATIONS

BARRIER VII uses a highly sophisticated barrier model and a somewhat simplified vehicle model. BARRIER VII allows for the configuration of vehicle specifications, barrier design, and impact parameters. A discussion of the model parameters is presented herein.

5.1 Vehicle Models

BARRIER VII uses idealized vehicles of an arbitrary shape that interact with the barrier through defined points. The part of the vehicle boundary that may interact with the barrier is defined by

specifying a number of points at which point contact with the barrier may be made. A discrete, nonlinear spring is then associated with each point.

These nonlinear springs have two stiffness coefficients in order to more accurately represent the physical behavior of the vehicle. The first stiffness is associated with sheet metal deformation, which occurs at relatively low force levels. However, after the sheet metal has "bottomed out" on the vehicle frame or other more rigid structure, a bottoming stiffness is used to represent the increased stiffness of the vehicle response. This bottoming stiffness also prevents unrealistic vehicle deformations.

Three vehicle models were used during simulation: a 2000-kg (4400-lb) pickup, a 2040-kg (4500-lb) sedan, and an 820-kg (1800-lb) small car. Vehicle models were designed to have realistic properties, including masses and rotational inertias. The vehicle dimensions and finite element mesh used for BARRIER VII simulation are shown in Figure 2. It was believed that this selection would give the reconstructionist sufficient guidance to reasonably perform a reconstruction.

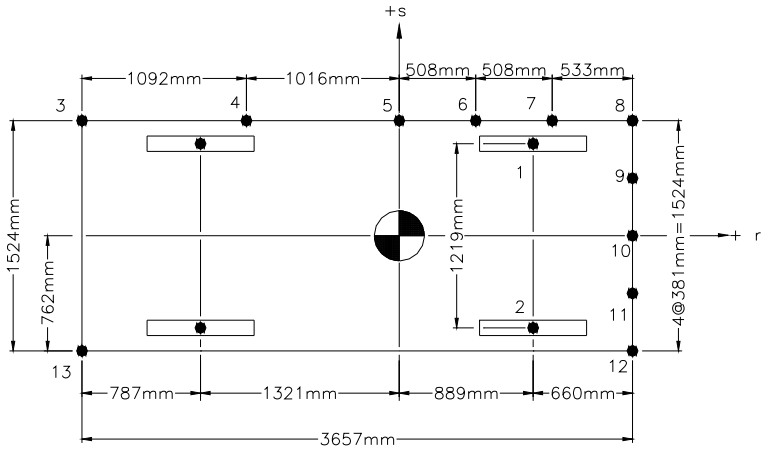

M = 820 kg

(1800 lb)

I_z = 1921 kg-m^2

(17 kip-in-sec^2)

a) NCHRP Report 350 820C Small Car Model

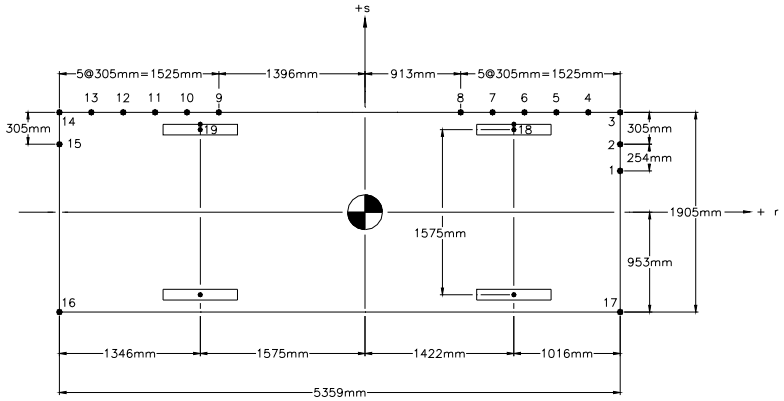

M = 2040 kg

(4500 lb)

I_z =5310 kg-m^2

(47 kip-in-sec^2)

b) NCHRP Report 230 4500-lb Sedan Model

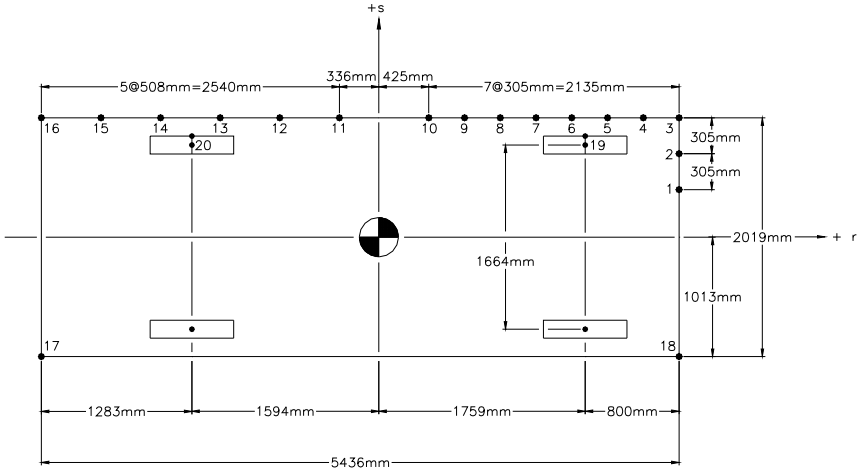

M = 2000 kg

(4400 lb)

I_z = 4520 kg-m^2

(40 kip-in-sec^2)

c) NCHRP Report 350 2000P Pickup Truck Model

Figure 9. Barrier VII Models Used in Simulation.

The three-quarter-ton truck, called a 2000P, and a small car, called an 820C, were chosen due to their incorporation into NCHRP Report 350. The FHWA adopted NCHRP Report 350 as the standard for determining safe and acceptable performance of roadside features for use on the National Highway System. The sedan was added to determine the sensitivity of the simulations to vehicle size and mass, in addition to providing the reconstructionist with an additional reference vehicle. The full-size sedan was also a standard test vehicle under NCHRP Report 230 and several prior safety hardware evaluation guidelines. Thus, a large number of tests with this vehicle were available.

5.2 Barrier Model

The barrier is idealized as a two-dimensional structural framework of an arbitrary shape. Discrete structural members possessing geometric and material nonlinearities are used, including beams, cables, columns, springs, dampers, posts, and composite members. The BARRIER VII model of the G4 (2W) strong-post W-beam guardrail system consisted of post elements to provide lateral and longitudinal support and beam members to model the W-beam guardrail. The beam model possesses both flexural and extensional bilinear elastic properties. BARRIER VII beam members are treated as a combination of a purely flexural and a separate, purely extensional member. Therefore, interaction between the bending moment and axial force is not considered. The extension member is assumed to yield over its full length when the axial force exceeds the yield force. The flexural member is assumed to yield by forming localized plastic hinges at either or both ends of the member. AASHTO specification M180-79 for corrugated sheet steel beams for guardrail was used for the W-beam material properties.

BARRIER VII posts have stiffnesses and yield strengths for displacements in two principal directions at right angles. Stiffnesses are used if the post is behaving elastically; elasto-plastic behavior commences after the posts yield.

Limiting deflections for which the post will fail completely are also specified. When a post fails, it is removed from the structure and the load that it was carrying prior to failure is transferred to the remaining structure over ten time steps. The posts were modeled using non-linear curves derived from bogie vehicle testing of guardrail posts embedded in soil [28,29]. This relationship is shown in Figure 3.

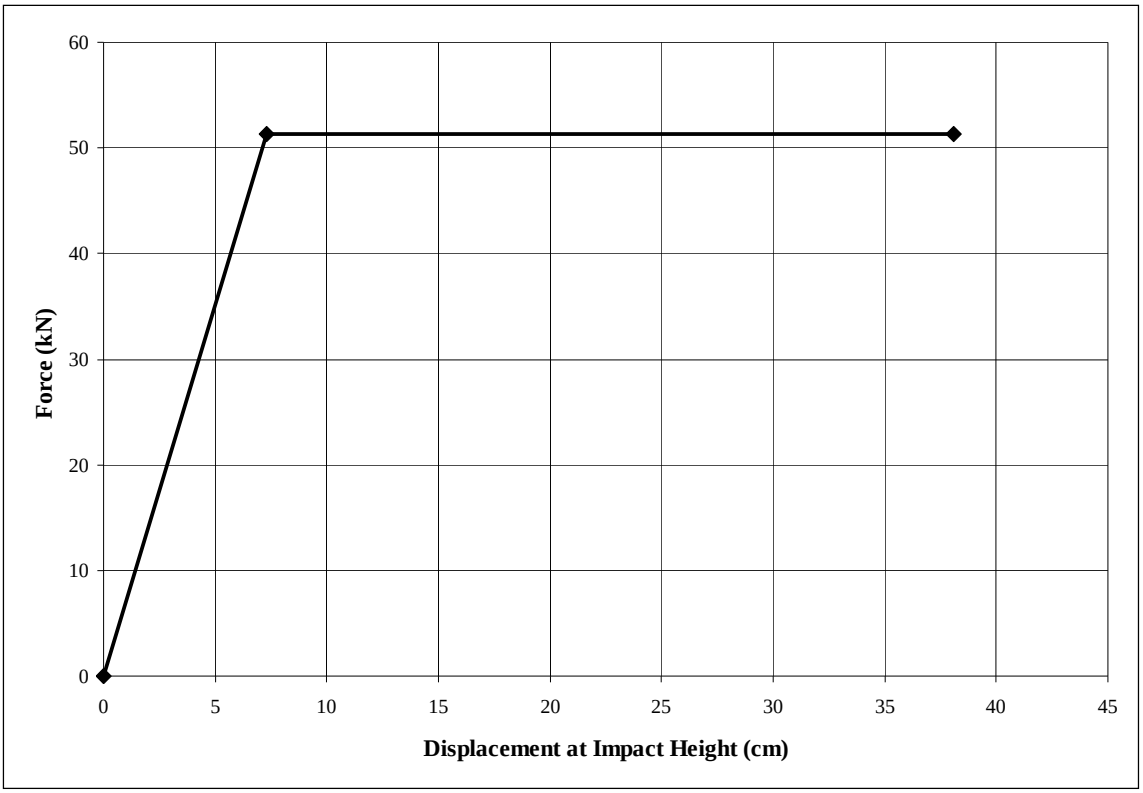

Figure 10. BARRIER VII Force-Deflection Relationship.

5.3 Impact Conditions

Velocities of 50, 75, and 100 km/h (31, 47 and 62 mph) were chosen as representative of most traveled velocities. It was assumed that as a vehicle begins an off-road excursion, the driver would make some corrective measures (e.g. applying brakes or corrective steering) that would reduce the actual impact velocity from the traveled way velocity.

It was assumed that angles steeper than 25° would not be simulated for two reasons: 1) Guardrail is not designed for higher impact angles and 2) Real-world crashes are rarely steeper than 25°. Five angles of 5°, 10°, 15°, 20°, and 25° were used.

Additionally, impacts at a post and at mid-span between two posts were performed. This yielded a total of 90 simulations: 3 vehicle models impacting at 2 locations at 3 velocities at 5 angles.

6 SIMULATION RESULTS

Simulation focused on determining which portions of the vehicle's initial kinetic energy were dissipated by which portions of the system, including vehicle crush, barrier deformation, post deformation (both permanent set and fracture), barrier-vehicle friction, and pavement-vehicle friction. Relating these values to measurable quantities at a crash site was the primary focus of the simulation.

6.1 Vehicle-Barrier Frictional Energy Losses

Frictional forces are calculated as the product of the normal force of the vehicle against the barrier and a dynamic frictional coefficient. As the vehicle is crushed, it becomes more rigid – as represented by the changing spring coefficient at spring bottoming in BARRIER VII. As

vehicle crush increases, so does the normal force exerted by the vehicle, increasing the frictional forces.

Vehicle-barrier friction was found to be a significant source of energy dissipation. For each of the three vehicles and three impact speeds, the impact angle was plotted versus the percent of the original kinetic energy dissipated by friction. These graphs were plotted for the vehicles impacting at the mid-span of the guardrail as well as at the post. These plots are shown in Figure 4.

It was observed that, for the truck model and to a lesser extent the sedan, lower speeds generated lower percentages of energy dissipated by auto-barrier friction. However, at higher speeds, the relationship appears to be convergent on the relationship found for the small car.

In order to account for this variation, a parameter study was performed. First, the effects of vehicle mass were examined. Decreasing the truck mass to that of the small car (2000 kg to 820 kg) showed no change in the relationship; lower speeds still saw lower percentages of energy dissipated by auto-barrier friction.

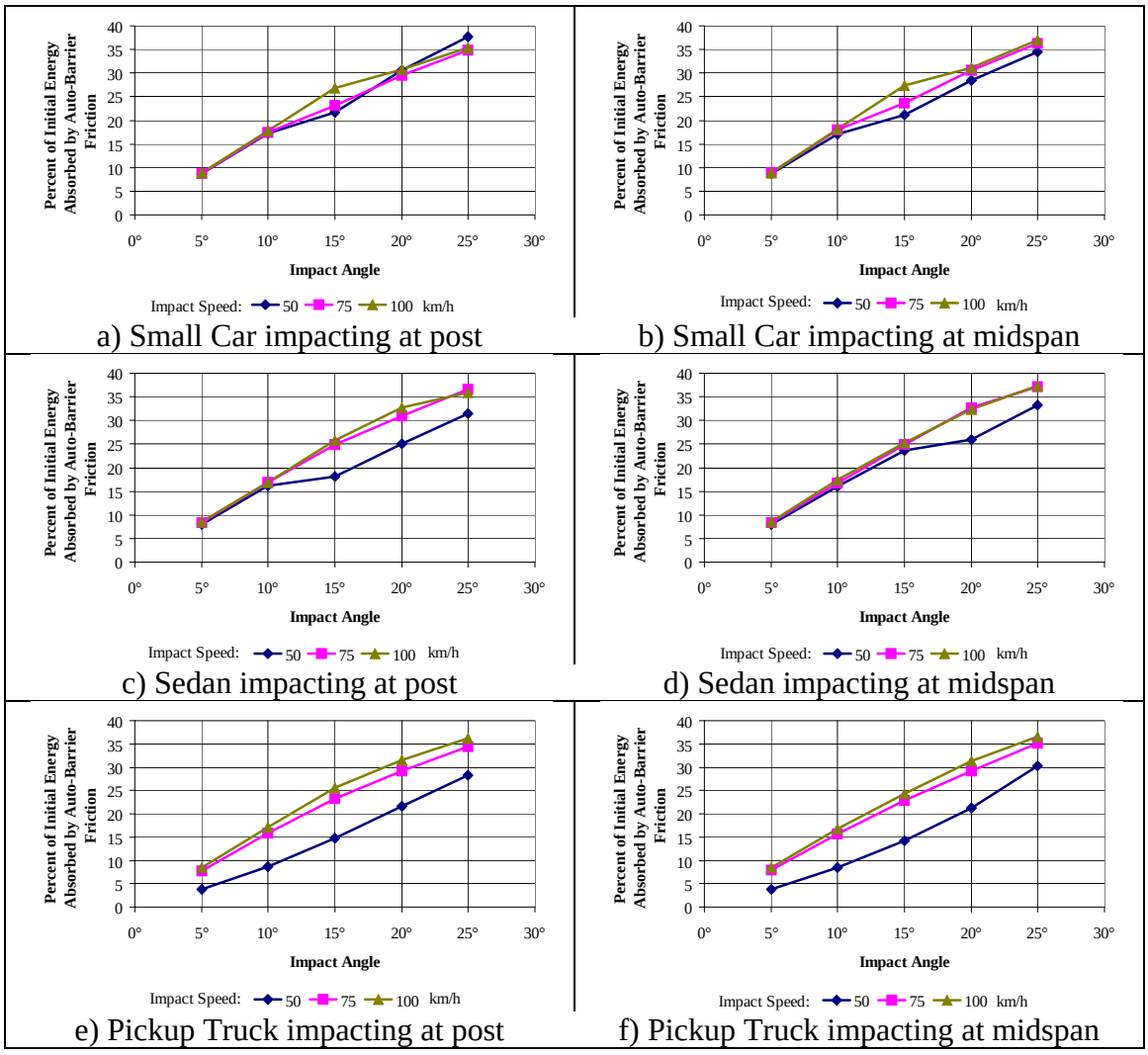

Figure 11. Energy Loss Due to Barrier Friction.

Next, the bottoming distances for the nonlinear springs representing vehicle stiffness were examined. It was believed that spring bottoming at the higher speeds might have resulted in higher frictional losses with the barrier.

When the bottoming distance was removed – the initial spring stiffness was the same of the bottomed stiffness – the curves converged. This relationship can be explained by the impact severity of the crash. The pickup and sedan models are stiffer vehicles and require more energy

to deform the sheet metal of the vehicle to the frame. This is in sharp contrast with the small car, where even small amounts of deformation crush the sheet metal skin of the vehicle to its frame. A velocity-dependent relationship for barrier-vehicle friction would create multiple variables for which iterative procedures would be required. For ease of use, it is desirable to consolidate the barrier-friction into one graph while still maintaining accuracy.

A single representative curve independent of speed created for each vehicle type by averaging the respective speed-dependent curves found in Figure 4. A linear regression was then performed on the resulting three curves. This regression and the average curves for the three vehicles are shown in Figure 5.

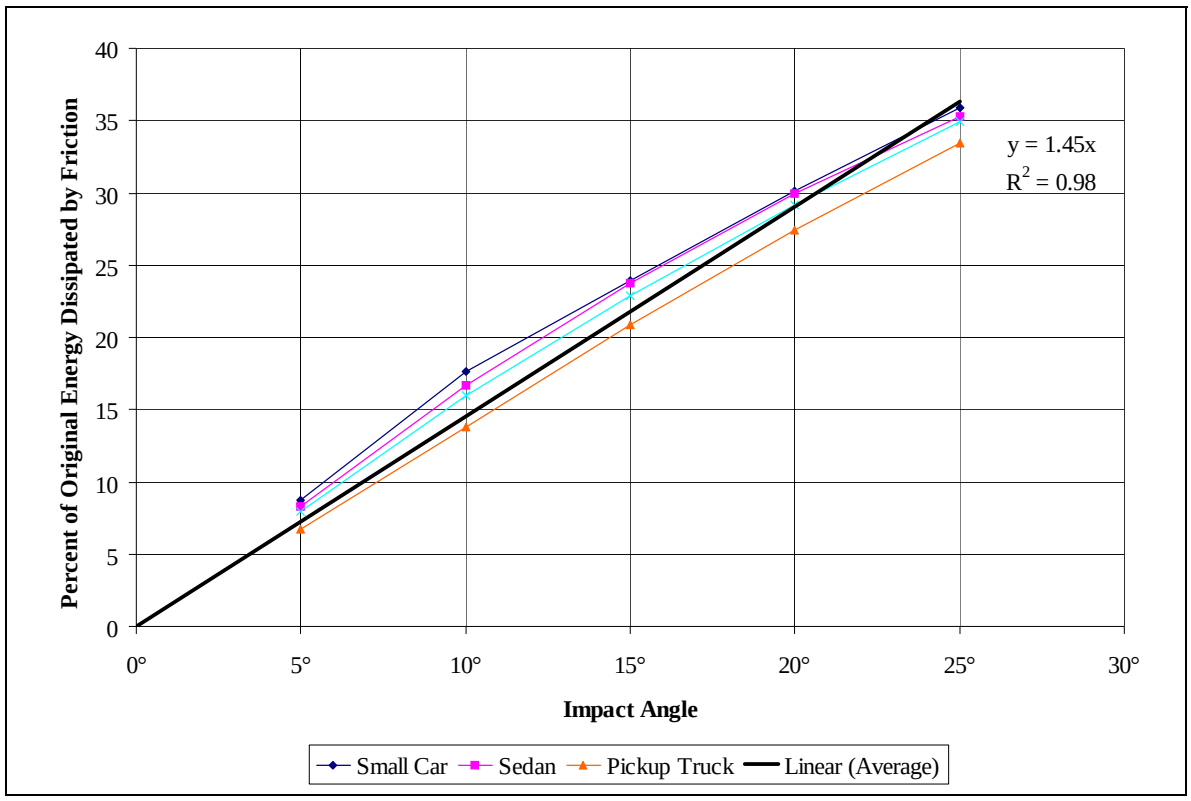

Figure 12. Relationship Between Barrier Friction and Impact Angle.

This relationship was considered reasonable, since the linear relationship for the three curves from the truck, sedan, and small car were found to be significant at $R^2 = 98.7\%$. This implies that 98.7% of the variation of the original energy dissipated by friction can be accounted for by a relationship with the impact angle.

However, the discrepancy found between velocities is biased towards higher velocities, since the small car represents the fully bottomed relationship at all velocities and the sedan represents the fully bottomed velocity at the majority of velocities. This is actually beneficial, since the greatest number of fatalities occur at higher impact speeds [30].

The energy lost from barrier friction can be quantified by the following equation:

$$\% \text{ Energy Loss} = 1.453 * \theta \quad [1]$$

where θ is the impact angle in degrees.

This formula can be used to estimate the percentage of the initial energy lost from barrier-vehicle friction for a given impact angle. At lower velocities, especially for larger vehicles, it may be prudent to use the individual curves for the relevant vehicle involved and perform multiple iterations until convergence upon an impact velocity is obtained.

6.2 Energy Absorption of Guardrail Posts

The behavior of guardrail posts is critical in several respects. First, guardrail posts provide the lateral resistance required to develop barrier-vehicle friction, which is a significant contributor to the energy dissipation of a guardrail system. Second, guardrail posts themselves dissipate energy through their rotation in soil as well as through post failure.

Significant effort has been undertaken to ascertain the force-deflection relationship of guardrail posts [**Error! Bookmark not defined.**]. This is the most difficult factor to determine in a longitudinal barrier impact, since soil conditions and, for the cases of wooden posts, wood quality, significantly affect performance.

In frozen soil, a guardrail post behaves much like it is embedded in a rigid foundation. Steel posts buckle and wooden posts fracture, both at the groundline. Because of this, the amount of energy dissipated in frozen soil is significantly less than posts allowed to rotate in soil. Standard W150x13.5 (W6x9) steel posts dissipate approximately 7.6 kJ (67 kip-in.) when embedded in a rigid foundation [31]. For wooden posts, however, significant deviations in post energies have been observed. The fracture energy of wooden posts in rigid foundations found in literature can vary from 1.4 kJ (12.3 kip-in.) to 15.4 kJ (136.3 kip-in.) [32,33]. However, a

reasonable performance envelope would be 6.2 kJ (54.9 kip-in.) to 8.0 kJ (70.8 kip-in) for DS-65 posts and 3.9 kJ (34.5 kip-in) to 5.0 kJ (44.3 kip-in) for Grade 1 posts [**Error! Bookmark not defined.**].

The relationship between posts rotating in soil is a more difficult number to quantify. For standard W150x13.5 (W6x9) steel posts, common force-deflection and energy absorption relationships are shown in Figure 6 and in Appendix A [34]. This research correlated well with previous research that had obtained numerically similar results for posts rotating in soil [**Error! Bookmark not defined.**]. The slope of the line in Figure 6b was found to be 0.46 kJ/cm (0.86 kip-ft/in.). This value can be used to directly calculate energy for any given deflection.

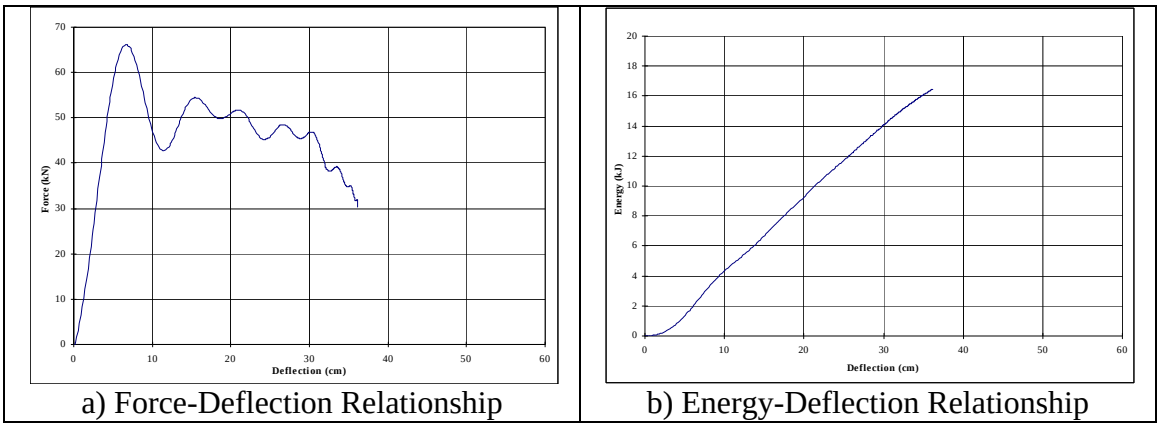

a) Force-Deflection Relationship b) Energy-Deflection Relationship

Figure 13. Post-Deflection Force and Energy Relationships (deflection at rail bolt height).

It has been noted that the differences between standard wooden and steel posts do not greatly affect the performance of any guardrail systems [35]. Because of this and the wide variability of soil strengths, Figure 6 is used to predict the energy dissipation of both steel and wooden posts. It is difficult, if not impossible, to accurately estimate individual post deflections from only the maximum lateral deformation and length of deformation of the barrier. It was found that a lack

of accurate measurements or photographic evidence made the estimation of individual post deflection inaccurate. Errors in individual post deflections create errors at an order of 0.92 kJ/cm (1.72 kip-ft/in.), since the barrier and post deformational energies are roughly equal, as discussed below.

Because of the importance of post deflections to the reconstruction processes, accurate post deflection measurements must be obtained at the crash site. Determination of post deflections from photographic evidence is difficult and will lead to significant inaccuracy.

6.3 Barrier and Post Deformation Relationship

Simulation using BARRIER VII indicated that, at low speeds, the barrier rail dissipates significantly more energy than the posts in the system. This was found to be independent of impacting angle or of vehicle type. However, at higher speeds, the ratio was found to approach unity – very rapidly with the truck and the sedan, but less rapidly with the small car model. These results are shown in Figure 7.

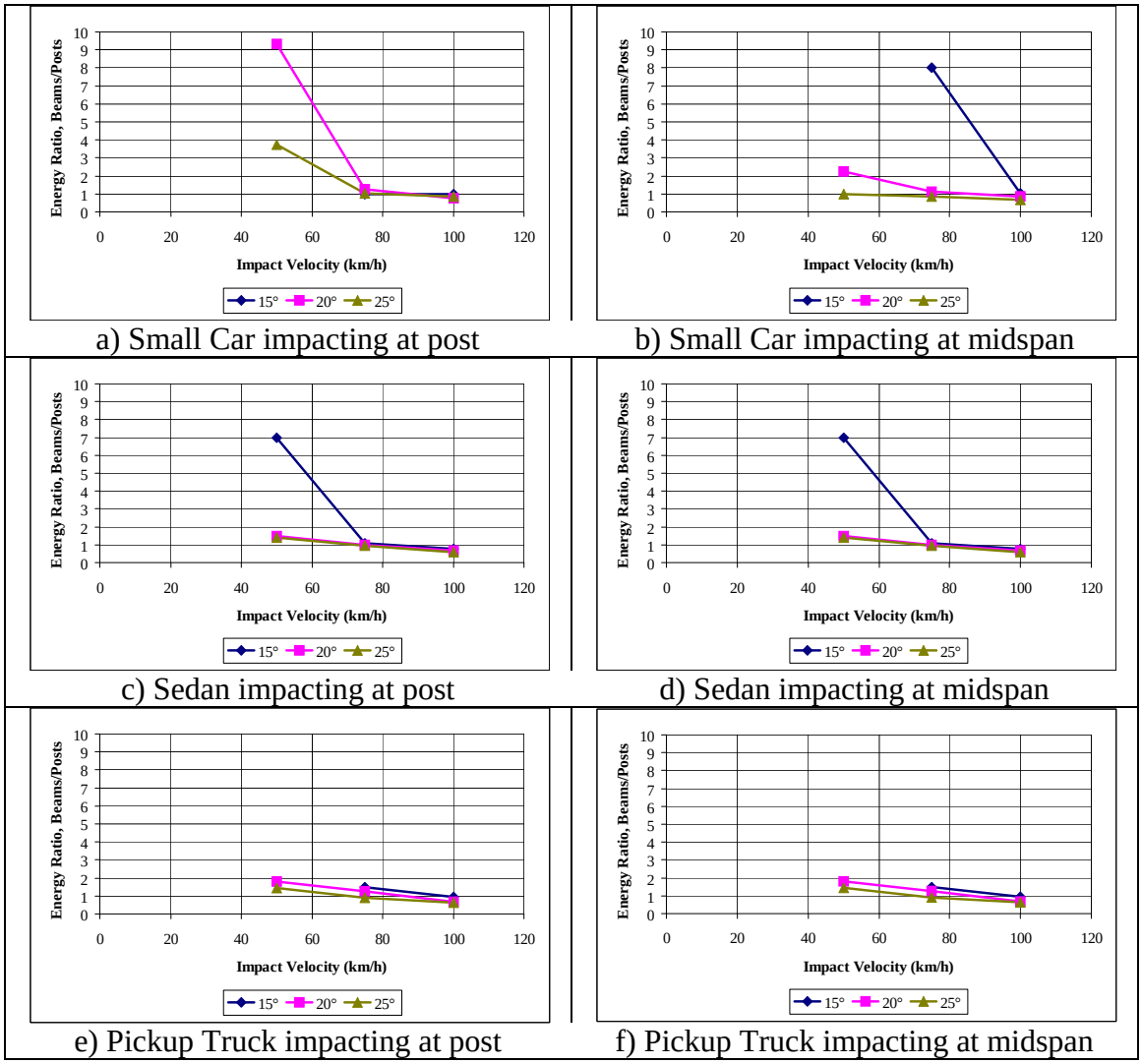

a) Small Car impacting at post b) Small Car impacting at midspan

c) Sedan impacting at post d) Sedan impacting at midspan

e) Pickup Truck impacting at post f) Pickup Truck impacting at midspan

Figure 14. Ratio of Beam Energy Absorption to Post Energy Absorption

In BARRIER VII, when a post fails, it is immediately removed from the structure and the load it carried immediately prior to failure is transferred to the remaining structure. Since the failure of a real post is unlikely to be sudden, the failure is assumed to extend over the ten time steps following initiation of failure.

This relationship was observed during physical testing by Powell prior to his creation of BARRIER VII [**Error! Bookmark not defined.**, **Error! Bookmark not defined.**]. Physically,

the guardrail is able to distribute loads across more posts at lower speeds, decreasing deflections. At higher speeds, the guardrail deforms locally and local posts see significantly higher loads and therefore more energy.

To determine the energy lost from barrier deformation, the post deformation energy obtained in Section 6.2 is multiplied by the appropriate energy ratio from Figure 7. Since it is velocity dependent, a reasonable estimate will initially need to be made; in most cases unity will provide the most accurate results. This yields the estimated energy dissipated from barrier deformation in kJ.

6.4 Vehicle Energy Losses

During longitudinal crashes, vehicle crush occurs due to impact with the barrier. The characteristic dual-stripe impacts that come from an impact with W-beam barrier cause it to be difficult to measure vehicle crush. Additionally, the longitudinal frictional forces can cause pulling and tearing of the vehicle body, which would not be measured in conventional crush measurements. Because of this, it may be more appropriate to use estimated vehicle damage rather than measured vehicle damage to determine energy losses due to vehicle crush.

Another source of energy that must be taken into account is the friction losses between the vehicle and the pavement. This energy is dissipated both in tracking and non-tracking modes and is proportional to a frictional coefficient times the mass of the vehicle.

These two forms of energy, frictional losses and vehicle crush energy, were combined because of their strong correlation ($R^2 \cong 0.99$) across velocities and vehicle platforms. The sum of these energies and their relationship to impact angle and vehicle type is shown in Figure 8.

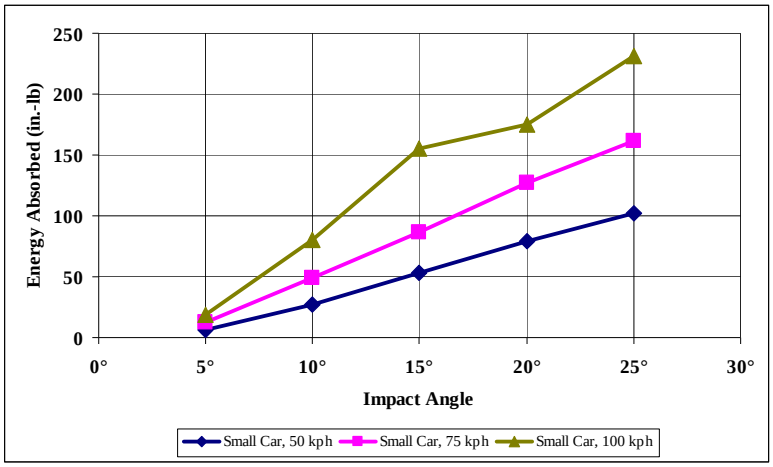

a) Percent Energy Loss, Small Car

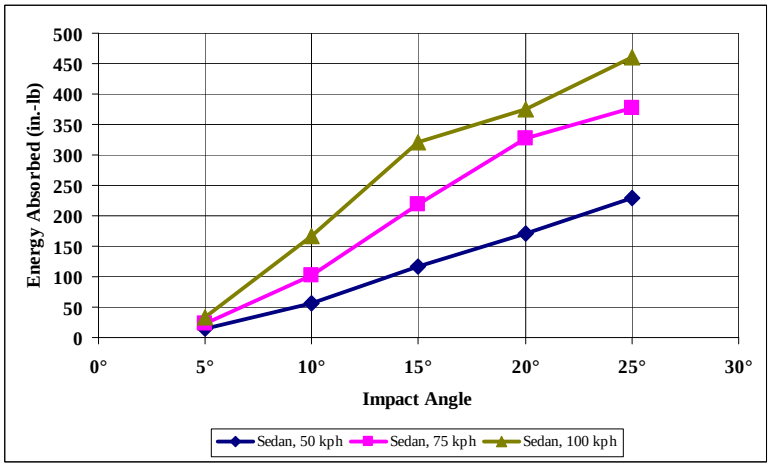

b) Percent Energy Loss, Sedan

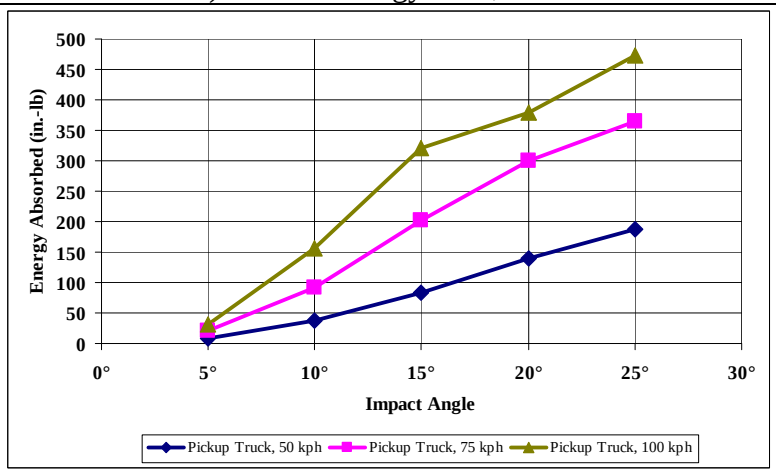

c) Percent Energy Loss, Pickup Truck

Figure 15. Energy Loss Due to Vehicle Crush and Pavement Friction.

Due to the divergent nature of the curves seen in Figure 8, a better, more linear relationship was desired. Additionally, since Figure 8 is plotted versus energy, it requires extensive calculation and either interpolation or extrapolation to determine the energy lost due to vehicle crush and tire-ground friction. To simplify the process, these values were divided by their corresponding initial energy, to yield a percentage of the initial vehicle kinetic energy absorbed by vehicle crush and tire-ground friction. This relationship is shown in Figure 9.

For lower impact angles, little deformation of the vehicle is seen. For increasing angles, roughly linear increases are seen. This is intuitive, given that impact severity is dependant on the impact angle.

At low impact angles, the percentage of energy absorbed by vehicle crush and tire-ground friction is very low, on the order of 1 percent. This percentage increases relatively linearly as the impact angle increases. However, the increase is both vehicle type and vehicle speed dependent. More energy is absorbed by a vehicle during high speed impacts relative to low speed impacts. However, the percentage of energy absorbed by the vehicle relative to the total energy dissipated during an impact is higher for lower speed vehicles than it is for higher speed ones. This is because at higher speeds, the crush space of the vehicle begins to bottom out and its energy absorbing capability is limited. At this point, the barrier is the weaker of the two structures, and as such, it absorbs a great deal of the remaining energy dissipated during the impact. The more energy absorbed by the barrier, the lower the percentage absorbed by the vehicle.

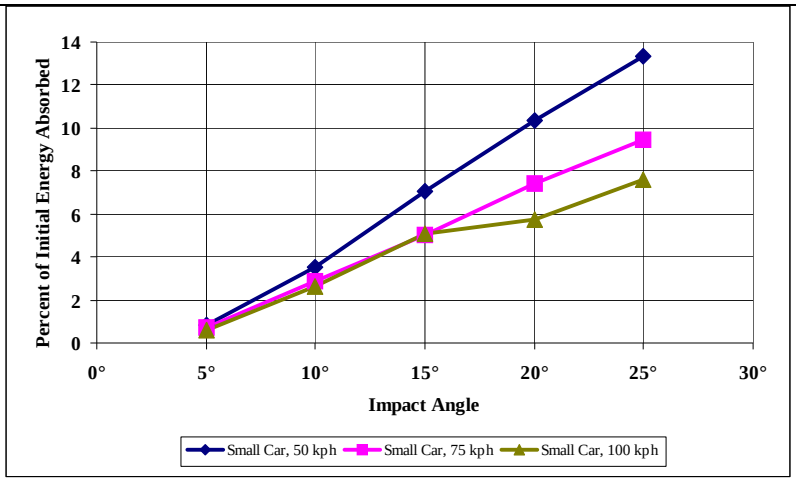

a) Percent Energy Loss, Small Car

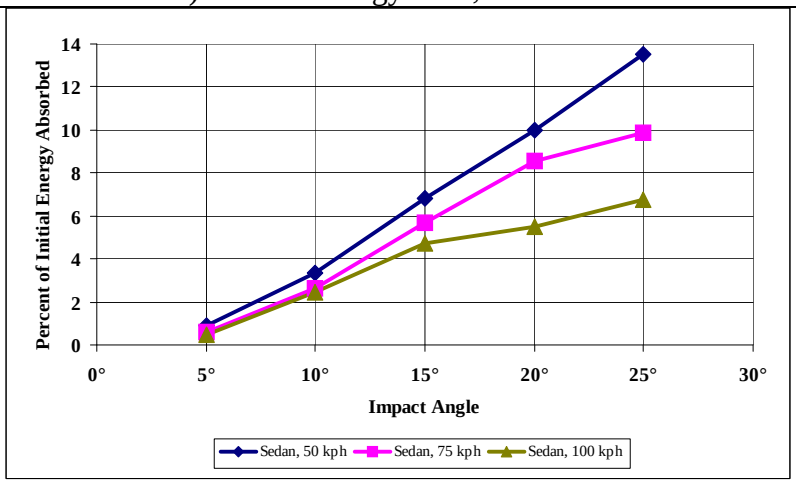

b) Percent Energy Loss, Sedan

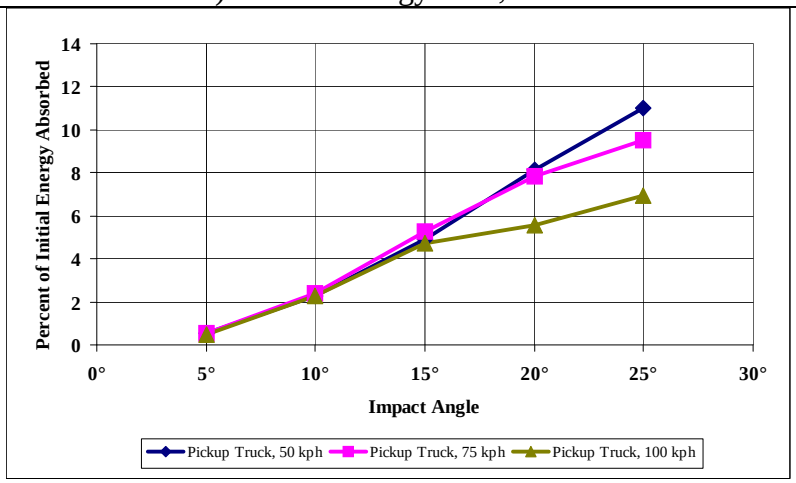

c) Percent Energy Loss, Pickup Truck

Figure 16. Energy Loss Due to Vehicle Crush and Pavement Friction.

12

7 RECONSTRUCTION PROCEDURE

The reconstruction procedure is based on conservation of energy. The impact angle must be determined either from scale diagrams or estimated from photographic evidence. The procedure uses the difference between the initial kinetic energy of the vehicle at the beginning of the impact and the kinetic energy of the vehicle after it departs from the barrier (or is stopped) and equates it to the energy losses sustained during the interaction between the barrier and the vehicle. By determining the departure kinetic energy of the vehicle and the energy losses during vehicle-barrier interaction, the initial kinetic energy can be calculated; which is easily converted to the initial velocity of the impact. This reconstruction procedure is valid only for strong-post W-beam guardrail systems.

Determine Departure Velocity and Departing Kinetic Energy

The departure velocity of the vehicle, V_d, is calculated from vehicle crush, rolling resistance, and other energy losses using traditional engineering approaches to crash reconstruction. This velocity is then converted to the departing kinetic energy using the following equation:

$$KE_{departing} = \frac{1}{2} M V_d^2 \quad [2]$$

This is important since events after departure are not interactions with the barrier; the difference between the initial kinetic energy of the vehicle and the departing kinetic energy of the vehicle is the energy losses sustained during the interaction between the barrier and the vehicle.

Estimate an Initial Velocity for the Impact

An initial velocity estimate must be made in order to determine the various energy-absorbing contributions made during the crash. Since this is an iterative process, the reconstructionist must use engineering judgment for an initial velocity for the first iteration. This velocity should be used, as needed, in Steps 3, 5, and 6 below.

Determine Energy Dissipation due to Barrier-Vehicle Friction

The percentage of energy dissipation due to barrier-vehicle friction is found from Figure 5 or using Equation 1. For larger vehicles at lower impact velocities, Figure 4 may be needed to ensure a more accurate calculation.

Determine Energy Dissipated by the Posts

For posts that rotate in the soil, Figure 6 provides estimates of energy dissipated by soil rotation. Posts that fracture or buckle without rotating in the soil dissipate approximately 7.6 kJ (67 kip-in.) of energy. This is common for posts that are placed in rigid foundations or frozen soil.

Determine Energy Dissipated by Guardrail Beam Deformation

The energy dissipated by the guardrail beam deformation is found by multiplying the energy dissipated from the post deformation (Step 4) by the factor found in Figure 7. Generally, at higher speeds where impact reconstructions are typically performed, the energy dissipated by the posts is equal to that dissipated by the guardrail beam deformation. However, at lower speeds and particularly for smaller vehicles, the posts do not dissipate as much energy proportionally and Figure 7 may be necessary to estimate the ratio.

Determine Energy Dissipated by Vehicle Damage and Tire-Ground Friction

The energy dissipated by vehicle damage and tire-ground friction is determined using Figure 9.

Calculate an Initial Kinetic Energy and Corresponding Initial Velocity

The vehicle's impact velocity is found by solving Equations 3 and 4 listed below. First, Equation 3 is solved for the initial kinetic energy. Then Equation 4 is solved for the initial velocity, $V_{initial}$.

$$KEinitial = KEdeparting + Efriction + Eposts + Ebeam + Evehicle \quad [3]$$

$$Vinitial = \sqrt{\frac{2 * KEinitial}{M}} \quad [4]$$

Where,

$KE_{initial}$ is the initial kinetic energy of the vehicle

$KE_{departing}$ is the departing kinetic energy of the vehicle (Step 1)

$E_{friction}$ is the energy dissipated by barrier-vehicle friction (Step 3)

E_{posts} is the energy dissipated by the guardrail posts (Step 4)

E_{beam} is the energy dissipated by the guardrail beam (Step 5)

$E_{vehicle}$ is the energy dissipated by vehicle damage and tire-ground friction (Step 6)

Iterate to Determine Initial Velocity

Compare the initial velocity calculated in Step 7 with the estimate from Step 2. If they are reasonably close, then the initial velocity has been determined. If the velocities are not close, iterate the procedure starting over with Step 2, but use the velocity calculated from Step 7 as the initial estimate.

13 8 SAMPLE RECONSTRUCTION

An example reconstruction, based on a Modified G4 (1S) W-beam system tested by the Texas Transportation Institute (TTI), is used to expressly show the procedures involved in the reconstruction [36]. The test consisted of a 2076-kg pickup impacting a W-beam guardrail on steel posts with timber blockouts. The vehicle impacted at 25.5° at a velocity of 101.5 km/h (63 mph) and exited at 16° at 55 km/h (34 mph).

Determine Departure Velocity and Departing Kinetic Energy

The departure velocity is converted to kinetic energy. For Test No. 405421-1, the vehicle mass was 2076 kg and exited the barrier at 55 km/h. Using Equation 2, the departing kinetic energy of the pickup is

$$KE_{departing} = \frac{1}{2} M\ Vd^2 = \frac{1}{2} (2076\ kg)\ (15.28\ m/s)^2 = 242\ kJ \quad [5]$$

Estimate an Initial Velocity for the Impact

An initial impact velocity of 120 km/h (75 mph) is selected as being representative of highway speeds. This is based on engineering judgment or other information available to the reconstructionist. This value is used to select velocity-dependent relationships estimate an initial kinetic energy using Equation 2.

$$KE_{initial} = \frac{1}{2} M\ Vi^2 = \frac{1}{2} (2076\ kg)\ (33.3\ m/s)^2 = 1{,}153\ kJ \quad [6]$$

Determine Energy Dissipation due to Barrier-Vehicle Friction

The percentage of energy dissipation due to barrier-vehicle friction is found from Figure 5. At 25.5°, barrier-vehicle friction dissipates approximately 36% of the initial kinetic energy.

Alternatively, Equation 1 may be used, yielding the same result. For an impact velocity of 120 km/h (75 mph), this equates to 427 kJ.

Determine Energy Dissipated by the Posts

The amount of energy dissipated by the posts is estimated. From photographic evidence from overhead cameras, post deflections were estimated. From Figure 6, the post defection energy is calculated to 38 cm (15 in.). After this, the posts are assumed to no longer contribute to the energy dissipation of the system. The corresponding deflections, corrected deflections (adjusted for a maximum deflection of 38 cm), and energies are given in Table 1:

Table 4. Summation of Post Energy Dissipation.

Post Number	Deflection (cm)	Corrected Deflection (cm)	Energy from Figure 6 (kJ)
10	0.0	0.0	0.0
11	20.8	0.0	9.5
12	41.6	20.8	17.4
13	62.4	41.6	17.4
14	83.2	38.0	17.4
15	83.2	38.0	17.4
16	62.4	38.0	17.4
17	41.6	38.0	17.4
18	0.0	0.0	0.0
Total:			114.0

Determine Energy Dissipated by Guardrail Beam Deformation

The energy dissipated by the guardrail beam deformation is estimated. This is found by multiplying the energy dissipated from the post deformation by the factor found in Figure 7. For the case of a pickup impacting at highway speed, the energies are assumed equal and assumed to be that of the deformed posts: 114.0 kJ.

Determine Energy Dissipated by Vehicle Damage and Tire-Ground Friction

The percentage of energy dissipated by the vehicle crushing and vehicle-pavement friction is found using Figure 9. This value varies between 7% and 11%; since we are assuming highway impact speeds, the value of 7% will be used. This yields 80.7 kJ.

Calculate an Initial Kinetic Energy and Corresponding Initial Velocity

The vehicle's impact velocity is found by solving Equations 3 and 4.

$$KE_{initial} = 242.3\ kJ + 427.4\ kJ + 114.0\ kJ + 114.0\ kJ + 80.7\ kJ = 978.5\ kJ \quad [7]$$

$$V_{initial} = \sqrt{\frac{2 * 978.5\ kJ}{2076\ kg}} = 110.5\ km/h \quad [8]$$

Iterate to Determine Initial Velocity

The initial estimate was 120 km/h, which is significantly different than our calculated velocity of 110.5 km/h. An iterative approach is then used, repeating the steps above assuming a new initial velocity of 110.5 km/h.

1. The energy at departure remains 242 kJ.

2. The new initial velocity is 110.5 km/h, with a $KE_{initial}$ = 978 kJ.

3. The energy dissipated by vehicle-barrier friction is 362.4 kJ.

4. Post energy unchanged, 114.0 kJ.

5. Barrier energy unchanged, 114.0 kJ.

6. Vehicle damage and tire-ground friction, 68.5 kJ

7. Summing, this yields 901.3kJ for a $V_{initial}$ = 106.1 km/h.

When repeated, the procedure converges to 102.4 km/h which is less than 1% from the actual impact speed of 101.5 km/h by less than 1 percent.

In Appendix A are the reconstructions of three G4 strong post guardrail systems from the Texas Transportation Institute, TTI, and the Midwest Roadside Safety Facility, MwRSF [37, 38, 39]. The results of the reconstruction were extremely close to the actual impact speeds, as shown in Table 2.

Table 5. Comparison of Reconstruction Results to Physical Test Data.

Testing House	Test Identifier	Post System	Reconstructed Speed (km/h)	Actual Speed (km/h)	Difference
MwRSF	BSP-5	G4(2W)	101.3	102.0	-0.7%
TTI	405421-1	G4(1S) (timber blockouts)	102.4	101.5	+0.9%
TTI	471470-26	G4(2W)	103.8	100.8	+3.0%

14 SENSITIVITY ANALYSIS

A sensitivity analysis was performed to determine the effect of impact angle on the reconstructed initial velocity. The reconstruction procedure was found to be relatively insensitive to the impact angle, varying by less than ±7.5% in the final reconstructed values with variations in impact angle of ±10°. The results of the parameter study are shown in Table 3 and graphically in Figure 10.

Table 6. Sensitivity Analysis of Reconstruction Procedure.

Impact Angle	Difference in Angle	Calculated Initial Velocity (k/hr)	Difference from Baseline
15.5°	-39.9%	94.7	-7.5%
20.5°	-19.6%	97.9	-4.4%
25.5°	Baseline	102.4	Baseline
30.5°	19.6%	106.1	3.6%

35.5°	39.2%	109.6	7.0%

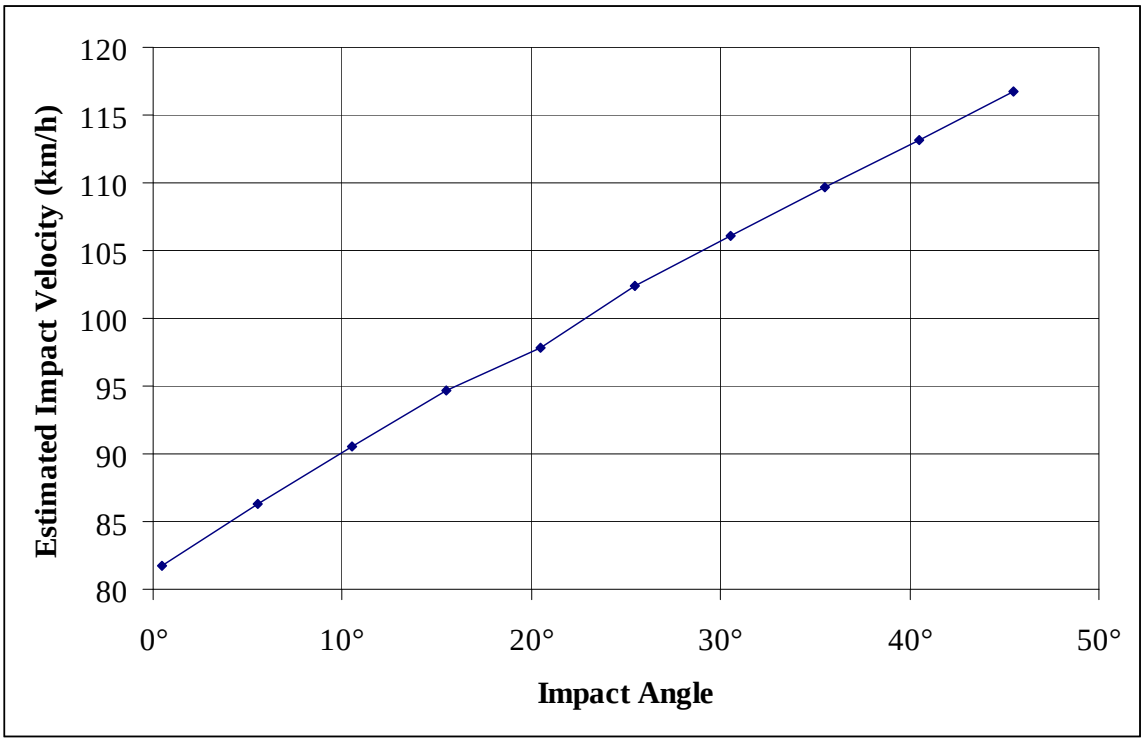

Figure 17. Sensitivity Analysis of Impact Angle.

A sensitivity analysis was also performed to examine the effects of post energy on the reconstructed initial velocity. The reconstruction procedure was found to be relatively insensitive to the post energy, varying less than ±15% with no post rotational/fracture energy or with the post rotational/fracture energy doubled. The results of the parameter study are shown in Table 4 and graphically in Figure 11.

Table 7. Sensitivity Analysis of Reconstruction Procedure to Post Energy.

Difference in Post Energy	Calculated Initial Velocity (k/hr)	Difference from Baseline
200%	116.5	-13.8%
180%	113.7	-11.0%

160%	110.9	-8.3%
140%	108.1	-5.5%
120%	105.3	-2.6%
Baseline (4.6 kJ/m)	102.4	Baseline
80%	99.6	2.8%
60%	96.7	5.6%
40%	93.8	8.5%
20%	90.8	11.3%
0%	87.9	14.2%

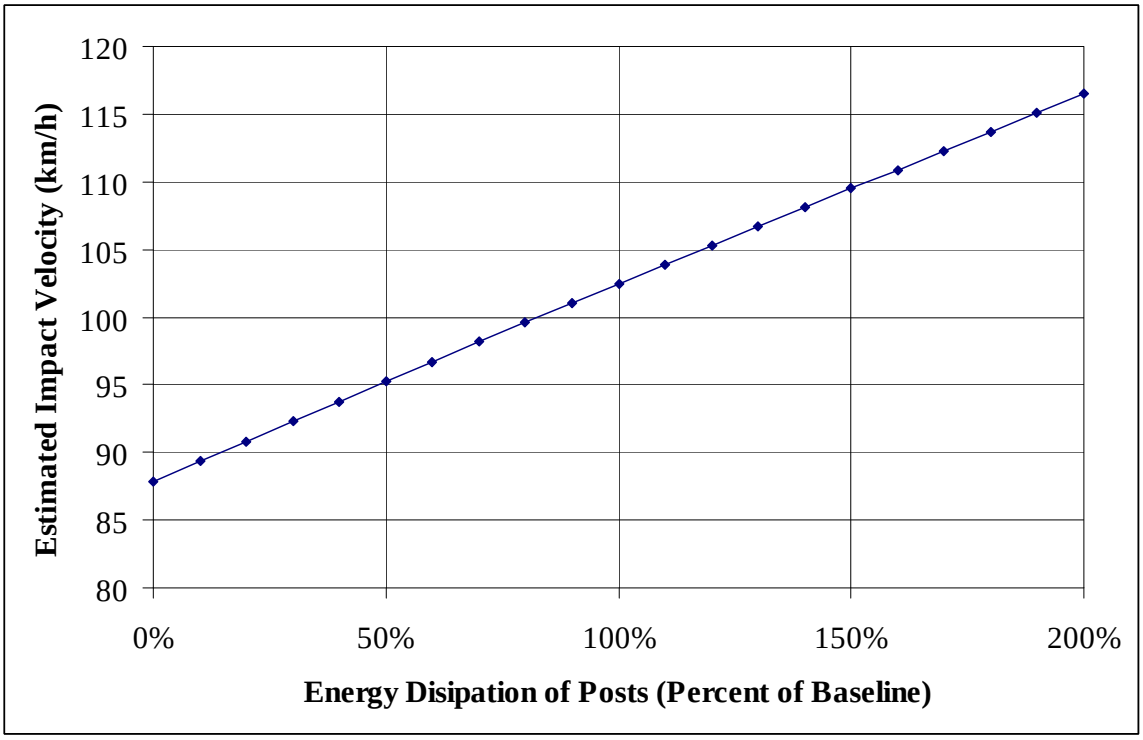

Figure 18. Sensitivity Analysis of Post Rotational / Fracture Energy.

15 10 CONCLUSIONS AND RECOMMENDATIONS

A method to simply and quickly estimate initial vehicle velocity for strong-post W-beam longitudinal barrier impacts was presented. This involved an iterative technique using relationships derived from BARRIER VII, a well-verified and commonly-used roadside barrier simulation program.

Significant portions of the initial vehicle energy are dissipated through friction between a longitudinal barrier and impacting vehicle. The relationship is dependent on vehicle impact angle and only to a negligible degree on vehicle type.

The energy to cause permanent deflections of the guardrail posts in a system is roughly equivalent to the amount of energy dissipated by the rail elements at higher speeds.

In order to perform the procedure, detailed information about the crash is required, including: the mass and type of vehicle, the angle at which the vehicle impacted, the velocity at which the vehicle lost contact with the longitudinal barrier, and post deflections.

Results from the reconstruction were within 3 percent of the actual impact velocity and can be produced without detailed knowledge of vehicle deformations. The process is highly dependent on impact angle, however, which must be determined from scale diagrams from accident reports or scene investigations or available evidence at the scene.

11 REFERENCES

Sicking, DL, KK Mak and WB Wilson, “Box-Beam Guardrail Terminal,” Transportation Research Record 1468, Transportation Research Board, National Research Council, Washington, DC, 1994.

National Highway Traffic Safety Administration (NHTSA), Fatal Accident Reporting System (FARS) Database, Washington, DC, 1999.

Powell, GH, “Computer Evaluation of Automobile Barrier Systems,” Federal Highway Administration No. FHWA-RD-73-73, August 1970.

Powell, GH, “BARRIER VII: A Computer Program for Evaluation of Automobile Barrier Systems,” Report No. FHWA-RD-73-51, Federal Highway Administration, Washington, D.C. (April 1973). Washington, D.C.

Barth, KE, JF Davalos, RG McGinnis, and MH Ray, “Development of an Improved Roadside Barrier System,” NCHRP Project 22-17, National Cooperative Highway Research Program, National Academies of Science, Washington, DC, March 2001.

Reid, JD, “Steel Post Simulation for the Buffalo Guardrail System,” AMD Vol. 225, Crashworthiness, Occupant Protection and Biomechanics in Transportation Systems, American Society of Mechanical Engineers, 1997.

AASHTO-ARTBA-AGC, “A Guide to Standardized Highway Barrier Hardware,” American Association of State Highway and Transportation Officials, Washington, DC, 1995.

Hunter, WW, JR Stewart, and FM Council. “Comparative Performance of Barrier and End Treatment Types Using the Longitudinal Barrier Special Study File.” Transportation Research Record No. 1419, Transportation Research Board, National Academy Press, Washington, D.C., 1993.

Erinle, O, W Hunter, M Bronstad, F Council, R Stewart, and K Hancock. “Analysis of Guardrail and Median Barrier Accidents Using the Longitudinal Barrier Special Studies (LBSS) File,” FHWA Publication No. FHWA-RD-92-098, Federal Highway Administration, Washington, DC, 1994.

Calcote, LR, “Development of Cost Effectiveness Model for Guardrail Selection,” Report FHWA-RD-78-75, Federal Highway Administration, Washington, D.C., 1980.

Post, ER, CY Tuan and SA Ataullah “Comparative Study of Kansas and FHWA Guardrail Transition Designs Using BARRIER VII Computer Simulation Model,” Transportation Research Report TRP-03-012-88, Midwest Roadside Safety Facility, University of Nebraska – Lincoln, December 1988.

Ataullah, S, “An Analytical Evaluation of Future Nebraska Bridgerail-Guardrail Transition Designs Using Computer Simulation Model BARRIER VII,” M.S. Thesis, Civil Engineering Department, University of Nebraska – Lincoln, August, 1988.

Tuan, CY, ER Post, S Ataullah, and JO Brewer, “Development of Kansas Guardrail to Bridgerail Transition Using BARRIER VII,” Transportation Research Record No. 1233, Transportation Research Board, National Academy Press, Washington, D.C., 1989.

Bligh, RP, and Sicking, DL, “Applications of Barrier VII in the Design of Flexible Barriers.” Transportation Research Record 1233, Transportation Research Board, National Research Council, Washington, D.C. (1989) pp. 117–123.

Mak, KK RP Bligh and DH Pope, “Wyoming Tube-Type Bridge Rail and Box-Beam Guardrail Transition,” Transportation Research Record No. 1258, Transportation Research Board, National Academy Press, Washington, D.C., 1990.

Ross, HE Jr., RP Bligh, and KK Mak, “Evaluation of Roadside Features to Accommodate Vans, Minivans, Pickup Trucks, and 4-Wheel Drive Vehicles,” NCHRP Report 471, National Cooperative Highway Research Program, Transportation Research Board, National Research Council, Washington, DC, 1994.

Reid, JD, DL Sicking, and R Bligh, “Critical Impact Point for Longitudinal Barriers,” ASCE Journal of Transportation Engineering, Vol. 124, No. 1, Jan./Feb. 1998.

Faller, RK, K. Soyland and DL Sicking, “Approach Guardrail Transition for Single-Slope Concrete Barriers,” Current Research on Roadside Safety Features, Transportation Research Record No. 1528, Transportation Research Board, National Academy Press, Washington, D.C., 1996.

Holloway, JC, MG Bierman, BG Pfeifer, BT Rosson, and DL Sicking, “Performance Evaluation of KDOT W-Beam Systems Volume II: Component Testing and Computer Simulation,” MwRSF Report No. TRP-03-39-96, Midwest Roadside Safety Facility, University of Nebraska – Lincoln, May 1996.

Wollyung, R, M Carpino, A. Scanlon, and B. Gilmore, “Performance of Timber Bridge Railings Under Vehicle Impact Using Barrier VII Simulation,” Proceedings of 76th Annual Meeting of the Transportation Research Board, Paper No. 971384, January 1997.

Plaxico, CA, "Response of Guardrail Posts under Parametric Variation of Wood and Soil Strength," Presentation at the 77th Annual Transportation Research Board Meeting, Washington, D.C., January 11-15, 1998.

Polivka, KA, RW Beilenberg, DL Sicking, RK Faller, and JR Rohde, “Development of a 7.62-m Longspan Guardrail System,” MwRSF Report No. TRP-03-72-99, Midwest Roadside Safety Facility, University of Nebraska – Lincoln, 1999.

Faller, RK, BT Rosson, MA Ritter, EA Keller, and SR Duwadi, “Development of Two Test Level 2 Bridge Railings and Transitions for Use on Transverse Glue-Laminated Deck Bridges,” Paper No. 01-0378, Transportation Research Record No. 1743, Transportation Research Board, National Research Council, Washington, D.C. 2001.

Ross, HE, Jr., RP Bligh, and KK Mak, “NCHRP Report 471: Evaluation of Roadside Features to Accommodate Vans, Minivans, Pickup Trucks, and 4-Wheel Drive Vehicles.” Transportation National Research Council, Washington, D.C. 2002.

Ray, MH, “The Use of Finite Element Analysis in Roadside Hardware Design,” International Journal of Crashworthiness, Vol 2, No 4, Woodhead Publishing, London, UK, 1997.

Wright, Frederick G. Jr., Program Manager, Safety, and Robert L. Wilson, Texas Transportation Institute, Federal Highway Administration Acceptance Letter, FHWA Reference No.: HSA-10/B47B,

September 4, 2001.

Ross, HE Jr, DL Sicking, RA Zimmer, and JD Michie, "NCHRP Report 350: Recommended Procedures for the Safety Performance Evaluation of Highway Features," National Cooperative Highway Research Program, National Research Council, Washington, DC. 1993.

Coon, BA, "Dynamic Impact Testing and Simulation of Guardrail Posts," Master's Thesis, Department of Civil Engineering, The University of Nebraska – Lincoln, 1999.

Bierman, MG, "Behavior of Guardrail Posts to Lateral Impact Loads," Master's Thesis, Department of Civil Engineering, The University of Nebraska – Lincoln, December 1995.

Solomon D, "Accidents on Main Rural Highways Related to Speed, Driver, and Vehicle," US Department of Commerce & Bureau of Public Roads, Washington, DC, 1964.

Herr, JE, "Development of Standards for Placement of Steel Guardrail Posts in Rock," Master's Thesis, Department of Civil Engineering, The University of Nebraska – Lincoln, December 2002.

Rohde, JR, JD Reid, and DL Sicking, "Evaluation of the Effect of Wood Quality on W-Beam Guardrail Performance," NDOR Report No. AFE-Z322, Midwest Roadside Safety Facility, University of Nebraska – Lincoln, November 1995.

Gatchell, CJ and JD Michie, "Pendulum Impact Tests of Wooden and Steel Highway Guardrail Posts," USDA Research Paper No. NE-311, United States Forest Service, United States Department of Agriculture, 1974.

Coon, BA, JD Reid, and JR Rohde, "Dynamic Impact Testiong of Guardrail Posts Embedded in Soil," Midwest Roadside Safety Facility Report No. TRP-03-77-98, University of Nebraska – Lincoln, July 21, 1999.

Jayapalan, JK, JF Dewey, TJ Hirsch, HE Ross and H Crooner, "Soil-Foundation Interaction Behavior of Highway Guardrail Posts," Transportation Research Record 970, 1983

TTI Test No. 205421-1, Texas Transportation Institute, University Texas A&M System, College Station, TX, November 16, 1995.

Bullard, DL Jr, WL Menges, and DC Albertson, "DNCHR Report 350 Compliance Test 3-11 of the Modified G4(1S) Guardrail with Timber Blockouts," TTI Project No. 405421-1, Texas Transportation Institute, Texas A&M University System, College Station, TX, January 1996.

Mak, KK, RP Bligh, and WL Menges, "Crash Testing and Evaluation of Existing Guardrail Systems," TTI Project No. DTFH61-89-C-00089, Texas Transportation Institute, Texas A&M University System, College Station, TX, December 1995.

Sicking, DL, JR Rohde, and JD Reid, "Development of a New Guardrail System," Interim Report to Buffalo Specialty Products, Midwest Roadside Safety Facility, University of Nebraska-Lincoln, April 15, 1997.

Coon, BA, "Development of Crash Reconstruction Procedures for Roadside Safety Appurtenances," Ph.D. Dissertation, Civil Engineering Department, University of Nebraska – Lincoln, August, 2003.

APPENDIX B

Reconstruction Techniques for Guardrail End Terminals

1 INTRODUCTION

Flexible longitudinal barriers protect errant vehicles from roadside hazards, redirecting the vehicles and minimizing the probability of serious injury. The introduction of these barriers onto the highway requires that the ends of the barriers be protected in an effective manner. Guardrail impacts are the third most common fixed-object impact, after only trees and embankments [1, 2]. Left untreated, the ends of the barrier are able to pierce into the occupant compartment. A particular type of guardrail end treatment, known as a "turndown," has been found to be responsible for 41% of all fatal guardrail crashes, whereas they constituted only 20% of nonfatal guardrail impacts [3].

Because of the frequency in which end terminals are involved in crashes, reconstruction of the impacts is critical. Crash reconstruction is the effort to determine, from whatever information is available, how the crash occurred. Crash reconstruction includes utilizing engineering concepts such as conservation of momentum and conservation of energy to estimate initial vehicle conditions and how the vehicle progressed through the crash.

The importance of crash reconstruction is two-fold: first, designers and testers of roadside safety devices must be certain they are designing and testing for real-world conditions. Secondly, departments of transportation must determine the impact severity of these impacts to determine appropriate warrants, maximizing the benefit-cost ratio for limited resources.

Guardrail end terminals are separated into two categories: energy-absorbing terminals and non-energy-absorbing terminals. Energy-absorbing terminals attenuate energy to slow the impacting vehicle. Non-energy-absorbing terminals act are designed to offer little resistance during end-on impacts and to create tension in the guardrail so that the system can redirect vehicles beyond the length-of-need.

This paper focuses on the identification of the numerous types of guardrail terminals and develops a technique for determining the initial velocity for impacts with guardrail end terminals based upon full-scale test results. However, care must be taken when comparing full-scale crash tests, which occur on ideally installed end terminals under optimal conditions, to real-world crashes. A second publication will focus on appropriate reconstruction techniques for crash cushions.

1.1 Crash Reconstruction Overview

In order to determine impact conditions, crash reconstructions must be performed. Vehicle mass, run-out trajectory, and the resulting deformed geometry of the barrier can generally be measured after the impact. However, the impact velocity must be estimated through crash reconstruction techniques.

For energy-absorbing guardrail end terminals, reconstruction is performed using conservation of momentum during the initial portion of the impact where the terminal impact head is accelerated by the impacting vehicle. Soon after the impacting vehicle and terminal impact head have reached the same velocity, the terminal impact head begins attenuating energy through a kinking, bursting, crushing or extruding process depending on the terminal type. The average force required to attenuate the energy was determined through literature; accelerometer traces, and traditional engineering dynamics equations. This average force can be used to determine estimated energy dissipations for any given deflection, since the energy attenuated is the area underneath the force-deflection curve.

For non-energy-absorbing terminals, conservation of momentum equations and the rotational and fracture energy of posts are used to estimate impact velocity. These terminals do not absorb significant amounts of energy during impact and are designed to protect the passenger compartment from being penetrated by the guardrail and to eliminate extreme decelerations.

2 HISTORY OF GUARDRAIL END TREATMENTS

Safe and economical methods of termination of strong-post W-beam guardrail have been a critical concern for more than three decades [4]. Early W-beam barriers were constructed with an untreated blunt end that was capable of piercing through impacting vehicles and causing serious injuries and/or fatalities.

In order to address this problem, guardrail turndowns were used, bending the guardrail into the earth or onto a concrete footing [5]. Unfortunately, small vehicles impacting these turndowns have a tendency to roll over. Because of this, another method of addressing the guardrail end problem was desired.

Development of several new end treatments occurred in the 1980's. These included the Safety End Treatment (SENTRE), the Transition End Treatment (TREND), the Vehicle Attenuating Terminal (VAT) and its second generation (CAT), the Controlled Release Terminal (CRT), the Eccentric Loader Terminal (ELT), the Modified Eccentric Loader Breakaway Cable Terminal (MELT), as well as modifications to the turndown and Breakaway Cable Terminal (BCT).

With the adoption of NCHRP Report 230 and its update, Report 350, slotted rail terminals (the Reduced Offset Slotted System (ROSS), the Slotted Rail Terminals (SRT) and the SRT-HBA) and the REdirective Gating End Terminal (REGENT) were developed. While these terminals met increasingly stringent test criteria, they were considered non-energy-absorbing and merely protect the vehicle from intrusion of the guardrail and severe impacts from full line posts rather than attempting to attenuate significant amounts of energy.

The Guardrail Extruder Terminal (GET) was the first in a family of energy-absorbing terminals that deformed the W-beam guardrail itself rather than adding crash cushions or other implements to the guardrail system. The energy-absorbing terminal concept consisted of a terminal head that dissipated energy through extruding the guardrail. New concepts, including kinking and cutting the W-beam, were then developed to safely attenuate the impact energy. These terminals were the Beam Eating Steel Terminal (BEST), the Sequential Kinking Terminal (SKT), and the FLared Energy Absorbing Terminal (FLEAT). End terminals for box-beam guardrail include the Wyoming Box-beam End Terminal (WY-BET) and the Box beam bursting Energy Absorbing Terminal (BEAT).

Approximately nineteen guardrail end treatments are currently approved under NCHRP Report 350 for usage on the National Highway System (NHS). The similarity in appearance among end treatments can cause confusion in determining the appropriate methods and values to be used to reconstruct a crash.

3 ENERGY ABSORBING TERMINAL IDENTIFICATION

Energy-absorbing end terminals rely on an impact head to kink, cut, or extrude the guardrail; in the case of box-beam guardrail, the terminal either bursts the beam or crushes pultruded fiberglass/epoxy tubes within the beam. There are six unique designs of energy absorbing end terminals: the BEAT family, the BEST, the ET-2000 family, the FLEAT family, the SKT, and the WY-BET. These terminals have distinctly different force-deflection behaviors, as well as significantly different masses, which must be differentiated before performing a reconstruction.

Each of the energy-absorbing terminals is identified by its distinguishing characteristics. The appearance of the deformed guardrail section, which is unique to each end terminal, is also examined.

3.1 Box Beam Bursting Energy Absorbing Terminal (BEAT)

Produced by Road Systems, Inc., the BEAT is designed as an energy-absorbing end terminal for standard 152x152x4.8-mm (6x6x3/16-in.) box beam barriers, which are weak-post barrier systems that are commonly used in regions that receive heavy snow [6, 7, 8, 9, 10]. The BEAT head weighs approximately 59 kg (130 lb) with a 508x508 mm (20x20 in.) front plate and overall length of 1.275 m (50.3 in.). The BEAT head is shown in Figure 1a. An installed BEAT is shown in Figure 1b.

The BEAT system is approximately 4.3 m (14 ft) long from its nose to the beginning of the standard box-beam guardrail. The BEAT may be installed parallel to the roadway or offset from traffic on a 50:1 flare rate.

As the impacting vehicle drives the BEAT head down the rail, the BEAT head assembly slides inside the box beam. As the head is pressed into the tubing, the tubing “bursts” apart into a curl, as shown in Figure 1c. This is the BEAT’s method of dissipating energy – splitting the beam apart at the corners and then curling the metal.

a) BEAT Terminal Head

b) Installed BEAT Terminal System

c) Bursted BEAT Box Beam

d) BEAT Median Terminal

e) BEAT Single-Sided Crash Cushion

f) BEAT Bridge Pier Protection System

Figure 19. Box Beam Bursting Energy Absorbing Terminal (BEAT).

3.1.1 BEAT Median Terminal (BEAT-MT)

The BEAT-MT is a terminal used for median box-beam guardrail systems, as opposed to the BEAT, which is used for box-beam guardrail systems installed along the roadside. The BEAT-MT uses the same energy-absorbing technique as that of the BEAT described previously. The BEAT-MT is shown in Figure 1d.

The BEAT and the BEAT-MT have many interchangeable parts – the main difference is that the I-beam posts are mounted underneath the box beam rail for the BEAT-MT and behind the rail for the roadside BEAT [11]. In addition, a sleeve is required to connect the 152x152-mm (6x6-in.) terminal tubing section to the 152x203-mm (6x8-in.) median barrier tubing. Finally, the BEAT-MT utilizes a tether cable behind the BEAT head to prevent the head from becoming a projectile during reverse hits.

3.1.2 BEAT Single Sided Crash Cushion (BEAT-SSSC)

The BEAT-SSCC is designed to attach directly to bridge abutments, rigid barrier ends and many bridge rails, as shown in Figure 1e [12]. The BEAT-SSCC is approximately 8.4 m (27.6 ft) from its nose to the beginning of the standard box-beam guardrail. The BEAT-SSCC is included as a guardrail terminal because of its similarity to the other BEAT designs and its implementation requires a run of box-beam rail as its energy attenuator. The BEAT-SSCC is similar in design concept to the BEAT and the BEAT-MT except for the following components:

A “Stage 1” energy absorber consisting of 152x152x3.2-mm (6x6x1/8-in.) box beam rail

(Identical to the BEAT)

An additional “Stage 2” energy absorber consisting of 152x152x4.8-mm (6x6x3/16-in.) box

beam rail

Eight breakaway steel posts

An end section for transitioning the BEAT-SSCC to a concrete barrier

3.1.3 BEAT Bridge Pier Protection System (BEAT-BP)

The BEAT-BP is designed to surround bridge abutments, rigid barrier ends and many bridge

rails, as shown in Figure 1f [13]. Specifically, no intermediate length-of-need is required

between the terminal system and the rigid hazard which it protects.

3.2 Beam Eating Steel Terminal (BEST)

Manufactured by Interstate Steel Corporation, the BEST is designed to fit onto standard W-beam guardrail. The BEST-350 head weighs approximately 125 kg (275 lb) with its 508x610 mm (20x24 in.) front plate. The head has an overall length of 1632 mm (64.25 in.) [14, 15, 16, 18, 19, 20, 21]. The BEST terminal is shown in Figure 2a.

The BEST system is approximately 11.4 m (37.5 ft) long from the first post to the beginning of the standard W-beam guardrail. It can be installed parallel to the roadway or offset from traffic on a 50:1 flare rate.

The BEST impact head uses three high-strength steel cutting teeth to cut the rail section into four ribbons of steel, as shown in Figure 2b. These four ribbons of steel then exit the backside of the head.

The first rail section is 15.2 cm (6 in.) longer than a standard 7.62-m (25 ft) guardrail section and uses ten bent tabs to lock into the cable anchor bracket. The additional length in the rail section provides three notches at the front end to line up with the cutting teeth of the impact head. It is one of three impact heads that has a center stiffener plate between the top and bottom plates.

a) Installed BEST System.

b) BEST System After Impact.

Figure 20. Beam Eating Steel Terminal (BEST-350)

3.3 Extruder Terminal 2000 Family (ET-2000)

Marketed and produced by Trinity Industries, the ET-2000 family consists of the ET-2000, the ET-2000 PLUS, and the LET [22, 23, 24, 25, 26, 27, 28, 29, 30, 31, 32, 33, 34, 35, 36, 37, 38, 39, 40, 41, 42]. The ET-2000 head weighs approximately 122 kg (268 lb) and its front plate measures 508x521-mm (20x20.5-in.). The terminal head has an overall length of 1.28-m (50.25-in.). The ET-2000 is shown in Figure 3a. The LET is identical to the ET-2000 except for changes in the guardrail post configuration and the offset block at Post 2.

The ET-2000 system is approximately 11.4 or 15.2 m (37.5 or 50 ft) long from the first post to the beginning of the standard W-beam guardrail. The ET-2000 may be installed parallel to the roadway or offset from traffic on a 50:1 flare rate.

The ET-2000 PLUS head weighs approximately 79 kg (175 lb) and its front plate measures 381x711-mm (15x28-in.). The terminal head has an overall length of 1.44-m (56.75-in.). The

ET-2000 PLUS is shown in Figure 3b. The ET-2000 PLUS uses the same energy dissipation method as the ET-2000 and the LET, but uses a different faceplate, is lighter, and has several other minor modifications. Both the ET-2000 and the ET-2000 PLUS use a six-hole cable anchor bracket locks into the into the first rail section.

The ET-2000 family's impact head has a narrowing throat area that extrudes the W-beam guardrail. This is achieved in two stages: a squeezing section and a bending section. Upon impact, the ET-2000 extrudes the guardrail away from the traveled way, as shown in Figure 3c.

a) ET-2000

b) ET-2000 PLUS

c) ET-2000 PLUS After Impact.

Figure 21. ET-2000 Terminal Family.

3.4 FLared Energy Absorbing Terminal (FLEAT)

Manufactured by Road Systems, the FLEAT head weights approximately 54.5 kg (120 lb) and its front plate measures 357x497 mm (14x19.6 in.). The terminal head has an overall length of 1557 mm (61.3 in.). The FLEAT is the lightest energy-absorbing terminal and is the only flared energy-absorbing terminal currently available [43, 44, 45, 46, 47, 48, 49, 50, 51, 52, 53, 54, 55, 56]. The flare used by the FLEAT is straight (as opposed to a parabolic curve) and is flared anywhere from 0.76 m to 1.2 m (2.5 to 4 ft) for the TL-3 design and 0.51 m to 0.81 m (1.7 to 2.7 ft) for the TL-2 design. The FLEAT is shown in Figure 4a.

The FLEAT system is approximately 11.4 m (37.5 ft) long from the first post to the beginning of the standard W-beam guardrail. The FLEAT is installed with a 0.762 to 1.219-m (2.5 to 4-ft) offset. A TL-2 design of the FLEAT system is approximately 7.62 m (25 ft) long from the first post to the beginning of the standard W-beam guardrail installed at a 0.51 to 0.81-m (1.7 to 2.7-ft) offset.

The FLEAT uses a bent deflector plate to sequentially kink the W-beam against the direction of the rail corrugations, as shown in Figure 4b. The FLEAT is the only system that deforms the guardrail toward the roadway. However, the kinking process prevents the rail from going out into the roadway by coiling the rail back towards the guardrail. It is one of three impact heads that has a center stiffener plate between the top and bottom plates.

The cable anchor uses a V-shaped bracket with four hooks on either side that lock into special bolts attached to the first rail section. The first rail section also has five slots along the top and bottom corrugations and, in some cases, three additional slots in the valley of the rail, making it completely interchangeable with the SKT first rail section.

The distinct shape of the deformed W-beam is shown in Figure 4c. The curling of the guardrail against the corrugations toward the roadway, in addition to the notable kinking that occurs during impact, is distinctive and unmistakable.

3.5 FLEAT Median Terminal (FLEAT-MT)

The FLEAT-MT is a terminal used for median W-beam guardrail systems, as opposed to the FLEAT, which is used for W-beam guardrail systems installed along the roadside. The FLEAT-MT uses the same energy-absorbing technique as that of the FLEAT described previously. The FLEAT-MT is shown in Figure 4b.

The FLEAT-MT is identical to the FLEAT system except that in severe impacts a second FLEAT head becomes active [57, 58, 59, 60]. The FLEAT and FLEAT-MT use the same impact head, rail, and anchor system.

a) FLEAT

b) FLEAT-MT

c) FLEAT System After Impact.

Figure 22. FLared Energy Absorbing Terminal (FLEAT-350).

3.6 Sequential Kinking Terminal (SKT 350)

Manufactured by Road Systems, Inc, the SKT head weighs approximately 78 kg (172 lb) and has a square front plate of 508x508 mm (20x20 in.). The end terminal head has an overall length of 2.11 m (83.3 in.) [**Error! Bookmark not defined.**, **Error! Bookmark not defined.**, 61, 62, 63, 64, 65, 66, 67, 68, 69,70]. Similar to the FLEAT, a deflector plate is used to sequentially kink the rail. However, the SKT kinks the rail away from the traveled way. The SKT 350 is shown in Figure 5a.

The SKT system is approximately 13.33 m (43.75 ft) long from the first post to the beginning of the standard W-beam guardrail. The SKT may be installed parallel to the roadway or offset from traffic on a 50:1 flare rate.

As with the FLEAT, the SKT leaves a unique kinking pattern in the rail, as shown in Figure 5b. This allows the determination of which impacting head was involved in a crash when the head is absent from the crash scene or is not visible in the photographic evidence. In comparison with the ET-2000, which leaves a smooth, flattened guardrail, both the SKT and the FLEAT leave a kinked pattern in the deformed guardrail. As mentioned before, the FLEAT kinks the guardrail toward the traveled way while the SKT kinks the guardrail away from the traveled way.

The SKT uses a rail section identical to that used for the FLEAT. The SKT is one of three impact heads that has a center stiffener plate between the top and bottom plates.

a) Installed SKT-350 System

b) After-Crash SKT-350 System

Figure 23. SKT-350, Sequential Kinking Terminal.

3.7 Wyoming Box beam End Terminal (WY-BET-350)

The Wyoming Box beam End Terminal, marketed by Trinity Industries, crushes fiberglass/epoxy composite tubes to dissipate energy [71, 72, 73]. The barrier uses standard 152x152x4.8-mm (6x6x3/16-in.) box beam mounted on S3x5.7 steel posts spaced 1.83 m (6 ft) apart. The WY-BET system is shown in Figure 6a. The WY-BET system is approximately 15.2 m (50 ft) long from the first post to the beginning of the standard W-beam guardrail. The WY-BET may be installed parallel to the roadway or offset from traffic on a 10:1 flare rate.

The telescoping tube terminal concept involves placing an oversized outer tube on the end of the standard box-beam rail element. A faceplate with a shortened, 914-mm (3 ft) piece of standard box beam is placed into the upstream end of the oversized outer tube.

During impact, the faceplate captures the impacting vehicle. The faceplate and shortened box beam slide backwards, fracturing the first post and releasing the tension in the cable. The faceplate then comes to rest against the outer tube, driving it downstream and crushing the composite tubes inside. The impacted system is shown in Figure 6b.

The WY-BET uses two “stages” of energy absorption obtained by using two stiffness levels of pultruded Fiber Reinforced Plastic (FRP) tubes. This allows for an increased energy-absorbing level for higher-severity impacts.

3.7.1 WY-BET Median Barrier (WY-BET (MB))

The WY-BET (MB) is a terminal used for median box-beam guardrail systems. The WY-BET (MB) uses the same energy-absorbing technique as that of the WY-BET described previously.

Whereas the WY-BET is used for box-beam guardrail systems installed next to the roadway, the WY-BET (MB) is used in median barrier applications.

The WY-BET and the WY-BET (MB) have many interchangeable parts. The main difference is that the system has the I-beam posts mounted underneath the box beam rail for the WY-BET (MT) and behind the rail for the roadside WY-BET. In addition, a sleeve is required to connect the 152x152-mm (6x6-in.) terminal tubing section to the 152x202-mm (6x8-in.) median barrier tubing and the WY-BET (MB) has a soil plate at the bottom of the first foundation tube or uses the alternate concrete foundation.

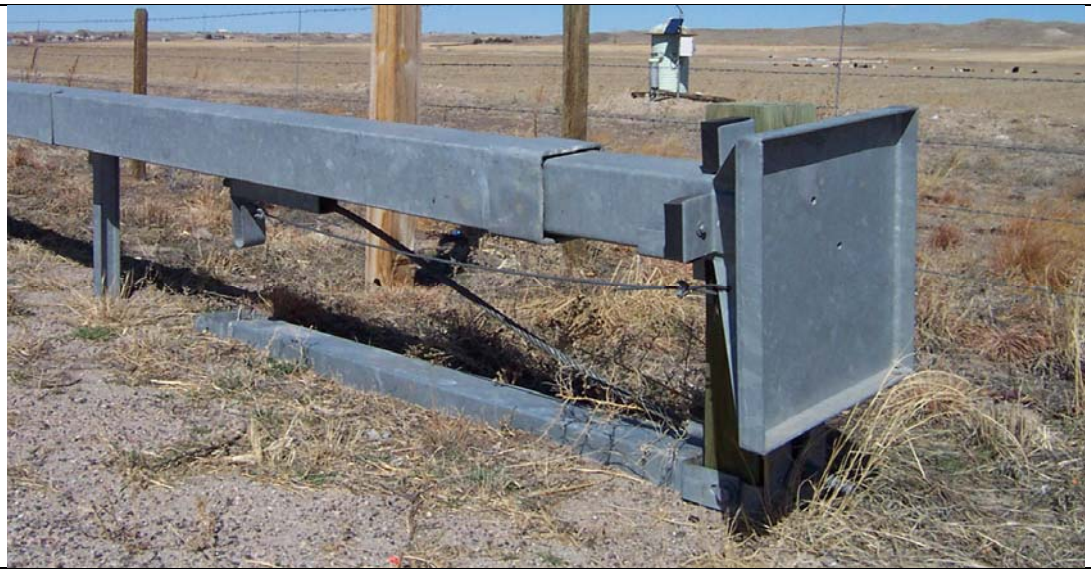

a) Installed WY-BET System

b) After-Crash WY-BET System

Figure 24. WY-BET, Wyoming Box Beam End Terminal.

4 PHYSICS OF ENERGY-ABSORBING TERMINALS

In an impact with a energy-absorbing guardrail end terminal, the acceleration of the impact head followed by the deformation of the rail element as the head is pushed down the rail dissipates the majority of the energy. During the initial impact, the vehicle contacts and accelerates the terminal head, fracturing the first Breakaway Cable Terminal (BCT) post, and releasing the tension in the rail. As the vehicle and terminal head reach the same velocity, the terminal head is driven down the guardrail, dissipating energy by either deforming the rail element or by crushing composite tubes, in the case of the WY-BET, in addition to fracturing posts. The terminal either comes to rest in contact with the end terminal or has a post-impact trajectry with possible subsequent impacts. These areas are examined individually, beginning from the point of impact to where the vehicle departs the rail.

4.1 Acceleration of Terminal Head

Either conservation of energy or conservation of momentum can be used to analyze the initial portion of the impact when the terminal head and vehicle eventually obtain the same velocity. While momentum is always conserved, kinetic energy is almost always not conserved in real-world impacts. If conservation of energy is applied, energy losses due to vehicle crush, friction, the deformation of terminal components, *et cetera*, must be determined. If conservation of momentum is applied and the impact is considered perfectly plastic, these energy losses do not need to be explicitly calculated.

Conservation of momentum demands that the total momentum must be the same before and after the collision. In the analysis of a one-dimensional collision, consider two objects with masses

M_1 and M_2 and initial velocities V_1 and V_2. After the collision, the objects will have new velocities $V'_1$and V'_2.

$$M1V1 + M2V2 = M1V'1 + M2V'2 \quad (1)$$

Conservation of kinetic energy implies that the total kinetic energy before and after the impact would be conserved. The combined velocity, V_c, can then be determined. Where two object reach the same final velocity, V_c, and applying both conservation of kinetic energy and conservation of momentum yields Equation 2.

$$\frac{1}{2} M1V^2 1 + \frac{1}{2} M2V^2 2 = \frac{1}{2} (M1 + M2) V^2 c \quad (2)$$

However, most real-world collisions are neither perfectly elastic (kinetic energy is conserved) nor perfectly inelastic (all available crush energy is dissipated as crush energy) but partially elastic. This means that a certain portion of the kinetic energy is lost to the system in the form of crush, *et cetera*. The ratio of the velocities before and after the impact is known as the coefficient of restitution, e.

$$e = \frac{V1' - V2'}{V2 - V1} \quad (3)$$

A perfectly plastic, or inelastic, collision has a coefficient of restitution of e = 0. An example of this would be two lumps of clay impacting each other. The two lumps of clay don't bounce at all, but stick together. A perfectly elastic collision has a coefficient of restitution of e = 1. An example of this is two glass marbles bouncing off each other. Conservation of kinetic energy exists only when e = 1.

As the vehicle impacts the terminal, there is a certain amount of elastic rebound experienced by the vehicle. This elastic rebound is caused by a non-zero coefficient of restitution. However, if the coefficient of restitution between the impact head and the vehicle is sufficiently low, it can be assumed that the collision is perfectly plastic with a high degree of accuracy. As the coefficient of restitution increases, conservation of energy must be used to examine the impact.

For high-speed frontal impacts, the coefficient of restitution is relatively low, as shown in Figure 7 [74]. This implies that the almost all of the kinetic energy is transformed into crush energy and that there is little elasticity to a frontal vehicle impact.

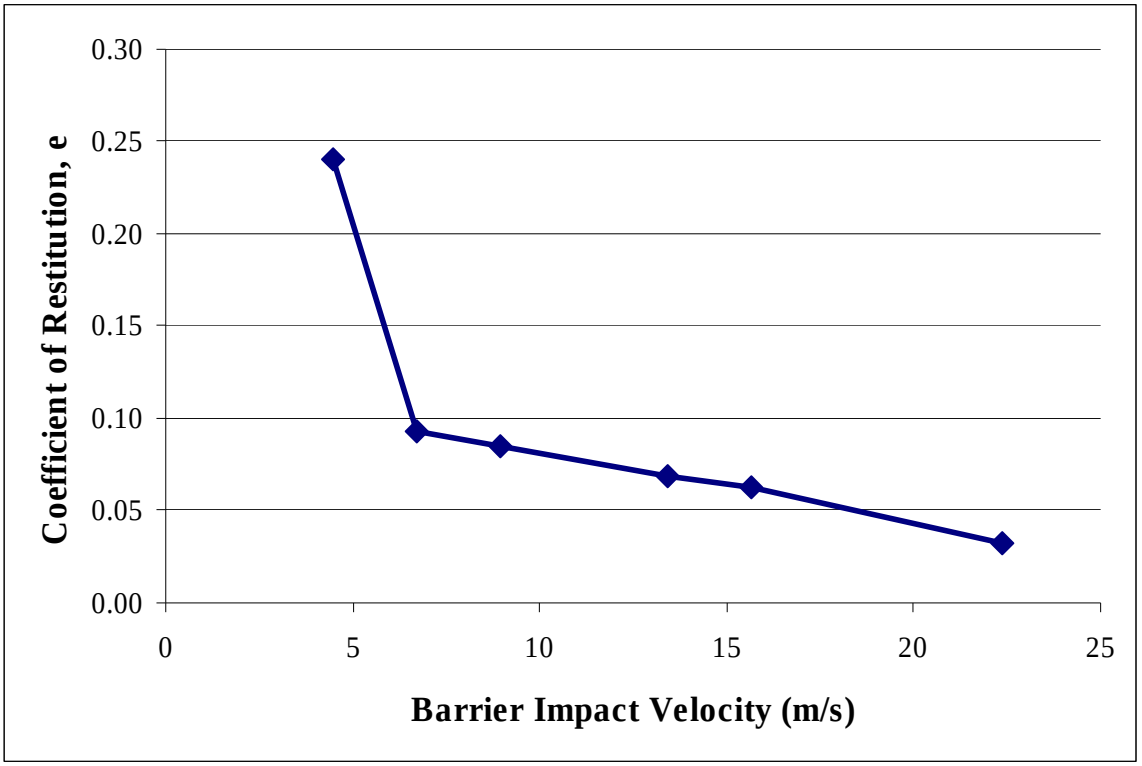

Figure 25. Coefficient of Restitution for Frontal Impacts [75].

Since the coefficient of restitution is relatively small, conservation of momentum is used, and the elastic restoration of vehicle crush during an impact with the terminal head may be

neglected. Equation 4 gives the combined velocity of the vehicle and head immediately after impact, V_c.

$$Vc = \frac{Vi * Mvehicle + Vhead * Mhead}{Mvehicle + Mhead} \quad (4)$$

where V_i is the initial velocity of the impacting vehicle

$M_{vehicle}$ is the mass of the impacting vehicle

V_{head} is the velocity of the end terminal head

M_{head} is the mass of the end terminal head

Initially, the head is at rest and must be accelerated. Given that the initial velocity of the impact head is zero, Equation 4 can be solved for the initial velocity of the vehicle, V_i, as shown in Equation 5.

$$Vi = \frac{Vc * (Mvehicle + Mhead)}{Mvehicle} \quad (5)$$

The combined velocity of the terminal head and vehicle, V_c, can be solved in terms of kinetic energy:

$$Vc = \sqrt{\frac{2\ KEc}{Mvehicle + Mhead}} \quad (6)$$

where KE_c is the corresponding combined kinetic energy.

4.2 Vehicle Crush Energy

Vehicle crush energy is generally determined using crush stiffness coefficients [76]. These stiffness coefficients are identical in concept to a spring coefficient, where deformation is related to impact force in a monotonically increasing manner. Since, the impacting vehicle encounters the highest force levels while accelerating the terminal head, the majority of the vehicle crush occurs during this stage. Additional forces are absorbed elastically and are not dissipated through vehicle deformation. Since the impact is considered a perfectly plastic reaction, the vehicle crush energy is taken into account using conservation of momentum as described in Section 4.1.

4.3 Energy Dissipation by the Rail

After the departing velocity (and corresponding kinetic energy) has been calculated, the energy dissipated by the terminal's specific energy-dissipating method must be found. For this, the area underneath the force-deflection curve representing the deformation of the rail is used. Since the deformation force levels of the guardrail end terminals are relatively constant, the energy dissipated by deformation of the rail, E_{rail}, is equal to the product of the average force required to displace the head along the rail, F_{ave}, times the distance the head is displaced, d. This relationship is given as:

$$Erail = Fave \cdot d \tag{7}$$

A guardrail end terminal with an average force of 67 kN (15 kips) displaced for a total of 2 m (78.4 in.) dissipates 134 kJ (98.4 kip-ft) of energy. Although force and displacement are vectors, the energy dissipated through work is a scalar value.

Ranges of force levels were determined through the reconstruction of full-scale crash testing and, when available, the examination of the corresponding accelerometer traces. Since the forces from the post fractures and acceleration of the system are inherently included in the accelerometer trace, they do not need to be accounted for individually. The values for the physical and mechanical properties of the end terminals are shown in Table 1.

Table 8. Terminal Head Summary.

	Faceplate Size mm (in.)	Head Mass kg (lb)	Head Length m (in.)	Average Force kN (kips)
BEAT	508x508 (20x20)	59 (130)	1.21 (83.3)	87 (20) to 122.5 (32.1) (Stage 1) 129 (29) (Stage 2)
BEAT-MT				
BEAT-SSCC*				
BEST-350 [**Error! Bookmark not defined.**]	502x610 (20x24)	125 (275)	1.63 (64.25)	83.4 (18.7) to 100 (22.5)
ET-2000	508x521 (20x20.5)	122 (268)	1.28 (50.25)	53.2 (12) to 94.7 (21.3)
ET-2000 PLUS	381x711 (15x28)	79 (175)	1.44 (56.75)	
FLEAT-350	357x497 (14x19.6)	54.5 (120)	1.56 (61.3)	60.2 (13.5) to 74.5 (16.7)
FLEAT-350 MT	357x497 (14x19.6)	54.5 (120)	1.56 (61.3)	First Head: Identical to FLEAT-350 Both Heads: 120.4 (17) to 149 (33.4)
REGENT	457x457 (18x18)	21 (46)	N/A	N/A
SKT-350 [**Error! Bookmark not defined.**]	508x508 (20x20)	78 (172)	2.11 (83.3)	46.7 (10.5) to 67.6 (15.2)
WY-BET*	508x508 (20x20)	57 (125)	0.96 (37.875)	Stage 1: 80.1 (18) to 95.27 (21.4) Stage 2: 155 (35)
WY-BET (MB)*				

* The BEAT-SSCC and the WY-BET both have two stages

4.5 Energy-Absorbing End Terminal Physical Properties

Since conservation of momentum is used to account for the energy dissipation during the initial acceleration of the end terminal head, the mass of the end terminal must be known.

Terminals masses were measured in the field, including the welds and the galvanizing required on all of the terminal heads. The end terminal masses are listed in Table 1.

5 ENERGY-ABSORBING TERMINAL RECONSTRUCTION PROCEDURE

In order to reconstruct an end terminal impact, the mass of the impacting vehicle, the amount of rail fed through the terminal, and the terminal type must be determined. Additionally, if the terminal did not stop the vehicle, sufficient information to reconstruct the departure velocity must be obtained.

The reconstruction is based on conservation of momentum for the initial portion of accelerating the terminal head. As the head is driven down the guardrail, conservation of energy is implemented. The procedure reconstructs the crash in reverse order of the actual crash.

1. The velocity at the point the vehicle departed from the rail must be determined. This point occurs when the vehicle loses contact with the end terminal or when the terminal ceases to dissipate energy in the manner in which it was designed. Reconstruction of the departure velocity can be achieved through conventional accident reconstruction techniques [**Error! Bookmark not defined.**]. This velocity is then converted to kinetic energy using Equation 8. This is important since events after departure are not interactions with the terminal.

2. The energy absorbed by the rail is calculated. This is determined using Equation 7 and the average force levels given in Table 1. This yields the total amount of energy attenuated through deformation of the guardrail and the fracturing of posts.
3. The departing vehicle energy found in Step 1 is added to the total deformation energy found in Step 2. This is the total energy of the vehicle and the terminal head before the initiation of the rail deformation, KE_c.
4. The velocity of the terminal head and vehicle are calculated using Equation 6. This yields the velocity of the vehicle and the terminal head before the initiation of the rail deformation.
5. Conservation of momentum is then applied to calculate the velocity of the impacting vehicle using Equation 5.

5.1 Sample Reconstruction

In order to clarify units and to detail the reconstruction procedure, a reconstruction of a full-scale crash of a FLEAT system run by the Southwest Research Institute is detailed below [**Error! Bookmark not defined.**]. The test, designated as type 3-30 in NCHRP Report 350, is a compliance test for a Test Level 3 (TL-3) end terminal.

Test 3-30 utilizes an 820-kg small car with an uninstrumented dummy. The test vehicle had a gross mass of 906 kg (1998 lb). The impact was end-on at 0° and 100 km/h (62.2 mph) with a ¼-car offset. The guardrail end terminal stopped the vehicle after deforming a total 5.48 m (18 ft) of guardrail.

1. First, the departing velocity of the vehicle must be estimated. In this case, the departing velocity was zero. If a vehicle departs the barrier, its departure velocity

must be found and converted to kinetic energy. However, in this case, $KE_{departing} = 0$.

2. The amount of energy dissipated by the terminal head on the system is equal to the force required to drive the head multiplied by the distance the head was driven. For a FLEAT head, the force levels are between 60.2 and 67 kN (13.5 and 15 kips). The average of 63.6 kN (14.25 kips) appears reasonable. For a deformed rail section of 5.48 m (18 ft), this yields 348.5 kJ (257 kip-ft).
3. The two energies found in Steps 1 and 2 are added to find the initial kinetic energy of the impacting vehicle and guardrail terminal immediately before the terminal head began to deform the guardrail. In this case,

$$KEc = KEdeparting + Erail = 0\ kJ + 348.5\ kJ = 348.5\ kJ \quad (9)$$

4. This value is converted to a velocity for the combined terminal head and vehicle.

$$Vc = \sqrt{\frac{2\ KEc}{Mvehicle + Mhead}} = \sqrt{\frac{2 * 348.5\ kJ}{906\ kg + 54.5\ kg}} = 26.9\ m/s = 97\ km/h \quad (10)$$

5. Conservation of momentum is applied to determine the initial velocity of the impacting vehicle. Using Equation 5, this yields:

$$Vi = \frac{Vc * (Mvehicle + Mhead)}{Mvehicle} = \frac{97\ km/h * (906\ kg + 54.5\ kg)}{906\ kg} = 102.8\ km/h \quad (11)$$

This estimate varies less than 3% from the physical test, which impacted at 100 km/hr. This is an extremely accurate estimate of the initial velocity of the impacting vehicle.

5.2 Comparison of Results

Reconstructions were performed for all available energy-absorbing end terminals crash test data. Typical results are shown in Table 2.

Table 9. Typical Results from End Terminal Reconstructions.

Terminal Type	Test Identifier	Velocity (km/h)		Rail Fed (m)	Reconstructed Velocity (km/h)		Percent Variation due to Variation in Force Levels
		Impact	Exit		Min. Force Level*	Max. Force Level*	
BEAT	SSC-1	99.0	0.0	6.91	89	100	12%
BEST	BEST-9	101.0	0.0	8.91	101	111	10%
ET-2000	400001-XT13	98.9	0.0	7.50	74	99	33%
ET-2000 PLUS	400001-LET1	100.3	0.0	11.60	91	122	34%
FLEAT	FLEAT-1	100.0	0.0	5.48	100	111	11%
SKT	SKT-6	100.1	81.0	4.11	97	103	3%
WY-BET	7202-3A	93.5	0.0	2.70	86	94	9%

*Velocities calculated using the minimum and maximum force levels as listed in Table 1.

Significant variation was found in the ET-2000 family, with a 31 km/h envelope between the low and the high velocity estimates. The differences may be due to the narrowness of the ET-Plus impact head. The narrow impact head can allow the front bumper to wrap around the impact plate and restrict the outlet for the flattened W-beam rail. However, these reports and corresponding accelerometer traces needed to explain the theory were not made available to the authors.

It should be noted that the range of force levels was obtained through the limited number of crash tests information available. These values, which vary up to 34% from each other, may or may not be representative of the population of each end terminal head type.

6 NON-ENERGY-ABSORBING END TERMINAL

Guardrail end terminals not specifically designed to dissipate impact energy still attenuate some energy through the rotation or fracture of guardrail posts and through barrier deformation. Two end terminals of this type are currently approved under NCHRP Report 350: (1) the SRT-350 and (2) the REGENT. The REGENT terminal is not covered in this paper due to an extremely low number of units in service.

In developing a crash reconstruction procedure for the SRT-350, it is critical to determine what information will be available at the scene to reconstruct the crash. This information includes vehicle damage, the number of fractured posts, the deflection of non-fractured posts, the number of buckled slots, and the amount of rail damaged. Additionally, identifying the specific design of the SRT is important.

Statistical analysis was performed on all available full-scale crash data in order to determine a relationship between the post-crash information that would be available at a typical crash site and the impact velocity. Conservation of energy was used to determine energy losses of individual system components.

It was determined that differences between design iterations of the SRT, including the SRT-75, SRT-100, ROSS, and the SRT-350, made a general correlation for all of the designs of

the SRT difficult due to the differences in energy dissipation in the barrier. However, a methodology relating the amount of post fracture energy, which is dependent on the number of fractured posts, was identified.

Longitudinal and lateral acceleration of the guardrail was also examined to determine energy losses. However, this energy was not considered due to the significant variations in the energy dependent on the eccentricity of the impact, which is dependent on the impact angle.

6.1 SRT-Slotted Rail Terminal

The Slotted Rail Terminal, SRT, is a gating end terminal marketed by Trinity Industries, and shown in Figure 8 [78, 79, 80, 81, 82, 83, 84, 85,86]. The slotted end terminal uses longitudinal slots in the W-beam rail to reduce its dynamic buckling strength sufficiently to accommodate small car impacts while maintaining sufficient tensile capacity in the barrier. The SRT-350 is shown in Figure 8.

When impacted head-on, the first BCT post fractures and releases the cable, removing tension from the system. The slotted rail buckles out of the way, since the longitudinal slots have reduced the dynamic buckling strength of the rail. The vehicle then breaks the line posts as necessary to gate through the system into the clear zone behind the downstream guardrail.

Figure 26. SRT, Slotted Rail Terminal.

6.2 Vehicle Crush Energy

Vehicle crush energy may be determined through several different methodologies, including crush stiffness coefficients, finite element simulation, or any other appropriate methodology [87]. The effects of friction may also be significant, depending on impact conditions, particularly in impacts where the side of the vehicle maintains contact with the barrier for any significant distance.

6.3 Post Fracture Energy

In order to reduce the impact severity of end-on impacts with end terminals, modern designs incorporate breakaway posts. Two non-propriety designs are in common use: Breakaway Cable Terminal (BCT) posts and Controlled Release Terminal (CRT) posts.

BCT posts are 140x190 mm (5.5x7.5 in.) and have 63.5-mm (2.5-in.) holes located parallel to the roadway, with the bottom of the hole located at the top of their foundation tube. These holes act to weaken the posts for end-on impacts while still maintaining significant

strength for redirecting impacts. The foundation tube facilitates the removal of broken posts during repair.

CRT posts are 150x200 mm (6x8 in.) and have two 88.9-mm (3.5-in.) holes located parallel to the roadway with the center of the top hole located at the ground line. CRT posts are embedded directly into the ground without a foundation tube.

Typical 150x200-mm (6x8-in.) wood posts weigh between 25 and 35 kg (55 and 77 lb) for the standard 1.83-m (6-ft) lengths. Because BCT and CRT posts are designed to fracture at relatively low force levels rather than rotate in the soil, the more complex analysis of posts rotating in soil is not required. Mechanical properties of BCT and CRT posts are listed in Table 3.

Table 10. Standard Values for Breakway Posts.

Post Type	b (mm) (in.)	h (mm) (in.)	Minimum Area (10^3 mm^2) (in^2)	I_x (10^6 mm^4) (in^4)	I_y (10^6 mm^4) (in^4)	S_x (10^3 mm^3) (in^3)	S_y (10^3 mm^3) (in^3)
BCT	140 (5.5)	190 (7.5)	17.7 (27.5)	77.5 (186.2)	29.8 (69.3)	813.7 (49.7)	413.1 (25.2)
Solid			26.6 (41.3)	80.5 (193.4)	43.3 (104.0)	845.0 (51.6)	619.6 (41.2)
CRT	150 (6)	200 (8)	16.5 (27.0)	97.6 (234.6)	33.7 (81.0)	960.9 (58.6)	442.5 (27.0)
Solid			31.0 (48.0)	97.6 (256)	59.9 (144)	1048.8 (64)	786.6 (48)

Typical values for fracture energy about the weak axis of BCT posts have been found to vary between 4.5 kJ (3.3 kip-ft) and 17 kJ (12.5 kip-ft) [88]. Reasonable CRT posts have fracture energies about the weak axis between 5.0 kJ (3.8 kip-ft) and 19.2 kJ (14.2 kip-ft) [89]. Extensive research has been performed on the behavior of guardrail posts. Even “identical” posts can have significantly different fracture energies and these values can only be given as a range of energies rather than specific values.

The fracture or buckling energies for non-breakaway steel posts have also been researched extensively. In frozen soil, a guardrail post behaves much like it is embedded in a rigid foundation. Standard W150x13.5 (W6x9) steel posts dissipate approximately 7.6 kJ (5.6 kip-ft) when embedded in a rigid foundation [90].

For wooden posts, however, significant deviations in post energies have been observed [91]. The fracture energy of wooden posts in rigid foundations found in literature can vary from 1.4 kJ (1.03 kip-ft) to 15.4 kJ (11.36 kip-ft) [92,93]. However, a reasonable performance envelope would be 6.2 kJ (4.57 kip-ft) to 8.0 kJ (5.90 kip-ft) for DS-65 posts and 3.9 kJ (2.88 kip-ft) to 5.0 kJ (3.69 kip-ft) for Grade 1 posts [94, 95].

6.4 Post Rotational Energy

In most energy-absorbing terminals, guardrail posts are designed to fracture and this is taken into consideration with the average force levels. However, while rigid posts fracturing in soil dissipate limited amounts of energy, posts rotating in soil dissipate significantly more, on the order of between 10.2 kJ (7.5 kip-ft) and 29.1 kJ (21.4 kip-ft), as shown in Figure 9 [96,97]. Because of this increased energy dissipation, if considerable rotation in the soil has occurred, this must be noted and taken into account.

Significant effort has been undertaken to ascertain the force-deflection relationship of guardrail posts rotating in soil [98]. This is a difficult parameter to determine, since soil conditions significantly affect performance. For standard W150x13.5 (W6x9) steel posts rotating in soil, force-deflection and energy absorption relationships are shown in Figure 9 [99]. This research correlated well with a previous study of posts [100].

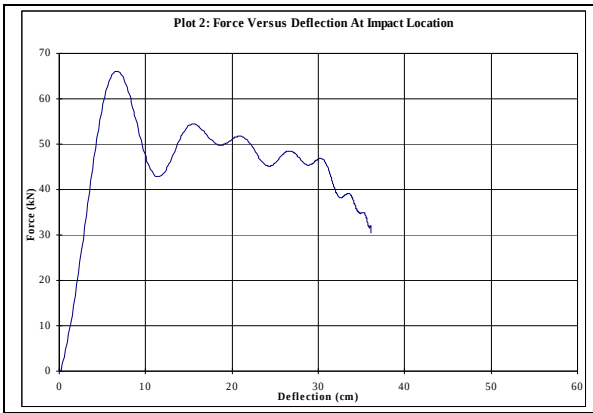

a) Force-deflection Relationship

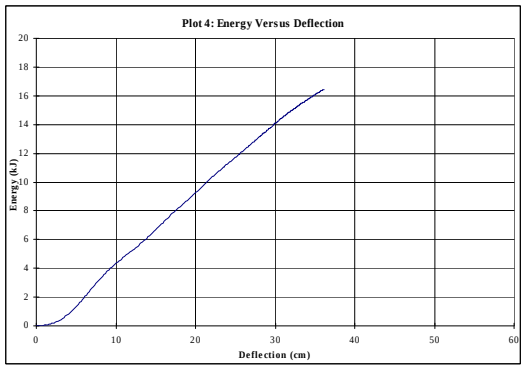

b) Energy-Deflection Relationship

Figure 27. Post-Deflection Force and Energy Relationships.

6.5 Barrier Deformational Energy of the SRT Terminal

Examination of photographic evidence from full-scale crash testing was performed in order to develop a correlation between the amount of energy dissipated by the rail elements of the SRT and information available from the crash scene. The available information was statistically examined to determine if correlations existed between the lengths and number of buckled slots, the length of system damaged, the number of damaged posts, and the amount of vehicle crush energy.

It was determined that the behavior of the different designs of the SRT system varied significantly. Since the SRT-350 is the most common design, only these points were used to determine the correlation between the energy absorbed by the rail and the total post fracture energy, as shown in Figure 10.

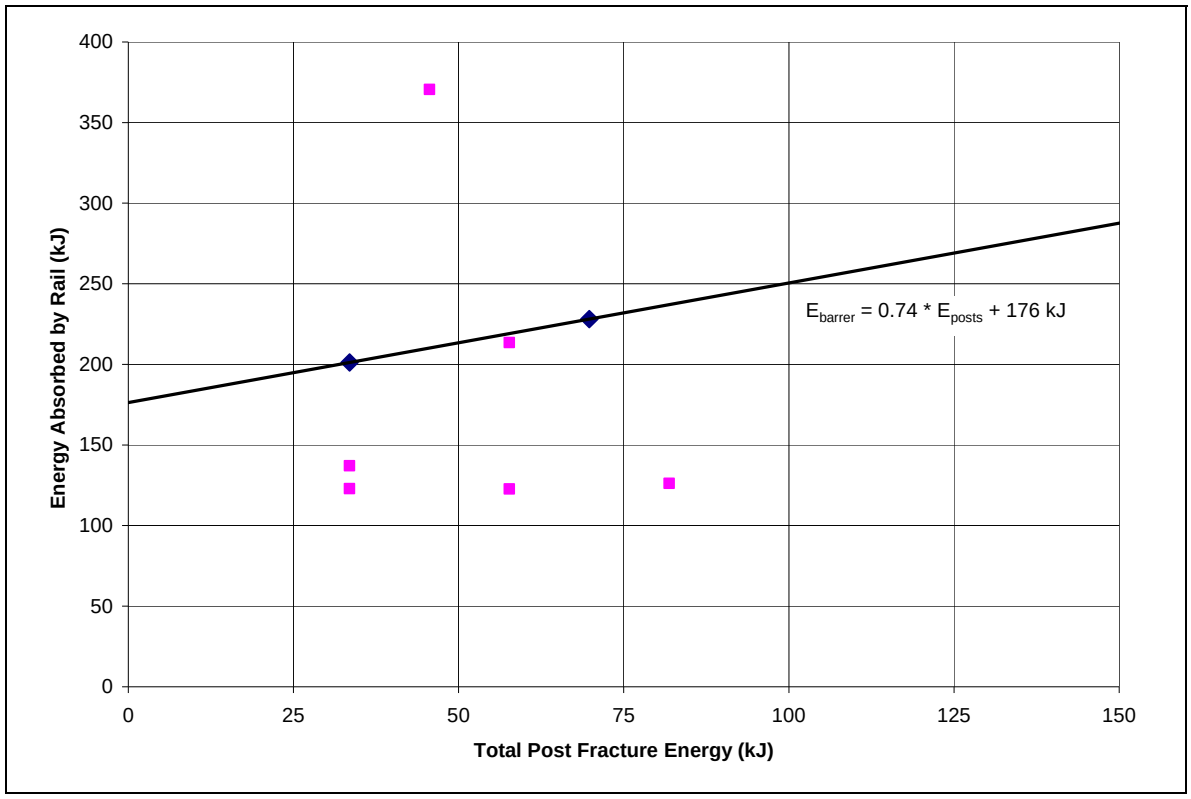

Figure 28. Correlation between Post and Rail Energy Absorption.

This empirical relationship implies that if an impact occurred where no posts were present but subject to their constraints, the rail would dissipate 176 kJ of energy. When posts are included in the system, the energy dissipated in the rail increases, since an increase in the number of fractured posts indicates an increase in the length of rail deformed.

6.6 Reconstruction Technique

The proposed reconstruction procedure for the SRT-350 is based on simple conservation of energy. The kinetic energy at the point where the vehicle departs the rail, the vehicle crush energy, the post fracture energy, and the energy required to crush the rail are summed to determine the initial kinetic energy of the vehicle through the following steps:

1. The velocity at the point the vehicle departed from the rail must be determined. This point occurs when the vehicle loses contact with the SRT-350. This velocity is then converted to kinetic energy using Equation 8. This is important since events after departure are not interactions with the terminal.
2. Energy losses due to vehicle crush are calculated through the procedures outlined in the Traffic Accident Investigation Manual or other appropriate means [**Error! Bookmark not defined.**]. Other energy losses not directly related with the terminal, such as energy losses to sideslip, elevation, et cetera, must also be considered when performing a reconstruction.
3. When post fracture occurs, the energy dissipated by their fracture is estimated as detailed in Section 6.3. When posts rotate in the soil, the deflection should be

determined and the deformation energy estimated as detailed in Section 6.4. These values are summed for the total energy of all posts, E_{posts}.

4. An empirical relationship, developed from the relationship in Figure 10, relates the energy absorbed by the rail element to the total fracture energy of the guardrail posts. This relationship relates the deformational energy in the barrier, $E_{barrier}$, with the total energy dissipated by the posts, E_{posts}. This relationship is shown in Equation 14.

$$Ebarrier = 0.74 * Eposts + 176 \text{ kJ} \quad (14)$$

5. The energy losses from Steps 1 through 4 are added together to find the impact energy.

$$Etotal = KEdeparting + Ecrush + Eposts + Ebarrier \quad (15)$$

6. Conservation of energy is assumed and the velocity is calculated from the total energy.

$$Vi = \sqrt{\frac{2\ Etotal}{Mvehicle}} \quad (16)$$

Where $M_{vehicle}$ is the mass of the vehicle.

6.7 Sample Reconstruction

In order to clarify units and to detail the reconstruction procedure, a reconstruction of a full-scale crash of an SRT-350 terminal run by the Texas Transportation Institute is detailed below. The test, TTI designation 220546-6, was a compliance test for a Test Level 3 (TL-3) end

terminal. Test 3-30 utilizes an 820-kg (1807-lb) small car with a dummy impacting end-on at 0° and 100 km/h (62.2 mph).

The vehicle impacted the system at 99.4.0 km/h (61.8 mph). The vehicle lost contact at a velocity of 43.6 km/h (27.1mph). Maximum exterior vehicle crush was documented as 300 mm (11.8 in.).

1. The departure velocity was 43.6 km/h (27.1mph). This equates to a departing kinetic energy of $KE_{departing}$ = 65.7 kJ (48.5 kip-ft).

$$KEdeparting = \frac{1}{2}(Mvehicle)\,Vd^2 = \frac{1}{2}(896\text{ kg})\,(12.1\text{ m/s})^2 = 65.7\text{ kJ} \qquad (17)$$

2. From photographic information, crush energy was estimated using vehicle stiffness characteristics [**Error! Bookmark not defined.**]. Energy loss due to vehicle crush was calculated as 41.2 kJ (30.4 kip-ft).
3. Two BCT and one CRT posts were fractured during impact. The two BCT posts absorb an estimated total of between 21.4 kJ (15.8 kip-ft). For the one CRT posts, an estimated total energy of 12.1 kJ (8.9 kip-ft) was absorbed. This yields a total of 33.5 kJ (24.7 kip-ft).
4. Equation 18 gives the energy absorbed by the barrier.

$$Ebarrier = 0.74 * (33.5\text{ kJ}) + 176\text{ kJ} = 201.1\text{ kJ} \qquad (18)$$

5. The total energy before impact is the sum of Steps 1 through 4 using Equation 18.

$$65.7\text{ kJ} + 41.2\text{ kJ} + 33.5\text{ kJ} + 201.1\text{ kJ} = 341.5\text{ kJ} \qquad (19)$$

6. This yields a total of 345.5 kJ (254.8 kip-ft) and a corresponding impact velocity of 100.2 km/h (62.3 mph).

$$Vi = \sqrt{\frac{2\ Etotal}{Mvehicle}} = \sqrt{\frac{2 * 341.5\ kJ}{896\ kg}} = 99.4\ km/h \qquad (20)$$

This is an exact match to the initial velocity, since this was one of the two end-on compliance tests on the SRT-350.

6.8 Comparison to Full-Scale Crash Testing

The SRT has been redesigned several times from its original design, including changes in post number and spacing, the slot locations and lengths, and the general design of slot protection. The crash reconstruction procedure outlined above was used to reconstruct all end-on impact tests available in the literature for systems of various designs. The results of these reconstructions are shown in Table 4.

In lower speed impacts where the vehicle was stopped by the system, the procedure significantly either underestimated or overestimated the impact velocity. However, for the higher-velocity impacts, the procedure was within 9% of the actual impact velocity. Statistical analyses were performed examining relationships between the number of posts fractured, the vehicle damage, the initial and final velocities, the length of guardrail damaged, and the number of slots of the system buckled. Unfortunately, none of these relationships provided a better correlation than that of the post fracture energy. However, it should be pointed out that the lower speed tests were not done on the same system that eventually received FHWA approval for installation on the National Highway System.

Table 11. SRT Reconstruction Results.

TTI Test No.	Date	System	Test Designation	Vehicle Type	Vehicle Mass (kg)	Departure Velocity (km/h)	Vehicle Crush (kJ)	Number of Buckled Slots	Number of Fractured Posts		Impact Velocity (km/h)		Error
									BCT	CRT	Actual	Reconstructed	
7199-8A	10/20/92	SRT	45	820C	893	0.0	23.25	4	2	1	75.0	86.52	15.4%
7199-15	04/14/93	SRT-75	41	Sedan	2041	0.0	30.33	4	2	2*	75.3	60.27	-15.9%
7199-14	04/27/93	SRT-75	45	820C	892	0.0	30.01	3	2	1	73.6	87.69	19.2%
220530-5	04/29/94	ISRT-100	45	820C	892	37.5	20.35	3	2	3	99.4	100.2	0.8%
220530-6	05/04/94	ISRT-100	41	Sedan	2043	83.1	26.12	4	2	3	97.6	106.2	6.2%
220530-10	06/26/95	SRT-350	3-31	2000P	2000	82.8	56.24	3	2	5	101.4	108.3	6.8%
Current Approved Design													
220546-5	04/02/98	SRT-350	3-31	2000P	2000	77.1	24.35	3	2	4	100.6	100.5	0%
220546-6	04/08/98	SRT-350	3-30	820C	896	43.6	41.19	2	2	1	99.4	99.4	0%

*A fifth steel line post was impacted

7 Conclusions

Procedures for reconstructing end-on impacts of guardrail end terminals were presented. These procedures included identification of the terminal impacted and reconstruction techniques that accurately estimate the velocity of a vehicle impacting a guardrail end terminal. This technique involved the conservation of momentum and the conservation of energy.

For energy-absorbing terminals, average force levels were derived from information, scale diagrams, and accelerometer traces from full-scale crash testing. Reconstructed velocities correlated well with full-scale crash data. However, the statistical variations could not be identified due to the limited full-scale crash tests performed on individual systems. Average force levels from test to test were found to vary from 3% to 34%, depending on the system.

A methodology was presented to examine crashes with SRT end terminals. This method uses conservation of energy and correlation of the energy dissipated by the rail to the energy dissipated by the fracture of the BCT and CRT posts. Reconstructed velocities correlated well with recent versions of the SRT.

8 REFERENCES

1. Sicking, DL, KK Mak and WB Wilson, “Box-Beam Guardrail Terminal,” Transportation Research Record 1468, Transportation Research Board, National Research Council, Washington, DC, 1994.
2. National Highway Traffic Safety Administration (NHTSA), Fatal Accident Reporting System (FARS) Database, Washington, DC.
3. Griffin, LI, “An Analysis of Accidents on Turndown Guardrail Ends in the State of Texas,” Final Report on Project 9901-H, Texas Department of Transportation, Austin, TX, May 1991.
4. Wendling, WH, “Roadside Safety Milestones,” Semi-Sesquicentennial Transportation Conference, HCR 71, P.O. Box 119, Camdenton, Missouri 65020, 1996.
5. Buth, CE and TJ Hirsh, “Improved End Treatment for Metal Beam Guardrail,” Research Report 189-1, Texas Transportation Institute, Texas A&M University, College Station, 1977.
6. Federal Highway Administration Approval Letter CC-69, November 9, 2000.
7. Federal Highway Administration Approval Letter CC-69a, February 1, 2002.
8. Federal Highway Administration Approval Letter CC-69b, February 22, 2002.
9. Sicking, DL and EA Keller, “Crash Testing of Box-Beam Bursting Energy Absorbing Terminal (BEAT),” MwRSF Report No. TRP-03-106-00, Tests BB 1-4, Midwest Roadside Safety Facility, University of Nebraska – Lincoln, September 22, 2000.
10. Reid, JE, JR Rohde, and DL Sicking, “A Box-Beam Bursting Energy Absorbing Terminal,” ASCE Journal of Transportation Engineering, TE/201/22485, June 21, 2001.
11. Polivka, KA, JR Rohde, JD Reid, DL Sicking, RK Faller, and J Holloway, “Evaluation of the Box-Beam Burster Energy-Absorbing Terminal - Median Barrier Terminal (BEAT-MT),” MwRSF Report No. TRP-03-110-01, Tests BMT 1-6, Midwest Roadside Safety Facility, University of Nebraska – Lincoln, December 14, 2001.
12. Bielenberg, B, RK Faller, J Holloway, JD Reid, JR Rohde, and DL Sicking. “Safety Performance Evaluation of a Single-Sided Crash Cushion,” MwRSF Report No. TRP-03-111-02, Tests SSC 1-5, Midwest Roadside Safety Facility, University of Nebraska – Lincoln, January 7, 2002.\
13. Bielenberg, B, RK Faller, J Holloway, JD Reid, JR Rohde, and DL Sicking, “Safety Performance Evaluation of the BEAT Bridge Pier Protection System,” MwRSF Report No. TRP-03-123-02, Midwest Roadside Safety Facility, University of Nebraska – Lincoln, December 2002.
14. Federal Highway Administration Approval Letter CC-37, November 20, 1996.

15. Federal Highway Administration Approval Letter CC-37a, February 19, 1997.

16. Federal Highway Administration Approval Letter CC-37b, February 19, 1997.\

17. Federal Highway Administration Approval Letter CC-37c, April 1, 1997.

18. Pfeifer, BG and DL Sicking, "Development of a Metal Cutting W-beam Guardrail Terminal," MwRSF Report No. TRP-03-43-94, Tests MCS 4,3, & 7, Midwest Roadside Safety Facility, University of Nebraska – Lincoln, September 1994.

19. Pfeifer, BG and DL Sicking, "Development of a Metal Cutting Guardrail Terminal," Transportation Research Record 1528, Transportation Research Board, National Research Council, Washington, DC, 1994.

20. Pfeifer and Sicking, "NCHRP Report 350 Compliance Testing of the BEST System," MwRSF Report No. TRP-03-63-96, Tests BEST 2-11,Midwest Roadside Safety Facility, University of Nebraska – Lincoln, December 4, 1996. Also referenced as: Pfeifer and Sicking, "Improved Guardrail Terminal. Development of a BEST Terminal to Comply with NCHRP Report 350 Requirements," MATC Report No. MATC UNL96-7, Mid-America Transportation Center, University of Nebraska – Lincoln, December 1998.)

21. Pfeifer, BG and DL Sicking, "NCHRP Report 350 Compliance Testing of the Beam-Eating Steel Terminal System," TRR Report No. 98-0765, Transportation Research Record 1647, Transportation Research Board, National Research Council, Washington, DC, 1998.

22. Federal Highway Administration Approval Letter CC-12c, August 22, 1995

23. Federal Highway Administration Approval Letter CC-12d, December 20, 1996.

24. Federal Highway Administration Approval Letter CC-12e, September 22, 1998.

25. Federal Highway Administration Approval Letter CC-12f, September 2, 1999.

26. Federal Highway Administration Approval Letter CC-12g, January 18, 2000.

27. Federal Highway Administration Approval Letter CC-12h, February 18, 2000.

28. Agent, KR, JG Pigman, D McAlister, and T Gatewood, "Evaluation of the ET 2000 Guardrail End Treatment," Kentucky Transportation Center University of Kentucky, December 1997.

29. Federal Highway Administration Approval Letter CC-12i, April 10, 2000.

30. Federal Highway Administration Approval Letter CC-12j, June 24, 2002.

31. Federal Highway Administration Approval Letter CC-12k, August 28, 2002.

32. Sicking, DL, AB Qureshy, and HE Ross, JR, "Development of Guardrail Extruder Terminal," Transportation Research Record 1233, Transportation Research Board, National Research Council, Washington, DC, 1989.

33. Ross, HE Jr, WL Menges, and DL Bullard, JR, “NCHRP Report 350 Compliance Tests of the ET-2000,” Transportation Research Record 1528, Transportation Research Board, National Research Council, Washington, DC, September 1996.

34. Sicking, DL et al, “Development of a New Guardrail End Treatments,” Research Report 404-1F, Texas Transportation Institute, Texas A&M, 1988.

35. Ross, HE, Jr, WL Menges, and DL Bullar, JR. “NCHRP Report 350 Compliance Tests of the ET-2000.” Transportation Research Record 1528, Transportation Research Board, National Research Council, Washington, DC, 1996.

36. Ross, HE, WL Menges, and DL Bullard, “NCHRP Report 350 Compliance Tests of the ET-2000,” TTI Projects 220510 & 220537, Texas Transportation Institute, College Station, TX. August 1995.

37. Ross, HE WL Menges, BG Butler, “Testing and Evaluation of the ET-2000 with 3.8-m W-beam Sections,” TTI Project 520201-1, Texas Transportation Institute, College Station, TX, August 1998.

38. Menges, WL, CE Buth, and SK Schoeneman, “Testing and Evaluation of the ET-2000 with Steel HBA Posts,” TTI Project No. 400001-XTI1-3, Texas Transportation Institute, College Station, TX, June 1999.

39. Menges, WL, CE Buth, and SK Schoeneman, “NCHRP Report 350 Test 3-35 On the ET-2000 With 4 HBA Posts and 4 CRT Posts,” TTI Project 400001-XTI4, Texas Transportation Institute, College Station, TX, August 1999.

40. Menges, WL, CE Buth, HE Ross, and SK Schoeneman, “NCHRP Report 350 Test 3-31 of the ET-2000 Plus,” TTI Project 400001-LET1, Texas Transportation Institute, College Station, TX, December 1999.

41. "NCHRP Report 350 Testing and Evaluation of the ET-PLUS with Steel Cable Release Post and Steel Yielding Terminal Posts," October 2001.

42. "NCHRP Report 350 Test 3-34 of the ET-PLUS with Steel Cable Release Post and Steel Yielding Terminal Posts," TTI Project 220547-6, Texas Transportation Institute, College Station, June 2002.

43. Federal Highway Administration Approval Letter CC-46, April 2, 1998.

44. Federal Highway Administration Approval Letter CC-46a, August 27, 1998.

45. Federal Highway Administration Approval Letter CC-46b, May 21, 1999.

46. Federal Highway Administration Approval Letter CC-46c, June 1, 2001.

47. Federal Highway Administration Approval Letter CC-46d, August 24, 2001.

48. Federal Highway Administration Approval Letter CC-61, August 27, 1999

49. Federal Highway Administration Approval Letter CC-61a, October 20, 2002.

50. Mayer, JB, "Full-Scale Crash Evaluation of a Flared Energy Absorbing Terminal," SwRI Project No. 06-1433, Test FLEET-1, Southwest Research Institute, San Antonio, Texas, March, 1998.

51. Mayer, JB, "Full-Scale Crash Evaluation of a Flared Energy Absorbing Terminal," SwRI Project No. 06-1433, Test FLEET-2, Southwest Research Institute, San Antonio, Texas, March, 1998.

52. Sicking, DL and EA Keller, "Full-Scale Crash Evaluation of a Flared Energy-Absorbing Terminal (FLEAT-350) with Reduced Offset" Test FLEAT-2, Midwest Roadside Safety Facility, University of Nebraska – Lincoln, March 14, 1998.

53. Sicking DL and EA Keller, "Full-Scale Crash Evaluation of a Flared Energy Absorbing Terminal (FLEAT-350)" MwRSF Report No. TRP-03-76-98, Test FLEAT-3, Midwest Roadside Safety Facility, University of Nebraska – Lincoln, July 1998.

54. Sicking DL and EA Keller. "Full-Scale Crash Evaluation of TL-2 Flared Energy Absorbing Terminal (FLEAT-TL2)," MwRSF Report No. TRP-03-85-99, Test FLEAT-4, Midwest Roadside Safety Facility, University of Nebraska – Lincoln, January 1999.

55. Sicking, DL, DJ Reid, and JR Rohde, "Development of a Flared Energy Absorbing Terminal for W-beam Guardrails," TRR No. 99-1053, Transportation Research Record, Transportation Research Board, Washington, DC, November 1999.

56. Kimball, CE and JB Mayer, "Full-Scale Crash Evaluation of Flared Energy Absorbing Terminal," SwRI Project No. 06-1433, Test SBD-1A, Southwest Research, Final Report, San Antonio, Texas, March 1998.

57. Mayer, JB, "Full-Scale Crash Evaluation of a Flared FLEAT-350 Terminal with Steel Breakaway Posts," SwRI Project No. 18-1433, Test SP-3, Southwest Research Institute, San Antonio, Texas, July 1999.

58. Mayer, JB, "Full-Scale Crash Evaluation of a FLEAT Median Terminal System," SwRI Project No. 18.01433.008, Test FMT-3M, Southwest Research Institute, San Antonio, Texas, July 2001.

59. Mayer, JB, "Full-Scale Crash Evaluation of a FLEAT Median Barrier Terminal," SwRI Project No. 18.01433.01.006, Test FMT-1, Southwest Research Institute, San Antonio, Texas, July 2001.

60. Mayer, JB, "Full-Scale Crash Evaluation of a FLEAT Median Barrier Terminal," SwRI Project No. 18.01433.01.007, Test FMT-2, Southwest Research Institute, San Antonio, Texas, July 2001.

61. Federal Highway Administration Approval Letter CC-40, April 2, 1997.

62. Federal Highway Administration Approval Letter CC-40a, February 4, 2000.

63. Strybos, JW, "Pendulum Evaluation and Full-Scale Crash Tests of a Guardrail End Terminal." SwRI Project No. 06-8538, Bogie Tests 1-10, Southwest Research Institute, San Antonio, Texas, November 15, 1996.

64. Reid, JD and DL Sicking, "Design of the SKT-350 Using LS-DYNA3D," Transportation Research Board 77th Annual Meeting, Washington, DC, January 11-15, 1997.

65. Strybos, JW and JB Mayer, "Full-Scale Crash Testing of a Sequential Kinking Terminal, SKT-350," SwRI Project No. 06-8631, Tests SBD 1-6, Southwest Research Institute, San Antonio, Texas, March 1997.

66. Reid, JD, "Tracking the Energy in an Energy-Absorbing Guardrail Terminal," International Journal of Crashworthiness, Vol 3, No 3, March 19, 1998.

67. Reid, JD and DL Sicking, "Design and Simulation of a Sequential Kinking Guardrail Terminal," International Journal of Impact Engineering, Vol. 21, No. 9, 1998.

68. Sicking, DL, JD Reid, and JR Rohde, "Development of a Sequential Kinking Terminal for W-beam Guardrails," TRB Report No. 98-0614, Transportation Research Record, 1998.

69. Sicking DL and EA Keller, "Full-Scale Crash Evaluation of Steel Post SKT-350 Terminal," MwRSF Report No. TRP-03-**-99, Test SP-1, Midwest Roadside Safety Facility, University of Nebraska – Lincoln, June 30, 1999.

70. Mayer, JB, Jr, "Full-Scale Crash Evaluation of a Straight Sequential Kinking Terminal with Steel Breakaway Posts," SwRI Project No. 18-1433, Test SP-2, Southwest Research Institute, San Antonio, Texas, July 1999.

71. Federal Highway Administration Approval Letter CC-60, August 19, 1999.

72. Mak, KK and DL Sicking, "Development of End Terminal for Box-Beam Guardrail, Phase II – Crash Testing and Evaluation," TTI Report No RF-72020, Texas Transportation Institute, Texas A&M University System, College Station, Texas, September 1992.

73. Mak, KK and WL Menges, "NCHRP Report 350 Evaluation of the Wyoming Box-Beam End Terminal (WYBET-350)", TTI Report No. RF-473160-01, Texas Transportation Institute, Texas A&M University System, College Station, Texas, June 1999.

74. Prasad, AK, "Energy Dissipation in Vehicle Crush – A Study Using the Repeated Test Technique," SAE Paper #900412, Society of Automotive Engineers, Warrendale, PA, 1990.

75. Kerkhoff, JF, SE Husher, MS Varat, AM Busenga, and K Hamilton, "An Investigation into Vehicle Frontal Impact Stiffness, BEV and Repeated Testing for Reconstruction," SAE Paper #930899, Society of Automotive Engineers, Warrendale, PA, 1990.

76. Cooper, GW, "Work, Energy, and Speed from Damage in Traffic Accidents," Northwestern University, Evanston, IL, 1990.

77. Fricke, LB, "Traffic Accident Reconstruction: Volume 2 of the Traffic Accident

Investigation Manual," Northwestern University Traffic Institute, Evanston, IL, 1990.

78. Federal Highway Administration Approval Letter CC-31, December 4, 1995.
79. Federal Highway Administration Approval Letter CC-31a, January 27, 1998.
80. Federal Highway Administration Approval Letter CC-51, June 18, 1998.
81. Federal Highway Administration Approval Letter CC-51a, June 4, 1999.
82. Mak, KK, RP Bligh, and WC Menges, "W-beam Slotted Rail End Terminal Design," TTI Project No. 220530, Texas Transportation Institute, Texas A&M University System, May 1994.
83. Mak, KK, RP Bligh, WL Menges. "Development of W-beam Slotted Rail End Terminal Design." Unpublished report prepared for the Tennessee Department of Transportation. Research Study RF 7199. 1994.
84. Mak, KK, HE Ross Jr, RP Bligh, and WL Menges. "NCHRP Report 350 Compliance Testing of the W-beam Slotted Rail Terminal." Texas Transportation Project No. 220546-14. The Texas A&M University System. College Station, TX. October 1995.
85. Mak, KK, HE Ross Jr, RP Bligh, and WL Menges. "Improved W-beam Slotted Rail Terminal with 1.22-m End Offset and Steel Line Posts." Texas Transportation Project No. 220546. The Texas A&M University System. College Station, TX. April 1999.
86. Mak, KK, HE Ross Jr, RP Bligh, and WL Menges. "Optimization of the W-beam Slotted Rail Terminal." Texas Transportation Project No. 220546. The Texas A&M University System. College Station, TX. May 1998.
87. Cooper, GW, "Work, Energy, and Speed from Damage in Traffic Accidents," Northwestern University, Evanston, IL, 1990.
88. Brown, CM, "Pendulum Testing of BCT Wood Posts: FOIL Tests: 91P039 through 91P045," FHWA No. FHWA-RD-95-023, Federal Highway Administration, Department of Transportation, McClean, VA. August 1991.
89. Denmann and Welch. "Development of a Flared End Terminal to NCHRP Report 350 REGENT™ System. E-TECH Testing Services, Inc. 1999.
90. Herr, JE, "Development of Standards for Placement of Steel Guardrail Posts in Rock," Master's Thesis, Department of Civil Engineering, The University of Nebraska – Lincoln, December 2002.
91. Rohde, JR, JD Reid, and DL Sicking, "Evaluation of the Effect of Wood Quality on W-beam Guardrail Performance," NDOR Report No. AFE-Z322, Midwest Roadside Safety Facility, University of Nebraska – Lincoln, November 1995.
92. Rohde, JR, JD Reid, and DL Sicking, "Evaluation of the Effect of Wood Quality on W-Beam Guardrail Performance," NDOR Report No. AFE-Z322, Midwest Roadside Safety Facility,

University of Nebraska – Lincoln, November 1995.

93. Gatchell, CJ and JD Michie, "Pendulum Impact Tests of Wooden and Steel Highway Guardrail Posts," USDA Research Paper No. NE-311, United States Forest Service, United States Department of Agriculture, 1974.
94. Rohde, JR, JD Reid, and DL Sicking, "Evaluation of the Effect of Wood Quality on W-beam Guardrail Performance," Midwest Roadside Safety Facility, University of Nebraska – Lincoln, November 1995.
95. Mayer, JB Jr, "Evaluation of the Dynamic Strength of Guardrail Posts Made from Recycled Plastic," SwRI Project No. 06-3906, Southwest Research Institute, San Antonio, Texas, October 1993.
96. Coon, BA, JD Reid and JR Rohde, "Dynamic Impact Testing of Guardrail Posts Embedded in Soil," MwRSF No. TRP-03-77-98, Midwest Roadside Safety Facility, University of Nebraska – Lincoln, July 1999.
97. Post, ER, CY Tuan and SA Ataulla "Comparative Study of Kansas and FHWA Guardrail Transition Designs Using BARRIER VII Computer Simulation Model," Transportation Research Report TRP-03-012-88, Midwest Roadside Safety Facility, University of Nebraska – Lincoln, December 1988.
98. Coon, BA, "Dynamic Impact Testing and Simulation of Guardrail Posts," Master's Thesis, Department of Civil Engineering, The University of Nebraska – Lincoln, 1999.
99. Coon, BA, JD Reid, and JR Rohde, "Dynamic Impact Testing of Guardrail Posts Embedded in Soil," Midwest Roadside Safety Facility Report No. TRP-03-77-98, University of Nebraska – Lincoln, July 21, 1999.
100. Bierman, MG, "Behavior of Guardrail Posts to Lateral Impact Loads," Master's Thesis, Department of Civil Engineering, The University of Nebraska – Lincoln, December 1995.

APPENDIX C

Reconstruction Techniques for Guardrail End Terminals

1 INTRODUCTION

Roadside objects, such as bridge piers, sign supports, or power poles, can pose a serious risk to drivers. One way to protect errant vehicles is to shield the object with crash cushions. Examples include arrays of sand-filled barrels to shield fixed objects such as concrete bridge piers, and crushable foam-filled cartridges to protect the ends of concrete median barriers. Crash cushions work by attenuating energy and decelerating the impacting vehicle to lessen the severity of a crash.

The importance of crash reconstruction is two-fold: first, designers and testers of roadside safety devices must be certain they are designing and testing for real-world conditions. Secondly, departments of transportation must determine the impact severity of crash cushion impacts to determine appropriate warrants, maximizing the benefit-cost ratio for limited resources.

1.1 Crash Reconstruction Overview

In order to determine impact conditions, crash reconstructions must be performed. Vehicle mass, run-out trajectory, and the resulting deformed geometry of the barrier can generally be measured after the impact using existing technology. However, verified techniques for estimating the impact velocity into crash cushions are currently unavailable.

Crash cushion technology can be divided into two basic categories: crash cushions that use energy-dissipating cartridges or similar refurbishable technologies, and crash cushions that are self-restorative and reusable. Crash cushion technology is difficult to reconstruct since test data on individual cartridges or units must be obtained.

Additionally, extensive modeling must be performed with full-scale crash test verification of the simulation.

1.2 Research Objectives

In order to reconstruct or document an impact with a crash cushion, the reconstructionist must first be able to identify the specific type of device impacted. This appendix documents crash cushions certified for use on the National Highway System (NHS) under NCHRP Reports 230 and 350 by their distinguishing characteristics, including physical appearance, number of bays, method of energy dissipation, *et cetera*.

Initially, it was envisioned that techniques for reconstructing impacts for several crash cushions would be developed. Unfortunately, for various reasons, many manufacturers of crash cushions are unable to share specific crash test data or component test information. Therefore, reconstruction techniques were developed only for three common crash cushions: 1) the REACT-350, 2) inertial barriers (sand barrels), and 3) the Box-Beam-Bursting, Energy-Attenuating Terminal Single-Sided Crash Cushion (BEAT-SSCC). The BEAT-SSCC is detailed in Appendix C, "Reconstruction Techniques for Guardrail End Terminals," due to its shared impact head and relationship to the BEAT family of end terminals, median barriers, and bridge pier protection systems [1]. These crash cushions were chosen due to their straightforward mechanical behavior. Other crash cushions would require a combination of extensive component testing, finite element modeling and full-scale crash testing in order to develop a reconstruction procedure, which is beyond the scope of this research.

2 TRADITIONAL CRASH CUSHIONS

Safe and economical methods of shielding hazards have been a critical concern for more than three decades [2]. In 1969, Philip E. Rollhaus, Jr. and associates founded the Quixote Corporation, designing energy-absorbing water-filled bumpers for vehicles. Using this technology, Quixote developed the first crash cushion to be placed in front of roadside hazards, the HiDro System. Since then, manufacturers have implemented sand barrel designs and then spawned the development of numerous designs for both narrow and wide hazards.

Because of the plethora of different crash cushion designs, it is difficult for the casual observer to note any difference between certain varieties of crash cushions. Each of the crash cushions is identified by its distinguishing characteristics. Widths, lengths, and approved test level severity are identified for the crash cushions.

Sand-filled barrels are often used as crash cushions, but because of their distinct appearance and behavior, they will be covered separately. Sand-filled barrels are referred to as inertial barrier systems, while the other systems discussed in this section are referred to as traditional crash cushions. A summary of crash cushions reviewed herein is provided in Table 1.

In addition to the physical dimensions detailed in Table 1, crash cushions are further identified by two qualities: (1) gating versus non-gating and (2) redirective versus non-redirective. A gating crash cushion, when impacted on the nose or the side of a crash cushion near the nose but at an angle, allows a vehicle to pass or gate through the crash cushion. A non-gating cushion prevents a vehicle from passing through the crash cushion

even under impacts at the nose or on the side of a crash cushion near the nose but at an angle.

A redirective crash cushion, when impacted along the side of the crash cushion but past the nose, acts as a safety barrier with the vehicle being sent back across its original path without causing any great danger to other vehicular traffic. When a vehicle passes through the crash cushion, such as the case with sand barrels, the crash cushion is considered non-redirective.

Table 1. Summary of Crash Cushions.

System Name	Temp. (T) Perm. (P)	System Width, m (ft)	System Length* m (ft)	Redirective or Non-Redirective / Gating or Non-Gating	NCHRP Report 350
Traditional Crash Cushions					
ABSORB 350	T / P	0.61 (2)	5.8 (19) 9.2 (30.2)	N / G	TL-2 (5 unit) TL-3 (9 unit)
ABSORB 350 QMB	T	0.61 (2)	5.4 (17.7) 8.2 (26.9)	N / G	TL-2 (5 unit) TL-3 (8 unit)
ADIEM 350	T / P	0.71 (2.67)	5.485 (18) 9.145 (30)	R / G	TL-2 TL-3
Brakemaster	P	0.61 to 0.91 (2 to 3)	9.6 (31.5)	R / G	TL-3
BEAT-SSCC	P	0.508 (1.67)	8.534 (28)	R / G	TL-3 (pending)
CAT	P	0.737 (2.42)	9.525 (31.25)	R / G	TL-3
CIAS	P	3.66 (12)	25.6	R / G	TL-3
EASI-cell	P	1.3 (4.3)	2.6 (8.5)	N / G	TL-1
GREAT	P	0.61, 0.76, 0.91 (2, 2.5, 3)	11.75 20.75	R / N	NHCRP 230
GREAT CZ	T	0.61, 0.76 (2, 2.5)	11.75 20.75	R / N	NHCRP 230
HexFoam Sandwich Hi-Dro Sandwich	P	9.15, 1.52, 2.29 (3, 5, 7.5)	?	R / N	NHCRP 230
Hi-Dro Cell Cluster	P	1.3 (4.33)	3.81 (12.5)	N / G	N/A
LMA	P	0.89 (3.5)	10.4 (33.2)	R / N	NCHRP 230
NCIAS	P	0.91 (3)	6.1 (24)	R / N	TL-3
N-E-A-T	T / P	0.61 (2)	3.0 (9.7)	N / G	TL-2
QuadTrend-350	P	0.457 (1.5)	6.1 (20)	R / G	TL-3
QuadGuard	P	0.61, 0.76, 0.91, 1.753, 2.286 (2, 2.5, 3, 5.75, 7.5)	2.16 (7.1) 4.0 (13.1) 6.74 (22.1) 12.23 (40.1)	R / N	(1-bay) TL-2 (3-bay) TL-3 (6-bay) TL-3 (12-bay)+
QuadGuard HS	P	0.61, 0.76, 0.91 (2, 2.5, 3)	9.474 (31)	R / N	TL-3 (9-bay)+
QuadGuard CZ	T	0.61, 0.76, 0.91 (2, 2.5, 3)	4 (13.1) to 9.49 (31.1)	R / N	TL-2 (3-bay) TL-3 (9-bay)
QuadGuard Elite	P / T	0.61, 0.76, 0.91, 1.753, 2.286 (2, 2.5, 3, 5.75, 7.5)	7.264 (23.83) 10.82 (35.5)	R / N	TL-2 (7-bay) TL-3 (11-bay)+
QuadGuard LMC	P	0.91, 1.75, 2.3 (3, 5.75, 7.5)	10 (32.8)	R / N	TL-3 (11-bay)+
QuadGuard 69 / 90	P	1.753, 2.286 (5.75, 7.5)	4.0 (13.1) to 12.23 (40.1)	R / N	TL-2 (4-bay) TL-3 (12-bay)
REACT Family REACT 350.4 REACT 350.6 REACT 350.9 (CZ)	 P P P / T	1.207 (3.92)	4.19 (13.75) 6.02 (19.75) 8.8 (28.75) 10.6 (34.75)	R / N	 TL-2 TL-2 TL-3

System Name	Temp. (T) Perm. (P)	System Width, m (ft)	System Length* m (ft)	Redirective or Non-Redirective / Gating or Non-Gating	NCHRP Report 350
REACT 350.HS	P				TL-3+
Medium REACT 350 AKA Wide REACT (Self-Contained)	P	0.914 - 1.83 (3 - 6)	3.66 (12) 6.32 (20.75) 8.76 (28.75)	R / N	TL-2 Tl-2 TL-3
		1.83 - 2.29 (6 - 7.5)	4.97 (16.25) 5.89 (19.33) 7.81 (25.67)	R / N	TL-2 TL-2 TL-3
		2.44 - 3.05 (8 - 10)	4.78 (15.67) 5.64 (18.5) 7.57 (24.83)	R / N	TL-2 Tl-2 Tl-3
Medium REACT 350 AKA Wide REACT (Side-Mounted)	P	0.914 - 1.83 (3 - 6)	3.08 (10.08) 5.77 (18.92) 8.21 (26.92)	R / N	TL-2 Tl-2 Tl-3
		1.83 - 2.29 (6 - 7.5)	4.42 (14.5) 5.33 (17.5) 7.27 (23.83)	R / N	TL-2 Tl-2 Tl-3
		2.44 - 3.05 (8 - 10)	4.27 (14') 5.14 (16.83) 7.04 (23.08)	R / N	TL-2 Tl-2 Tl-3
REACT Wide (60") REACT Wide (96") REACT Wide (120") (Self-Contained)	P	1.525 (5) 2.440 (9.5) 3.050 (10)	9.52 (31.25) 10.62 (34.83) 10.43 (34.17)	R / N	TL-3
REACT Wide (60") REACT Wide (96") REACT Wide (120") (Side-Mounted)	P	1.525 (5) 2.440 (8) 3.050 (10)	8.91 (29.25) 10.01 (32.83) 9.82 (32.17)	R / N	TL-3
REACT 350 CZ	T	1.207 (3.92)	8.8 (28.75)	R / N	TL-3
SENTRE	P	0.457 (1.5)	5.182 (17)	R / G	NHCRP 230
TAU-II	P	0.889 (2.92)	4.718 (15.5) 8.185 (26.9)	R / N	TL-2 (4-bay) TL-3 (8-bay)
SHORTRACC TRACC FASTRACC WideTRACC	T / P	0.8 (2.58) 0.8 (2.58) 0.8 (2.58) Various	4.3 (14) 6.4 (21) 7.89 m (25.9) Various	R / N	TL-2 TL-3 TL-3+ TL-3
TREND	P	0.457 (1.5)	6.096 (20)	R / G	NCHRP 230
Inertial Barriers					
Energite III	P / T	1.07 (6.5)	27.9	N / G	TL-3+
Fitch	P / T	1.07 (6.5)	30	N / G	TL-3+
Big Sandy	P / T	1.07 (6.5)	10.1 (33)	N / G	TL-3+

+ The QuadGuard, REACT, FASTRACC and the inertial barrels systems have configurations that are designed to exceed the requirements of NCHRP Report 350. QuadGuard HS is designed for impacts up to 113 km/h (70 mph) in FHWA Approval Letter CC-35E. The FASTRACC is designed for impacts up to 112.3 km/h in FHWA Approval Letter CC-54B. The REACT-350 HS has designs at 113 km/h (70 mph) and 120 km/hr (75 mph). The Fitch, Energite, and the Big Sandy all offer configurations for higher speeds. The Fitch system has been tested at 109.4 km/hr and the QuadGuard HS system has been tested at 113 km/h (70 mph).

2.1 ABSORB 350 and ABSORB 350 QMB

Made by Barrier Systems, Inc., the ABSORB 350 is a non-redirective, gating crash cushion for protecting the ends of permanent or portable concrete barriers and Barrier Systems' Quickchange® Movable Barriers (QMB) without the need to anchor the system to the roadway surface [3, 4, 5]. The ABSORB 350 is shown in Figure 1.

Figure 1. ABSORB 350 Crash Cushion (Picture from Barrier Systems, Inc.).

The ABSORB 350 system consists of a series of steel-reinforced plastic units, each measuring 1000-mm (39.5-in.) long, 812-mm (32-in.) high, and 610-mm (24-in.) wide. A steel and aluminum nosepiece is required to attach to the first unit and the system requires appropriate transition hardware.

The ABSORB 350 units are placed on-site empty and then filled with water. Each unit holds approximately 300 L (80 gal) of water. The units have a mass of approximately 50 kg (110 lbs) empty and 325 kg (717 lbs) when filled.

For protecting concrete barriers, a five-element, 5.7 m (19 ft) long system is required for TL-2, while a nine-element, 9.7-m (32-ft) long system is required for TL-3.

The ABSORB 350 QMB uses a five-element system, 5.4-m (17.7-ft) long for TL-2 or an eight-element system, 8.2-m (27-ft) long for TL-3. However, configurations with capacity less than TL-2, between TL-2 and TL-3, and more than TL-3 can be created and used. Barrier Systems Inc. designates ten separate configurations as being acceptable configurations in specific circumstances.

2.2 ADIEM, Advanced Dynamic Impact Extension Module

The ADIEM, marketed by Trinity Industries, is a redirective, gating end treatment for protecting the ends of permanent or portable concrete barriers bridge parapets and rails, bridge piers, and other hazards placed on concrete, asphalt, or compacted base or soil [6, 7, 8, 9, 10]. The ADIEM is shown in Figure 2.

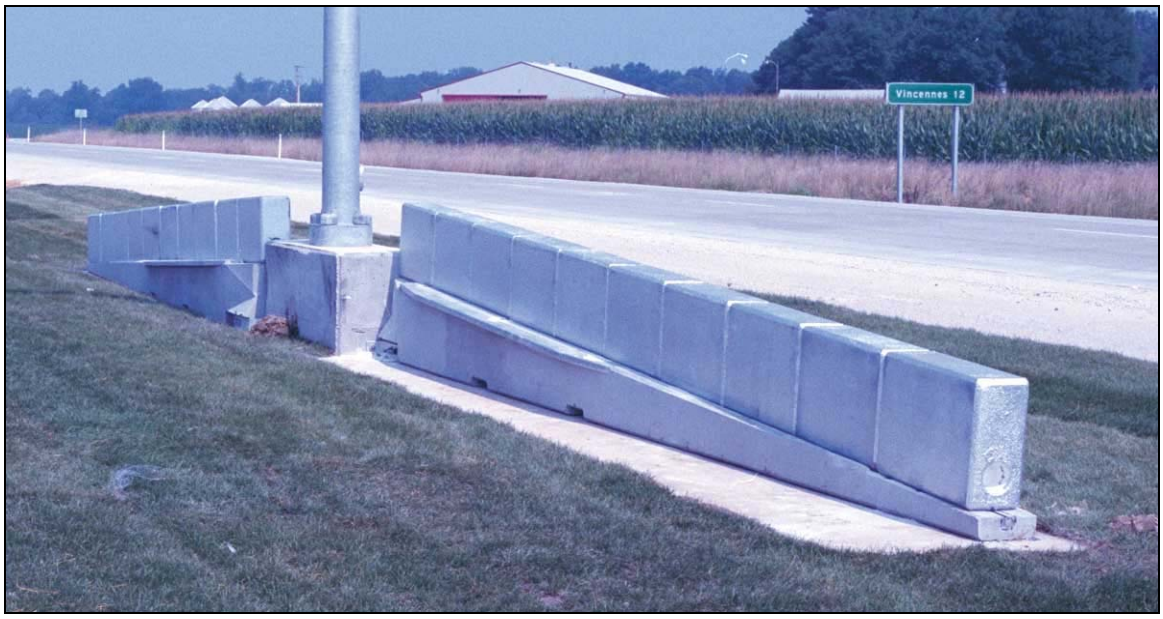

Figure 2. ADIEM Crash Cushion (Picture from Trinity Industries).

The ADIEM depends on the crushing of ten lightly reinforced, ultra-low-strength Perlite concrete modules placed on a 9.144-m (30-ft) inclined base to dissipate energy.

All of the modules are identical with no specific order needed during installation. Each module is 910-mm long, 610-mm tall, and 292-mm wide (3-ft long, 2-ft tall, and 11.5-in. wide). A penetrometer is used to ensure the correct 28-day strength of the ultra-low-strength Perlite concrete, which must be between 620 and 827 kPa (90 and 120 psi) in the top 177.8 mm (7 in.), between 138 and 276 kPa (20 and 40 psi) in the middle 355.6 mm (14 in.), and 3448 kPa (500 psi) in the bottom 76 mm (3 in.).

Some states have expressed concerns that when the protective coating is damaged, the Perlite concrete can be significantly weakened if it becomes wet [11]. The manufacturer has addressed this with a plastic cover intended to keep the modules dry.

The nose of the ADIEM's carrier arm tapers over the first 3.35 m (11 ft) from an initial width of 0.305 m (1 ft) at the groundline to a final width of 0.610 m (2 ft). The ADIEM has a total length of 9.133 m (30 ft) and is approved as a TL-3 crash cushion.

2.3 BEAT-SSCC, Single-Sided Crash Cushion

Developed by Safety by Design, Inc., the Beam-Bursting, Energy-Absorbing Terminal, Single-Sided Crash Cushion, the BEAT-SSCC, is designed to attach directly to bridge abutments, rigid barrier ends, and many bridge rails, as shown in Figure 3a [12,13].

The BEAT-SSCC attenuates energy by bursting open two stages of box-beam, as shown in Figure 3b. The first energy absorber, a 152x152x3.2-mm (6x6x1/8-in.) box beam, is 2.328-m (8-ft) long; the second stage energy absorber, a 152x152x4.8-mm (6x6x3/16-in.) box beam, is 4.94-m (16-ft) long.

The BEAT-SSCC is a redirecting, gating system 8.42-m (27.6-ft) long from its nose to the beginning of the standard box-beam guardrail, 0.508-m (20-in.) wide, and is approved as a TL-3 crash cushion. A complete reconstruction technique for the BEAT family of impact attenuators is available [14].

a) Installed BEAT-SSCC.

b) Bursted BEAT Box Beam.

Figure 3. BEAT-SSCC Crash Cushion.

2.4 Brakemaster System

The Brakemaster, manufactured by Energy Absorption Systems, is a redirective, gating crash cushion designed for protecting rigid objects, median barriers, and as an end treatment for W-beam guardrail [15, 16, 17, 18, 19]. The Brakemaster is shown in Figure 4.

Figure 4. Brakemaster Crash Cushion (Photograph from Energy Absorption, Inc.).

The Brakemaster utilizes a cable brake mechanism that uses friction to decelerate the impacting vehicle. During impact on the nose of the system, the panels nest back onto each other, telescoping out the panels. After 1.27 m (50 in.), a brake/tension support assembly begins to move on the cable, dissipating energy through friction.

When used to shield a rigid object, a transition section is required to prevent pocketing. The Brakemaster should be placed on standard firm soil, compacted subbase, oiled crushed rock, asphalt, or concrete.

The Brakemaster is 9.957 m (32.67 ft) in length, 610-mm (2-ft) wide, and is approved as a TL-3 crash cushion. However, during impact, the Brakemaster's panels can flare out up to three meters (10 ft), so median applications of the Brakemaster should be limited to widths of three meters (10 ft) or greater.

2.5 CAT 350, Crash Cushion Attenuator Terminal

The CAT 350, produced by Syro, a subsidiary of Trinity Industries, was originally named the "Combination Attenuating Terminal" and was developed from a FHWA project [20, 21, 22, 23]. The name was later changed to the Crash Cushion Attenuator Terminal. The CAT 350 is an end treatment for W-beam guardrail and can be used for concrete barrier if a transition is provided. A redirective, gating crash cushion, the CAT 350 is shown in Figure 5

Figure 5. CAT 350, Combination Attenuating Terminal.

CAT 350 absorbs energy in stages, or progressively increasing amounts, beginning with 1) the nose section, 2) the lighter gage guardrail section, and finally, 3) the heavier gauge guardrail section. When impacted end-on, the nose section folds up across the front of the errant vehicle and the second stage then begins to telescope downstream over the third stage guardrail. Energy is dissipated by using a pin that shears the steel between the slots in the CAT 350 panels. If necessary, the third, heavier-gauge section of the CAT 350 is activated, absorbing more energy.

The CAT is a minimum of 9.525-m (31.25-ft) long and can vary between 60.96 cm (2 ft) and 1.524 m (5 ft) in width and is a TL-3 crash cushion.

2.6 CIAS, Connecticut Impact Attenuation System

The CIAS, developed by the Connecticut Department of Transportation, is a redirective, gating crash cushion designed to protect rigid objects [24, 25, 26, 27, 28, 29, 30, 31]. The CIAS is shown in Figure 6.

Figure 6. CIAS (Photo from CDOT).

The CIAS consists of 12 steel cylinders, 1.22 m (48 in.) in diameter and 2 cylinders 0.91 m (36 in.) in diameter. Each cylinder is 1.22 m (48 in.) high, with wall thicknesses of 6.35 mm (0.25 in.) for the three cylinders attached to the concrete backup structure, 7.94 mm (5/16 in.) for the next two cylinders, and 4.76 mm (3/16 in.) for the remaining large diameter cylinders. The two 0.91-mm (36-in.) diameter cylinders are made from 4.176-mm (8-gauge) plate steel.

The CIAS array is set on two steel skid rails bolted to a concrete pad and is connected to a 1980-mm (78-in.) wide concrete backup wall with L-brackets on each side of the wall. The changing of the width of the concrete back wall from 2.7 to 2.0 meters (106 to 78.7 inches) and the introduction of these L-brackets are the only significant modifications from the original 1980s design.

The CIAS attenuates energy through the deformation of the steel cylinders. The CIAS is 3.81-m (150-in.) wide and 6.86-m (270-in.) long. It is approved as a TL-3 crash cushion.

2.7 NCIAS, Narrow Connecticut Impact Attenuation System

Developed by the Connecticut Department of Transportation, the NCIAS is a redirective, non-gating crash cushion designed to shield concrete barriers [32, 33, 34]. The NCIAS is similar to the CIAS, but with a single row of cylinders and two steel tension cables to keep the system in place and provide redirective capability in the system. The system is shown in Figure 7.

Figure 7. Narrow Connecticut Impact Attenuation System (Photo from CDOT).

The NCIAS consists of eight steel cylinders in a single row with two anchored wire ropes along each side. All cylinders are 900 mm (36 in.) in diameter and 1200-mm (36-in.) tall.

The system attenuates energy through the crushing of the steel cylinders. The system is 7.3-m (24-ft) long and 914-mm (3-ft) wide. The NCIAS is approved as a TL-3 crash cushion.

2.8 EASI-cell System

The EASI-cell (Energy Absorption Systems, Inc. cell) system, manufactured by Energy Absorption Systems, Inc., is designed to protect rigid objects, such as utility poles, railroad crossing signals, and traffic lights [35]. The EASI-cell system is shown in Figure 8. The EASI-cell attenuates energy through the deformation of the plastic cylinders. The EASI-cell is a non-redirective, TL-1 crash cushion. The EASI-cell is a self-restoring version of the Hi-Dro Cell Cluster system.

Figure 8. EASI-Cell System (Energy Absorption Systems, Inc.).

The EASI-cell consists of eight rows of four High Density Polyethylene (HDPE) cylinders, making the total unit 1.3-m (51.2-in.) wide by 2.6-m (102.4-in.) deep. Individual cylinders have an outside diameter of 324 mm (12.75 in.) and a height of 990 mm (39 in.). Each cylinder in the first row has a wall thickness of 19 mm (3/4 in.) and all the others have wall thicknesses of 10 mm (3/8 in.).

2.9 GREAT and GREAT CZ Systems, GuardRail Energy Absorbing Terminal

The GREAT (Guard Rail Energy Absorbing Terminal) is a redirective, non-gating terminal previously developed by Energy Absorption Systems, Inc. The GREAT consists of crushable material cartridges surrounded by a framework of steel thrie-beam guardrail. Original versions of the GREAT used Hi-Dri brand lightweight concrete. Subsequent versions used HexFoam and HexFoam II cartridges instead. The GREAT system is shown in Figure 9.

Figure 9. GREAT System.

When hit head-on, the energy absorbing cartridges crush to dissipate the energy of the impact. The sections of thrie-beam guardrail are fastened through slotted holes that allow the system to collapse like a telescope. After the impact, only the cartridges and plastic nose cover are required to be replaced.

Both the GREAT and the GREAT CZ (Construction Zone) were certified under NCHRP Report 230 but were not tested under NCHRP Report 350. The GREAT CZ is a portable version of the GREAT, using the same technology.

2.10 Hex-Foam and Hi-Dro Sandwich Systems

The Hex-Foam and Hi-Dro Sandwiches are redirective, non-gating crash cushions developed by Energy Absorption Systems, Inc. to protect rigid objects. A Hex-Foam Sandwich is shown in Figure 10.

Figure 10. Hex-Foam Sandwich.

The Hex-Foam and Hi-Dro Sandwich systems used energy-absorbing cartridges placed between rigid steel or wooden diaphragms in a multi-layered "sandwich" construction. A flexible belt protects the nose of the system while the sides of the system are constructed of steel fenders.

The Hex-Foam and Hi-Dro Sandwiches were approved under NCHRP Report 230 but were not tested under Report 350.

2.11 LMA, Low Maintenance Attenuator System

Developed by the Texas Transportation Institute and marketed by Energy Absorption Systems, Inc., the LMA was designed as a crash cushion for concrete barriers. The LMA is a redirective, non-gating system. The LMA is shown in Figure 11.

Figure 11. Low-Maintenance Attenuator, LMA.

The LMA consists of a thrie-beam fender panel filled with energy-absorbing rubber cylinders. Upon impact, energy is attenuated through inertia, damping, and elastic deformation. The LMA is 1.08-m (3.5-ft) wide, 10.16-m (33.2-ft) long, and was certified under NCHRP Report 230.

2.12 NEAT, Narrow, Non-Redirective Energy-Absorbing Terminal

Developed by Energy Absorption Systems, Inc., the NEAT is designed to protect the ends of concrete barriers [36, 37, 38]. The NEAT is designed to attach to the end of a barrier using the barrier's existing pen and loop connection. The NEAT is shown in Figure 12.

Figure 12. NEAT System (Photo from Energy Absorption, Inc.).

The NEAT is made from aluminum cells encased in an aluminum shell and attenuates energy through the deformation of these cells and casing. The NEAT is 570-mm (22.4-in.) wide and 2.96-m (9.7-ft) long. The NEAT is approved as a TL-2 non-redirective, gating crash cushion.

2.13 QuadGuard

The QuadGuard crash cushions, developed by Energy Absorption Systems, Inc., are redirective, non-gating crash cushions available in several incarnations from construction-zone temporary barriers to high-speed designs exceeding the capacity required by NCHRP Report 350 TL-3 [39, 40, 41, 42, 43, 44, 45, 46, 47, 48]. The QuadGuard CZ system, shown in Figure 13, comes in several different varieties, including:

- TL-2 QuadGuard Elite (3 Bay)

- TL-3 QuadGuard Elite (6 Bay)
- TL-3 QuadGuard-Wide
- TL-3 QuadGuard LMC Low Maintenance
- TL-3 QuadGuard HS (High Speed, tested to 113 km/h (70 mph))
- TL-3 QuadGuard CZ (Crash Zone)
- QuadGuard CEN (European Standard)

Figure 13. QuadGuard System.

The QuadGuard is similar to the GREAT in function, consisting of a monorail assembly anchored to a concrete pad, steel diaphragms, specially fabricated steel fender panels, a nose assembly, and a steel strut backup. The system must be grouted in place

using fifty anchors embedded in a two-part polyester epoxy. Each bay contains energy absorbing cartridges identified as type 1 or type 2.

The QuadGuard Elite and QuadGuard LMC use HDPE cylinders instead of disposable cartridges like the other versions of the QuadGuard implement. This makes these versions, to a great extent, self-restoring and reusable.

The QuadGuard is available in all test level configurations and in a considerable number of widths and lengths. Depending on the configuration, all NCHRP Report 350 test levels are available.

2.14 QuadTrend

The Quad TRansition section and ENd Treatment, QuadTrend, is based on the original TREND, or TRansitioning END Terminal, system, which the Federal Highway Administration accepted for use as an NCHRP Report 230 device on January 8, 1986 [49]. The TREND and QuadTrend are redirecting, gating terminals designed as treatments for rigid barriers as well as transition sections. The Trend and QuadTrend are shown in Figure 14.

a) TREND System.

b) QuadTrend System.

Figure 14. TREND Family of Crash Cushions.

The TREND systems consist of nested fender panels fabricated from 3.416-mm (10-gauge) steel Quad-beam™ corrugated rail sections, slip bases, a tension strap, a redirective cable, and sand-filled boxes for dissipating collision energy. The systems require a cable to be placed 3.2 m (10.5 ft) from the front of the barrier, creating a maintenance issue.

The primary difference between the TREND and the QuadTrend is the use of quad-beam fender panels in place of the original thrie-beam panels used on the TREND.

The TREND and QuadTrend are 6.096-m (20-ft) long and 0.457-m (18-in.) wide. The original TREND was approved under NCHRP Report 230. The QuadTrend is a TL-3 approved crash cushion.

2.15 REACT 350

The Reusable Energy Absorbing Crash Terminal 350 (REACT 350) is a redirective, non-gating crash cushion composed of high molecular weight, high-density polyethylene cylinders of varying wall thicknesses to shield concrete barriers or, with a transition, steel beam median barriers [50, 51, 52, 53, 54, 55, 56, 57, 58]. The REACT 350, marketed by Energy Absorption Systems, Inc., is shown in Figure 15.

Figure 15. REACT 350.6, the Six-Bay REACT 350.

Each cylinder is 910 mm (3 ft) in diameter, 1220-mm (4-ft) high, with cylinder wall thicknesses shown in Table 2. Two 25.4-mm (1-in.) cables are located on either side of the attenuator to provide redirection of side impact. These cables are connected to anchor plates at the front of the REACT 350 and to a backup assembly at the rear of the unit. It should be noted that the width of the system is greater than the width of the cylinders due to the cables and cable clamps on the outside of the cylinders. The REACT 350 unit rests on a steel support structure and is stiffened laterally by three chain assemblies attached to rods in the support structure on either side and to steel pates located between the cylinders 6-7, 7-8, and 8-9 in the center.

Table 2. REACT Cylinder Thickness.

Cylinder Number	REACT System Cylinder Wall Thickness, mm (in.)				
	350.4	350.6	350.9	350.9HS	350.11
1	43 (1.714)	25.4 (1.0)	20 (0.8)	23 (0.9)	20 (0.8)
2	35 (1.385)	25.4 (1.0)	20 (0.8)	23 (0.9)	54 (2.1)
3	25.4 (1.0)	25.4 (1.0)	23 (0.9)	25.4 (1.0)	20 (0.8)
4	23 (0.9)	25.4 (1.0)*	23 (0.9)	25.4 (1.0)	20 (0.8)
5	N/A	43 (1.714)	25.4 (1.0)	35 (1.385)	23 (0.9)
6	N/A	43 (1.714)	25.4 (1.0)	35 (1.385)	23 (0.9)
7	N/A	N/A	28 (1.108)	43 (1.714)	25.4 (1.0)
8	N/A	N/A	35 (1.385)	43 (1.714)	25.4 (1.0)
9	N/A	N/A	35 (1.385)	43 (1.714)	37 (1.5)
10	N/A	N/A	N/A	N/A	37 (1.5)
11	N/A	N/A	N/A	N/A	54 (2.1)

*Or 28 mm (1.108 in.), depending on the date of manufacture [53].

The REACT 350 uses metal frames located at the top of the first two cylinders to decrease deflection in the top portion of the cylinder. This minimizes the chances of the vehicle climbing up the cylinders, crushing the tops, and ramping over the top of the system.

2.16 Wide REACT 350

The Wide REACT 350 is based on the REACT 350, but uses internal steel spacers to increase the effective width of the system up to 3.05 m (10 ft) [59, 60, 61, 62, 63, 64, 65]. Initially, a design of the Medium REACT was named the Wide REACT, but was changed through an FHWA approval letter.

Figure 16. Wide REACT (Photo from Energy Absorption Systems, Inc.).

2.17 SENTRE

The Safety barrier ENd TREatment (SENTRE) is a redirective, gating crash cushion used as a barrier end treatment [66, 67]. The SENTRE System, developed by Energy Absorption Systems, Inc., is shown in Figure 17.

Figure 17. SENTRE System.

The SENTRE uses sand-filled cartridges to attenuate energy through momentum transfer. The SENTRE requires a redirecting cable to be placed a distance away from the system, which must remain uncovered from soil or other debris. The SENTRE is 5.182-m (17-ft) long and was approved under NHCRP 230.

2.18 TAU-II

The TAU-II is a redirective, non-gating crash cushion designed to protect the ends of rigid barriers, tollbooths, utility poles, and other narrow roadside hazards [68]. The TAU is an Italian design, named *Terminale Attinuatore d'Urto*, which translates literally

as, “End Terminal Attenuator for Collisions.” The TAU-II, manufactured by Barrier Systems, Inc., is shown in Figure 18.

Figure 18. TAU-II System (Photo from Barrier Systems, Inc.).

The TAU-II is a modular crash cushion using air compression. It consists of a metal framework and external thrie-beam panels that telescope back into the base. Inside each section is a bag made of a plastic-coated high-resistance fabric filled with air at atmospheric pressure. Upon impact, the air inside increases in pressure providing a cushioning effect and continues increasing until a diaphragm gives way and discharges the air to prevent rebounding.

The TAU-II consists of two levels of cartridges separated by steel diaphragms. The TAU-II is 0.889-m (35-in.) wide and is available in TL-2 and TL-3 lengths. The TL-2 configuration consists of four bays with a total length of 4.718 m (185.75 in.); the TL-3 configuration consists of eight bays with a total length of 8.185 m (322.25 in.).

2.19 The TRACC Family

The TRinity Attenuating Crash Cushion, TRACC, consists of 3.416-mm (10-gauge) fender panels on an impact "sled" designed to protect concrete barriers, bridge parapet rails, or W-beam and thrie-beam median barriers [69, 70, 71, 72, 73, 74]. The TRACC is a redirective, non-gating crash cushion and is shown in Figure 19.

Figure 19. TRACC System.

The TRACC, FASTRACC, SHORTRACC, and WideTRACC are identical in design except for variations in length and test level. The four TRACC systems are 0.8-m (31-in.) wide and installed on either a concrete or asphalt pad. All units ship complete without requiring field assembly. The TRACC is 6.4-m (21-ft) long, the FASTRACC is 7.89-m (25.9-ft) long and the SHORTRACC is 4.3-m (14-ft) long.

The WideTRACC, with a length of 6.4 m (21 ft), can be used to shield objects 1.47-m (58-in.) wide and wider. The WideTRACC is widened from 1.47 m (58-in.) in 0.71-m (28-in.) increments, each increment adding 0.17 m (6.7 ft) to the overall length of the system. As an example used in the FHWA approval letter, a 3.56-m (11.7-ft) extension would result in a rear width of 2.34 m (7.7 ft) and the WideTRACC would be a total of 9.94 m (32.6 ft) long. The TRACC and WIDETRACC are NCHRP 350 TL-2 and TL-3 crash cushions; the SHORTRACC is a TL-2 crash cushion; and the FASTRACC was tested to exceed TL-3, but since no higher certification exists, is a TL-3 crash cushion.

3 ANALYSIS OF TRADITIONAL CRASH CUSHIONS

In order to perform an engineering analysis of crash cushions, it is helpful to separate their behavior into two categories: non-self-restoring and self-restoring. While the physical outcome may be identical – attenuating kinetic energy from the vehicle – the development of a crash reconstruction procedure is markedly different.

3.1 Non-Self-Restoring Crash Cushions

Most crash cushion designs require the replacement of damaged structural and spent energy-dissipating components after impact. Of the crash cushion designs listed in Table 1, only three are not of this type (the EASi-cell, LMA, and REACT systems). Until these repairs are made, the crash cushion is largely ineffective since its energy-dissipating abilities no longer conform to their original design specifications.

Creating a reconstruction procedure requires extensive physical test data, including vehicle accelerometer traces and system damage from full-scale crash. However, quantifying vehicle damage or proprietary energy-absorbing cartridges to describe the behavior may not be necessary, since the energy dissipated by the crash cushion can be found directly from energy-deflection plots derived from physical testing.

3.2 Self-Restoring Crash Cushions

For crash cushions subjected to significant numbers of impacts, low-maintenance, reusable crash cushions are desirable. For example, the REACT-350, which uses “smart” energy-dissipating thermoplastic cylinders to restore itself, was specifically designed for end-on impacts in high impact locations.

Unfortunately, impacts with self-restoring crash cushions are difficult to reconstruct since the crash cushion has returned to its original position. Unlike replaceable cartridges, that are designed to dissipate a specific amount of energy for a certain amount of permanent crush, the self-restoring devices leave little, if any, evidence of the severity of an impact. Therefore, reconstruction of impacts with self-restoring crash cushions must be performed strictly based on vehicle crush.

Creating a reconstruction procedure requires extensive physical test data, including vehicle accelerometer traces, system damage, and vehicle damage from full-scale crash testing as well as component testing of the unique modules that frequently compose proprietary crash cushion systems.

It is believed that it is possible to relate final vehicle crush to initial velocity of the vehicle for an end-on impact with a self-restoring crash cushion. However, in order to create such relationships for several different vehicle classes, a large amount of physical test data and detailed finite element models would be required for each type of crash cushion. Crashes cushions using High Density Polyethylene (HDPE), such as the REACT, are strain-rate sensitive, and would require crash testing at multiple velocities. Initial finite element simulation performed to examine the feasibility of lumped-parameter modeling determined that strain-rate effects must be identified and modeled for an accurate simulation. Because that information is not available, developing reconstruction procedures for these crash cushions is not feasible at this time.

4 INERTIAL BARRIER CRASH CUSHIONS – SAND-FILLED BARRELS

Inertial systems are primarily sand-filled plastic barrels used to attenuate energy. Upon impact, each barrel absorbs a portion of the momentum of the vehicle. The barrels are constructed of a frangible plastic designed to fracture upon impact. However, this requires barrels to be inspected regularly, since damaged barrels retain little, if any, of their original energy-attenuating ability.

Three inertial barrier systems are currently approved under NCHRP Report 350: Big Sandy by TrafFix, Energite III by Energy Absorption Systems, Inc., and the Fitch Barrier System. When the Federal Highway Administration approves an inertial barrier system, the manufacturer will frequently publish guidelines for installations of lower-level arrays of crash cushions based on that approval. The subsequent lower-test-level arrays are developed using conservation of momentum, as detailed in Section 4.4. Each of the barrier systems, along with their unique identifying characteristics, is identified below.

4.1 Big Sandy by TrafFix

Big Sandy, manufactured by TrafFix Devices, Inc., uses a number of 0.9144-m (3-ft) diameter, sand-filled, polypropylene and polyethylene plastic modules that are installed in a specific geometric array in front of a hazard [75, 76]. The Big Sandy is shown in Figure 20.

Figure 20. TrafFix's Big Sandy.

Three separate barrels are available. The largest holds 960 kg (2100 lb) of sand; the second largest holds 640 kg (1400) of sand. The smallest barrel can be filled to 90, 180, or 320 kg (200, 400, or 700 lb), depending on placement in the array. The original design of the Big Sandy required the inversion of the 320 kg (700 lb) module. TL-3 approval as a non-redirecting, gating crash cushion was granted based on a design using twelve barrels in the configuration, shown in Table 3, from front to back.

Table 3. TrafFix Big Sandy TL-3 Tested Array.

Row	Barrel Mass, kg (lb)	
1	90 (200)	
2	180 (400)	
3	180 (400)	
4	320 (700)	
5	320 (700)	320 (700)
6	320 (700)	320 (700)
7	640 (1400)	640 (1400)
8	960 (2100)	960 (2100)

TrafFix Devices recommends that 300 mm (1 ft) be left between the system and object being protected and a minimum of 150 mm (6 in.) be left between barrels longitudinally. A maximum spacing of 150 mm (6 in.) may be left between barrels laterally.

4.2 Energite III System

The Energite III, manufactured by Energy Absorption Systems, Inc., uses a number of 0.9144-m (3-ft) diameter, sand-filled, polyethylene plastic modules that are installed in a specific geometric array in front of a hazard [77, 78, 79, 80]. Each module consists of a one-piece barrel, a lid, and, in some modules, a cone insert. The cone insert is used to adjust the center of gravity and mass of the barrel. The Energite III system is shown in Figure 21.

Figure 21. Energite III System.

The Energite III modules come in 90, 180, 320, 640, and 960-kg (200,400, 700, 1400, and 2100-lb) sizes. These masses are accomplished using two different barrel designs: Model 640 and Model 960. The Model 640 is used to create all of the lighter modules. TL-3 approval as a non-redirective, gating crash cushion was granted based on a design using twelve barrels in the following configuration shown in Table 4 (from front to back). Energy Absorption Systems recommends that 300 mm (1 ft) be left between the system and object being protected and 150 mm (6 in.) be left between barrels.

Table 4. Energite III TL-3 Tested Array.

Row	Barrel Mass, kg (lb)	
1	90 (200)	
2	180 (400)	
3	180 (400)	
4	320 (700)	
5	320 (700)	320 (700)
6	320 (700)	320 (700)
7	640 (1400)	640 (1400)
8	960 (2100)	960 (2100)

4.3 Fitch Universal Module Crash Cushion

The Fitch Universal Module Crash Cushion uses a number of 0.9144-m (3-ft) diameter, sand-filled, polyethylene plastic modules that are installed in a specific geometric array in front of a hazard [81, 82]. The Fitch system is shown in Figure 22.

Figure 22. Fitch Sand Barrel System.

The Fitch sand barrel system consists of two identical half-cylinders that connect together using two plastic “Zip Strip” fasteners on either side. Fitch’s Unicore allows the utilization of identical barrels for the various required barrel masses by adjusting the depth of the bottom of the barrel. The modules can be configured in 90, 180, 320, 640, and 960 kg (200, 400, 700, 1400, and 2100 lb) weights.

Approval as a TL-3 non-redirective, gating crash cushion was granted based on a design using fourteen barrels in the configuration shown in Table 5 (from front to back).

Table 5. Fitch TL-3 Tested Array.

Row	Barrel Mass, kg (lb)	
1	90 (200)	
2	90 (200)	
3	180 (400)	
4	180 (400)	
5	180 (400)	180 (400)
6	320 (700)	320 (700)
7	640 (1400)	640 (1400)
8	640 (1400)	640 (1400)
9	960 (2100)	960 (2100)

4.4 Physics of Inertial Barriers

Inertial barriers are design to dissipate the kinetic energy of an impacting vehicle through momentum transfer. Although other factors influence energy dissipation during an impact, simple momentum transfer is used as the basis for predicting a system's performance [83]. In addition to inertial barrier design, this methodology can also be used as a technique for crash reconstruction. The derivation of the equations for inertial barrier impacts is performed below.

If constant deceleration is assumed (losing the distinction between average acceleration and instantaneous acceleration), the average deceleration, D, of the vehicle is [84].

$$D = \frac{\Delta V}{\Delta t} = \frac{v_i - v_f}{t} \qquad \text{[Eqn. 1]}$$

Where v_f is the final velocity in m/s

v_i is the initial velocity in m/s and

t is the deceleration time in seconds

The deceleration distance, d_{decel}, traveled during deceleration is given as [ibid]:

$$d_{decel} = v_i\, t + \frac{1}{2}\, D\, t^2 \qquad \text{[Eqn. 2]}$$

For an impact with a single sand barrel, or a single row of sand barrels, the deceleration occurs over the entire diameter of a barrel; since it is made of frangible plastic, the vehicle breaks apart the barrel and accelerates through the sand independent of the barrel [85]. TrafFix's sand barrel design has an outside diameter of 0.900 m (35.4 in.) at the top, making it slightly narrower than the Fitch and Energite designs of 0.9144 m (36 in.); however, this variation affects the deceleration of the vehicle by less than 2%. Therefore,

$$d_{decel} = d_{barrel} = 0.9144 \text{ m (36 in.)} \qquad \text{[Eqn. 3]}$$

Combining Equations 1 and 2 yields the deceleration in terms of the initial and final velocities and the diameter of the barrel.

$$D = \frac{1}{2\, d_{barrel}} (v_f^2 - v_i^2) \qquad \text{[Eqn. 4]}$$

It is assumed that the impacting vehicle and the sand barrel obtain the same final velocity after impact, implying a perfectly plastic collision (i.e. the coefficient of restitution, e = 0.). Using conservation of momentum:

$$v_i * M_v = v_f\, (M_s + M_v) \qquad \text{[Eqn. 5]}$$

Where M_s is the mass of the sand impacted (single barrel or row mass)

M_v is the mass of the vehicle

Solving Equation 4 for initial velocity,

$$v_i = \frac{v_f\, (M_s + M_v)}{M_v} \qquad \text{[Eqn. 6]}$$

Frequently, the maximum deceleration, D_g, in Gs, is desired for an estimate of the occupant risk from ridedown decelerations. This can be calculated as:

$$D_g = \frac{D}{g} \qquad \text{[Eqn. 7]}$$

Where g is free-fall acceleration, 9.81 m/s^2 (32.2 f/s^2)

NCHRP Report 350 lists a preferred value of 15 Gs and a maximum value of 20 Gs for occupant ridedown decelerations. By combining Equations 3 and 4, the maximum deceleration for any impact velocity, vehicle mass, sand mass, and barrel diameter can be calculated as:

$$D_g = \frac{v_i^2}{2\ g\ d_{barrel}} \left(\left(\frac{M_v}{(M_v + M_s)} \right)^2 - 1 \right) \qquad \text{[Eqn. 8]}$$

Or, rewriting, where R is the ratio of the mass of the vehicle to the combined mass of the vehicle and the sand barrels being impacted,

$$D_g = \frac{v_i^2}{2\ g\ d_{barrel}} (R^2 - 1) \qquad \text{[Eqn. 9]}$$

Where $R = \frac{M_v}{M_v + M_s}$

This procedure is applied in a sequential manner for each row of sand barrels impacted.

4.5 Inertial Barrier Design Charts

Design charts are frequently used to facilitate the analysis of inertial barrier impacts rather than explicitly solving Equations 6 and 8. Design charts are developed for specific vehicles to quickly and easily calculate the average deceleration and exit velocity when the mass of the sand in any given impact is known. A simplified design chart is shown in Figure 23.

The two straight lines sloping from upper right to lower left, designated v_f = 40 km/h and v_f = 45 km/h, are constant final velocity curves. For a given vehicle mass and final velocity, Equation 4 becomes a linear relationship between the impact velocity and the mass of sand impacted. To create the two constant final velocity curves shown in Figure 23, a vehicle mass of 2000 kg (4410 lb) was used.

The curved lines sloping from upper left to lower right, designated D_g = 3.0 G and D_g = 4.0 G, are constant deceleration curves. For a given vehicle mass and final velocity, Equation 7 becomes an exponential relationship between the impact velocity and the mass of sand impacted. To create the two constant deceleration curves shown in Figure 23, a vehicle mass of 2000 kg (4410 lb) was used.

An example of using the simplified design charge in Figure 23 is as follows: A 2000-kg (4410-lb) pickup truck impacts a 480-kg (1058-lb) sand barrel at 50 km/h (31 mph). First, on the horizontal axis, "Velocity Entering Row," a vertical line is drawn at the velocity impact velocity of the pickup truck, 50 km/h (31 mph). Next, on the vertical axis, "Sand Weight in Row," a horizontal line is drawn at the weight of the sand barrel, 480 kg (1058 lb). The point at which these lines intersect is designated as Point "A."

The final velocity curves are used to determine the final velocity of the pickup truck. In this case, point "A" lies between the v_f = 40 km/h and v_f = 45 km/h, very close to the v_f= 40 km/h (24.9 mph) curve. Interpolating, the final velocity of the pickup truck was approximately 40.3 km/h (25.1 mph).

The sloping curves indicate the average deceleration seen by the pickup truck. In this case, Point "A" lies three-fourths of the way between the D_g = 3.0 G and D_g = 4.0 G

lines. Interpolating, the average deceleration of the pickup truck was approximately 3.75 Gs. Interpolation is performed along the normal of the two curves and passing through the point of interest.

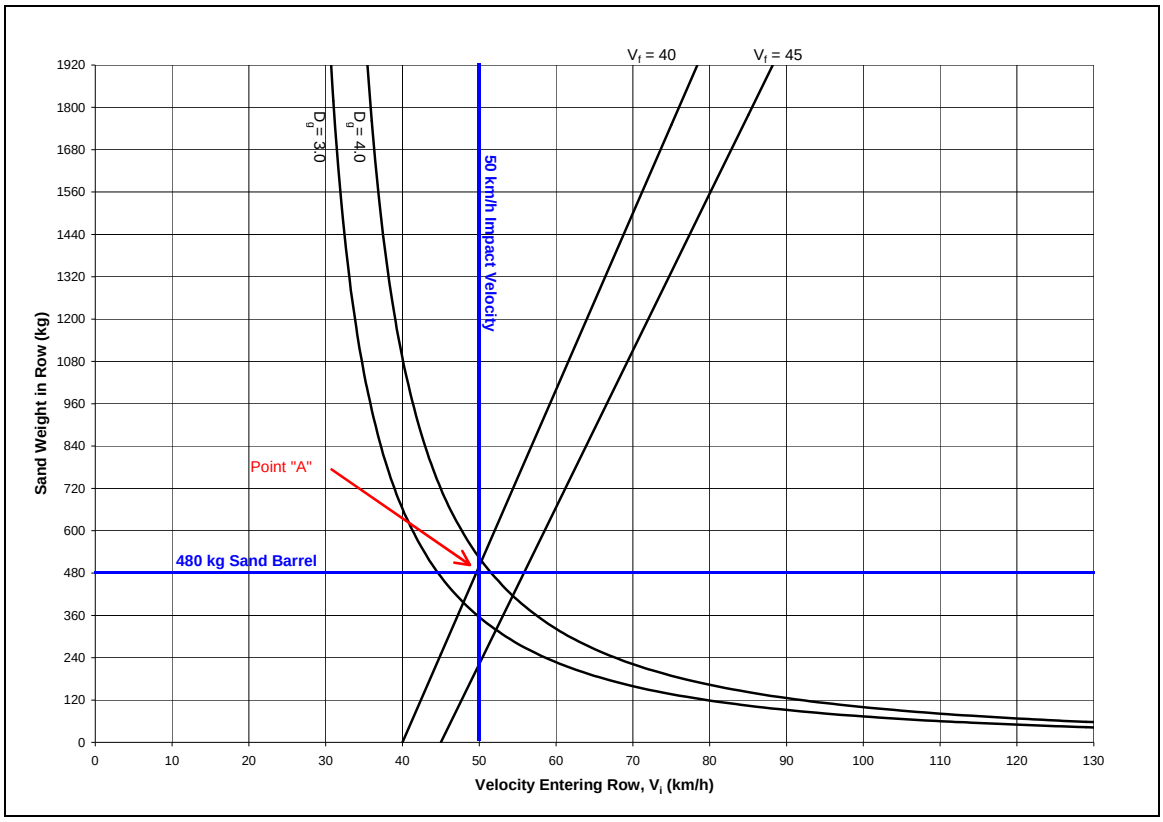

Figure 23. Simplified Inertial Barrier Design Chart.

Curves were developed for both a 2000-kg (4010-lb) pickup truck and an 820-kg (1808-lb) small car with a 75-kg (165-lb) occupant. These curves are shown in Figure 24 and Figure 25. These curves conform to the specifications for testing under NCHRP Report 350. These curves can be used instead of equations for determining the performance of a crash cushion or for reconstructing an impact with a crash cushion.

It is important to note that NCHRP Report 350 requires a 75-kg (165-lb) dummy be used in testing. This is to represent the 50th percentile male and increases the overall

mass to 895 kg (1874 lb). The overall mass, not just the mass of the vehicle, should be used whenever working with inertial barrier design.

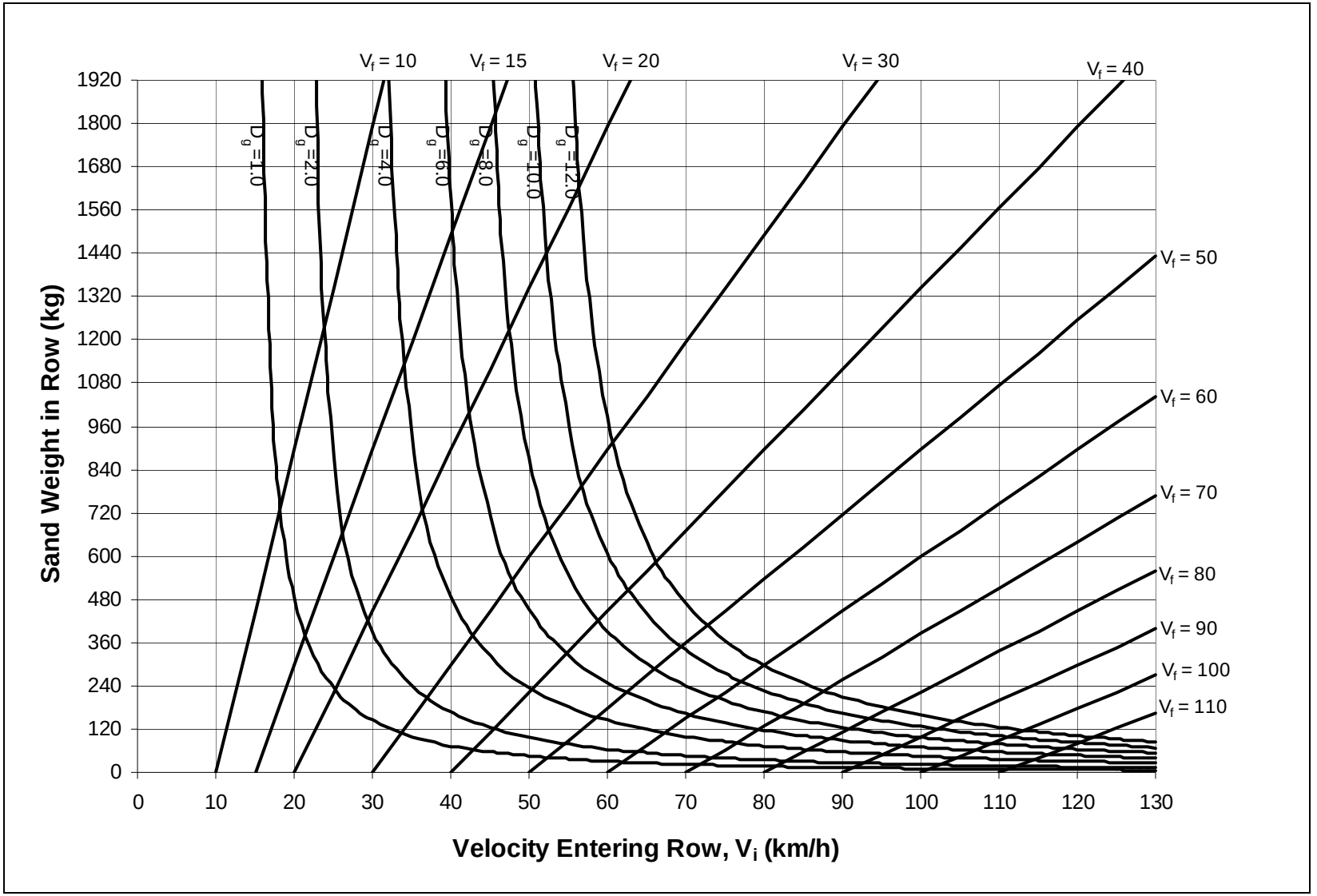

Figure 24. Inertial Barrier Design Chart for an 895-kg (1973-lb) Total Vehicle Mass.

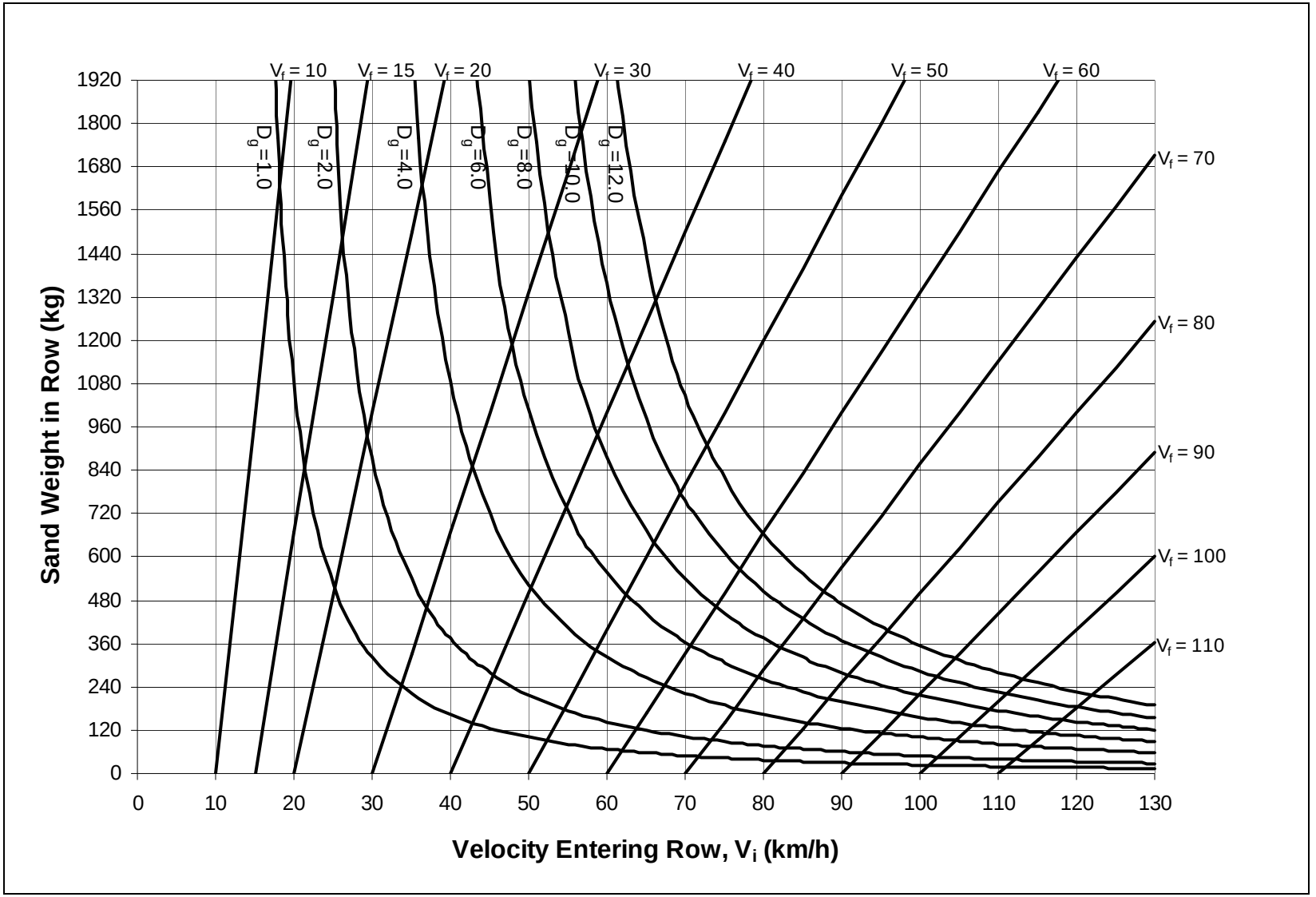

Figure 25. Inertial Barrier Design Chart for 200-kg (4410-lb) Total Vehicle Mass.

5 INERTIAL BARRIER SYSTEM RECONSTRUCTION PROCEDURE

In order to reconstruct an end-on impact with an inertial barrier system, the vehicle mass, departure velocity, and the number and masses of the barrels impacted must be known. The reconstruction is based on conservation of momentum. The procedure reconstructs the crash in reverse order of the actual crash.

1. The velocity at the point the vehicle departed from the crash cushion must be determined. This point occurs when the vehicle loses contact with the crash cushion. Reconstruction of the departure velocity can be achieved through conventional accident reconstruction techniques [86]. This is important since events after departure are not interactions with the crash cushion.
2. Conservation of momentum is used to determine the impacting velocity for each barrel or set of sand barrels impacted. This is achieved using Equation 6 in Section 3. If the barrels are impacted simultaneously, then the barrel masses should be summed together for a total impacted mass. Otherwise, each barrel is treated individually. The mass of the vehicle remains constant, since the sand is dispersed after each sand barrel is impacted. To calculate the initial impact velocity, these calculations are performed sequentially until the first sand barrel is impacted.

5.1 Sample Reconstruction

In order to clarify the units and to detail the reconstruction procedure, a reconstruction of a full-scale crash test of an Energite III sand barrel crash cushion system run by Energy Absorption Systems, Inc. (EASI) was performed [81]. The

NCHRP Report 350 designation 3-41 is a compliance test for a Test Level 3 (TL-3) crash cushion.

Test 3-41 utilizes a 2000-kg (4410-lb) pickup truck without a dummy. The test vehicle had a gross mass of 2005 kg (4420 lb). The impact was end-on at 0° and 102.8 km/h (63.9 mph). The test vehicle impacted a barrier system as shown in Table 4.

The test vehicle, after impacting every sand barrel, proceeded to impact a rigid concrete barrier behind the system. Crush measurements, estimated from photographic evidence, are shown in Table 6.

Table 6. Estimated Vehicle Crush Measurements from Test 177.015.

Permanent Vehicle Crush Measurements			
C_1:	6.05 in.	C_4:	12.1 in.
C_2:	12.1 in.	C_5:	12.1 in.
C_3:	12.1 in.	C_6:	6.05 in.

Impact Parameters	
W:	18 in.
θ:	0°

Vehicle Stiffness Coefficients	
A:	480 lbf/in
B:	50 lbf/in^2
G:	2304 lbf

1. The departing velocity of the vehicle must be estimated. In this case, the departing velocity was reconstructed using vehicle damage caused by an impact with a rigid concrete barrier. The impact velocity can be found using traditional reconstruction techniques by estimating crush energy, E_{crush} [86]:

$$E_{crush} = \frac{W\,(1 + \tan^2\theta)}{30}\,(30G + 3A(C_1 + 2C_2 + 2C_3 + 2C_4 + 2C_5 + C_6) + B(C_1^2 + 2C_2^2 + 2C_3^2 + 2C_4^2 + 2\,C_5^2 + C_6^2 + C_1C_2 + C_2C_3 + C_3C_4 + C_4C_5 + C_5C_6)) \quad \text{[Eqn. 10]}$$

For the values in Table 6, Equation 8 yields 11.96 kJ (8.825 kip-ft). Converting to velocity through the definition of kinetic energy produces:

$$v_f = \sqrt{\frac{2\,E_{crush}}{M_{vehicle}}} = \sqrt{\frac{2 * 11960\ J}{2005\ kg}} = 3.45\ m/s = 12.4\ km/h = 7.7\ mph \qquad \text{[Eqn. 11]}$$

Where $M_{vehicle}$ is the mass of the vehicle.

2. Conservation of momentum is used to determine the impacting velocity for each barrel or set of sand barrels impacted. This is achieved using Equation 6. The results of the impact with each row of cylinders are shown in Table 7. Alternatively, the nomograph shown in Figure 25 can be used.

Table 7. Inertial Crash Cushion Reconstruction.

Row	Barrel Mass, kg		Velocity Entering Row, km/h	Velocity Exiting Row km/h (mph)
8	960	960	$v_8 = \frac{v_f\,(1920 + 2005)}{2005} = 24.3$	$v_f = 12.4$
7	640	640	$v_7 = \frac{v_8\,(1280 + 2005)}{2005} = 39.8$	$v_8 = 24.3$
6	320	320	$v_6 = \frac{v_7\,(640 + 2005)}{2005} = 52.5$	$v_7 = 39.8$
5	320	320	$v_5 = \frac{v_6\,(640 + 2005)}{2005} = 69.2$	$v_6 = 52.5$
4	320		$v_4 = \frac{v_5\,(320 + 2005)}{2005} = 80.3$	$v_5 = 69.2$
3	180		$v_3 = \frac{v_4\,(180 + 2005)}{2005} = 87.5$	$v_4 = 80.3$
2	180		$v_2 = \frac{v_3\,(180 + 2005)}{2005} = 95.3$	$v_3 = 87.5$
1	90		$v_i = v_1 = \frac{v_2\,(90 + 2005)}{2005} = \mathbf{99.6}$	$v_2 = 95.3$

The reconstructed initial velocity was found to be 99.6 km/h (61.9 mph), which is within 3% of the actual impact velocity of 102.8 km/h (63.9 mph). However, it should be noted that the reconstructed initial velocity is sensitive to the final velocity. Given the above reconstruction procedure, the initial velocity, v_i, can be calculated for any final velocity, v_f, which is calculated from vehicle crush energy. As an example, if the final velocity determined in Step 1 above was 20% off, then using v_f = 14.9 km/h, the predicted initial velocity would be 20% off, a 20 km/h error. This highlights the importance of accurate estimates of the departure velocity.

6 CONCLUSIONS AND RECOMMENDATIONS

Detailed descriptions and identification of crash cushions was presented. This included identification of the test levels, redirective and gating qualities, and descriptions of crash cushions and physical measurements of the crash cushions.

A method for developing reconstructing techniques for self-restoring and non-self-restoring crash cushions was suggested. This included an examination of the data required to create the reconstruction procedure, extensive physical test data, including vehicle accelerometer traces, system damage, and vehicle damage from full-scale crash testing as well as component testing of the unique modules that frequently compose proprietary crash cushion systems.

For inertial barriers (sand-filled barrels), a crash reconstruction procedure using the principles of conservation of momentum was derived. Methods for estimating impact velocity from post-impact damage and vehicle exit velocity, velocities correlated extremely well with full-scale crash data. Additionally, the importance of determining the velocity of a vehicle as it departs a sand barrel array was also highlighted.

7 ACKNOWLEDGEMENTS

The authors would like to thank the National Cooperative Highway Research Program and Dr. Dean Sicking for funding this research; Bob W. Bielenberg, for his invaluable assistance in finite element modeling of the REACT 350 system, Karla Polivka for her help editing and valuable input, and the entire staff of the Midwest Roadside Safety Facility.

8 REFERENCES

1. Bielenberg, BW, RK Faller, JC Holloway, JD Reid, JR Rohde, and DL Sicking, "Safety Performance Evaluation of a Single-Sided Crash Cushion," Final Report to Safety By Design Company, Inc., Transportation Research Report No. TRP-03-111-02, Midwest Roadside Safety Facility, University of Nebraska-Lincoln, January 7, 2002.
2. Wendling, WH, "Roadside Safety Milestones," Semi-Sesquicentennial Transportation Conference, HCR 71, P.O. Box 119, Camdenton, Missouri 65020, 1996.
3. Federal Highway Administration Acceptance Letter CC-66, May 11, 2000.
4. Federal Highway Administration Acceptance Letter CC-66A, Jun 27, 2000.
5. Barrier Systems, Inc., Press Release: "New absorb 350 Crash Cushion from Barrier Systems Inc Meets Both NCHRP 350 NL-2 and TL-3 Recommendations," Undated.
6. Federal Highway Administration Acceptance Letter CC-38, March 3, 1997.
7. Syro, "ADIEM 350: Installation and Maintenance," Undated.
8. Ivey, DL and MA Marek, "ADIEM: Low-Cost Terminal for Concrete Barriers." Transportation Research Record 1367, Transportation Research Board, Washington, DC, 1992.
9. Ivey, DL and MA Marek, "Development of a Low Cost High Performance Terminal for Concrete Median Barriers and Portable Concrete Barriers," Texas Transportation Institute Project No. 9901-E, Texas A&M University System, College Station, Texas, August 1991.
10. Alberson, DC, "Test Report 220517-5," Texas Transportation Institute Project No. 220517, Texas A&M University System, College Station, Texas, October 1993.
11. AASHTO. "Roadside Design Manual." American Association of State Highway Transportation Officials. Washington, DC. 2003.
12. Bielenberg, B, RK Faller, J Holloway, JD Reid, JR Rohde, and DL Sicking. "Safety Performance Evaluation of a Single-Sided Crash Cushion," MwRSF Report No. TRP-03-111-02, Tests SSC 1-5, Midwest Roadside Safety Facility, University of Nebraska – Lincoln, January 7, 2002.
13. Bielenberg, B, RK Faller, J Holloway, JD Reid, JR Rohde, and DL Sicking, "Safety Performance Evaluation of the BEAT Bridge Pier Protection System," MwRSF Report No. TRP-03-123-02, Midwest Roadside Safety Facility, University of Nebraska - Lincoln. 2003
14. Coon, BA and JD Reid, "Reconstruction Techniques for Guardrail End Terminals," 2003.

15. Federal Highway Administration Acceptance Letter CC-41, June 19, 1997.
16. Energy Absorption Systems, Inc., “Brakemaster System Installation Manual,” undated.
17. Energy Absorption Systems, Inc., “Brakemaster System Maintenance Manual,” undated.
18. Energy Absorption Systems, Inc., “Brakemaster Design Manual,” Form ENE 704-0897, 1997.
19. Energy Absorbsion Systems, Inc., “Brakemaster NCHRP 230 Certification Report,” September 1989.
20. Federal Highway Administration Acceptance Letter CC-33, May 1, 1996.
21. Federal Highway Administration Acceptance Letter CC-33A, September 5, 2002.
22. Mayer, JB and ME Bronstad, “Experimental Evaluation of the Combination Attenuator Terminal (CAT), Final Report on SwRI Project 06-1618, Southwest Research Institute, San Antonio, TX, 1988.
23. Syro Product Brochure, “America’s Most Affordable Crash Cushion Attenuating Terminal,” Undated.
24. Carney, JF, “Development and Experimental Evaluation of a Steel Pipe Vehicle Impact Attenuation System,” FHWA Report No. FHWA-CT-RD-722-1-80-13, Federal Highway Administration, July 1980.
25. Federal Highway Administration Acceptance Letter CC-77, April 9, 2002.
26. Logie, DS, JF Carney, and MH Ray,”Computer-Based Methodology for the Generalized Design of the Connecticut Impact Attenuation System,” Transportation Research Record 1233, Transportation Research Board, Washington, DC, 1989.
27. Carney, JF, CE Dougan, and MW Hargrave, “The Connecticut Impact-Attenuation System,” Transportation Research Record 1024, Transportation Research Board, Washington, DC, 1985.
28. Lohrey, EC, “Field Evaluation of the Connecticut Impact-Attenuation System at Four High-Hazard Locations,” Connecticut Department of Transportation Report Number 876-F-88-2, March 1988.
29. Logie, DS and JF Carney, “CADS (Connecticut Attenuator Design System) Manual, Connecticut Department of Transportation Report No. 1222-1-88-14, December 1988.
30. Carney, JF, “A Generalized Design for the Connecticut Impact Attenuation System, “Connecticut Department of Transportation Report Number 1222-F-88-15, December 1988.

31. Juan, YLM, “Construction of the Connecticut Impact Attenuation System at Four High-Hazard Locations,” Federal Highway Administration Report No FHWA-CT-RD-876-3-84-12, December 1984.
32. Federal Highway Administration Acceptance Letter CC-58, March 26, 1999.
33. Lohrey, EC, “Construction of the Narrow Connecticut Impact-Attenuation System at Five High-Hazard Locations,” Transportation Research Record 1367, Transportation Research Board, Washington, DC, ?.
34. Carney, JF, “Connecticut Narrow Hazard Crash Cushion,” Transportation Research Record 1233, Transportation Research Board, Washington, DC, 1989.
35. Federal Highway Administration Acceptance Letter CC-71, December 6, 2000.
36. Federal Highway Administration Acceptance Letter CC-25, February 10, 1995.
37. Energy Absorption, Inc., “N E A T General Specifications,” undated.
38. Energy Absorption, Inc., NEAT Product Description, undated.
39. Federal Highway Administration Acceptance Letter CC-35, June 21, 1996.
40. Federal Highway Administration Acceptance Letter CC-35A, August 5, 1996.
41. Federal Highway Administration Acceptance Letter CC-35B, October 17, 1996.
42. Federal Highway Administration Acceptance Letter CC-35C, June 17, 1999.
43. Federal Highway Administration Acceptance Letter CC-35D, October 13, 2000.
44. Federal Highway Administration Acceptance Letter CC-35E, October 19, 2001.
45. Federal Highway Administration Acceptance Letter CC-43, December 1, 1997.
46. Federal Highway Administration Acceptance Letter CC-45, March 19, 1998.
47. Federal Highway Administration Acceptance Letter CC-57, December 30, 1998.
48. Federal Highway Administration Acceptance Letter CC-57A, June 17, 1999.
49. Federal Highway Administration Acceptance Letter CC-49, June 18, 1998.
50. Federal Highway Administration Acceptance Letter CC-26, March 3, 1995.
51. Federal Highway Administration Acceptance Letter CC-26A, April 12, 1995.
52. Federal Highway Administration Acceptance Letter CC-26B, August 14, 1995.
53. Federal Highway Administration Acceptance Letter CC-26C, September 25, 1995.
54. Federal Highway Administration Acceptance Letter CC-26D, December 19, 1996.
55. Federal Highway Administration Acceptance Letter CC-26E, June 25, 1997.
56. Federal Highway Administration Acceptance Letter CC-26F, September 23. 1997.
57. Federal Highway Administration Acceptance Letter CC-26G, July 24, 1998.
58. Roadway Safety Service, “REACT 350 System Installation Instruction for Narrow Units,” Wauconda, IL, undated.

59. Federal Highway Administration Acceptance Letter CC-50, June 16, 1998.
60. Federal Highway Administration Acceptance Letter CC-50A, June 9, 1999.
61. Federal Highway Administration Acceptance Letter CC-50B, December 9, 1999.
62. Carney, JF, DC Alberson, DL Bullard, S Chatterjee, and W Menges, “Reusable High Molecular Wight / High Density Polyethylene Crash Cushions for Wide Hazards,” 78th Annual Meeting, Transportation Research Board, Washington, DC, January 1999.
63. Federal Highway Administration Acceptance Letter CC-73, May 3, 2001.
64. Federal Highway Administration Acceptance Letter CC-73A, April 30, 2002.
65. Carney, JF, MI Farawawi, and S Chatterjee, “Development of Reusable High-Molecular-Weight-High-Density Polyethylene Crash Cushions,” Transportation Research Record 1528, September 1996.
66. Noureldin, AS, "Final Report, SENTRE Guardrail End Treatments, Experimental Project NO. 7" Indiana Department of Highways, West Lafayette, IN (February 1988).
67. Stanley, MT, "Evaluation of the SENTRE Guardrail Anchor System, Final Report" Experimental Project 170-3, North Carolina Department of Transportation, Raleigh, NC (April 1990).
68. Federal Highway Administration Acceptance Letter CC-75, September 14, 2001.
69. Federal Highway Administration Acceptance Letter CC-54, November 13, 1998.
70. Federal Highway Administration Acceptance Letter CC-54A, September 8, 2000.
71. Federal Highway Administration Acceptance Letter CC-54B, April 10, 2001.
72. Federal Highway Administration Acceptance Letter CC-54C, July 3, 2002.
73. Federal Highway Administration Acceptance Letter CC-54D
74. Federal Highway Administration Acceptance Letter CC-54
75. Federal Highway Administration Acceptance Letter CC-52, July 10, 1998.
76. Federal Highway Administration Acceptance Letter CC-52A, October 10, 1998.
77. Federal Highway Administration Acceptance Letter CC-29, June 28, 1995.
78. Energy Absorption Systems, Inc., “The Energite III Inertial Barrier System,” January 1983.
79. Energy Absorption, Inc., “Energite III System General Specifications,” December 19, 1995.
80. Energy Absorption, Inc., “Energite III System Design Manual,” Form ENE 671C-1/C, 1996.
81. Federal Highway Administration Acceptance Letter CC-28, June 28, 1995.

82. Roadway Safety Service, Inc., Fitch product brochure, undated.
83. Energy Absorption Systems, Incorporated. "Energite III Design Manual." Form ENE 671C-1/96. Chicago, IL. 1996.
84. Halliday, D and R Resnick, "Fundamentals of Physics," Third edition, Wiley & Sons, 1988.
85. Energy Absorption Systems, Inc., "Energite II Design Manual." Chicago, IL. 1996.
86. Fricke, LB, "Traffic Accident Reconstruction, Volume 2 of the Traffic Accident Investigation Manual," Northwestern University Traffic Institute, 1990.